SLAC-PUB-992

PHOTOPRODUCTION OF PSEUDOSCALAR MESONS*

Bjorn Wiik
Stanford Linear Accelerator Center
Stanford University, Stanford, California 94305

ERRATA

The computed ratio $R = \frac{\gamma n \to \pi^o n}{\gamma p \to \pi^o p}$ contain a misprint. The correct expression is:

$$R = \frac{(I_V - 1/3\ I_s)^2 + 8/9\ I_s^2}{(I_V + 1/3\ I_s)^2 + 8/9\ I_s^2} \quad .$$

The plotted values of R in Fig. 6 are correct.

The prediction of Worden (Nucl. Phys B, 37, 253 (1972)) for the asymmetry in π^o photoproduction from a polarized target was mistakenly plotted against $\sqrt{-t}$ instead of against -t as shown in Fig. 7.

I thank Dr. Worden for pointing out this mistake to me.

(1971 International Symposium on Electron and Photon Interactions at High Energies, Cornell University, Ithaca, New York, Aug. 23-27, 1971.)

*Work supported by the U. S. Atomic Energy Commission.

March 1972

SLAC-PUB-992
(TH) and (EXP)
December 1971

PHOTOPRODUCTION OF PSEUDOSCALAR MESONS*

Bjorn Wiik
Stanford Linear Accelerator Center
Stanford University, Stanford, California 94305

(1971 International Symposium on Electron and Photon Interactions at High Energies, Cornell University, Ithaca, New York, Aug. 23-27, 1971.)

*Work supported by the U. S. Atomic Energy Commission.

In the first part of the talk I'll discuss the new data on high energy photoproduction of pseudoscalar mesons. For this purpose new is taken to mean since the Liverpool Conference(1-3) and high energies will start at 3 GeV. In the second part, the data on photon induced inclusive reactions will be presented.

I. Pseudoscalar Meson Photoproduction

It is probably fair to say that it is not what you see, but what you don't see that makes the photoproduction data so difficult to understand and therefore so interesting. For example, none of the reactions shows the strong shrinkage which can be taken as evidence for Regge-exchange. In fact, whereas there are some deviations from a k^{-2} behavior in the forward direction, the cross sections for backward π^+ and π^o photoproduction are both decreasing as k^{-3} over a large range in u-values. A dip, which can be associated with a nonsense-wrong-signature (NWS)-zero , is only observed in forward π^o- photoproduction. Although the various reactions differ markedly at small t-values, they all become rather similar at larger t-values, decreasing nearly proportional to exp(3t).

It is by now generally accepted that this simple behavior in s and t cannot be reproduced in a pure Regge model, which would most naturally lead to structure in the angular distributions as well as shrinkage. The data can only be represented within the framework of an exchange model by including large contributions from cuts or absorption. It is therefore tempting to speculate that these reactions are approaching their asymptotic limits. In

this case the phases of the amplitudes can be extracted from the observed energy dependence(4). Consider charged pion photoproduction, $\gamma + p \rightarrow \pi^+ + n$ and $\gamma + n \rightarrow \pi^- + p$. The cross sections for these reactions are to a good approximation proportional to $1/s^2$ and the most natural assumption would be for the amplitudes to decrease as $1/s$. However for such an energy dependence the the isoscalar and isovector amplitudes would be 90° out of phase, and we would predict $d\sigma/dt(\gamma p \rightarrow \pi^+ n)$ to be equal to $d\sigma/dt(\gamma n \rightarrow \pi^- p)$ in disagreement with the available data(1-3). We are therefore forced to conclude that the amplitudes for photoproduction of pseudoscalar mesons have not yet reached asymptotic limits, and that the simple behavior of the observed cross section in s and t does not reflect a simple behavior of the amplitudes. To fully understand these reactions will therefore require detailed experimental information involving both polarized beam and target.

At present the data are fitted in terms of Regge cut models. These models, depending upon the structure of the pole term, can be divided into two classes known as the Argonne(5) and the Michigan(6) models. The Argonne(5) model in general incorporates exchange degeneracy with the same residue function for both even and odd signature Regge poles. The odd signature exchanges (ω,ρ--) then have NWS-zeros for $\alpha(t)=0$. Because of large cancelling effects, the contributions from cuts or absorption are in general small and the observed structure in the angular distributions is caused by NWS-zeros in the pole term. In the

Michigan model(6), the pole term contains no NWS-zeros. In this model, the dip structure results from destructive interference between the pole term and the absorption term. However, the dip structure can only be reproduced by increasing the absorption terms by a factor of two.

Both models, although they are able to fit a large number of observation, have serious short-comings(7). A critical discussion of the various Regge cut models has recently been given by Contogouris(8). Harari has shown(9), using arguments based on duality, that only the imaginary part of the amplitude should be dominated by the peripheral waves as assumed in the absorption model, whereas in general the real part is not known. This observation offers a possible explanation for the failures of the two models. Fits to the photoproduction data using such a "duality" model have been made by Contogouris(8).

π^o Photoproduction

The previous data(10) by the Ritson Group on π^o-photoproduction have now been extended down to t-values of $-.1(GeV/c)^2$. The process was identified, as in the earlier experiment, by observing the recoil proton with the SLAC 1.6 GeV/c spectrometer. The new data(11), together with the old re-analyzed data are plotted in Fig. 1 for incident energies of 6, 9, 12, and 15 GeV and for values of t between $-.1(GeV/c)^2$ and $-1.4(GeV/c)^2$. The data show a smoothly varying cross section with a dip around $t = -.5(GeV/c)^2$. The relative depth of this dip is nearly independent of energy, in slight disagreement with

the earlier data. This difference is due to an improved Compton subtraction. Since only the recoil proton is detected, the resolution is not sufficient to separate the π^o events from the Compton events and therefore only the sum of these reactions is measured. The corresponding correction factor is the largest in the dip region, where at high energies, the Compton cross section is considerably larger than the π^o cross section. The Compton cross section has now been measured(12) by essentially the same apparatus as used in the π^o experiment. Therefore no relative normalization error is involved in the subtraction and the results should be very reliable. This has been confirmed by detecting one of the photons from the π^o decay in coincidence with the recoil proton. With this technique, the Compton contribution can be excluded, and the results(11) obtained at 17 GeV are in excellent agreement with the single arm data.

Gomez et al.(13) have extended the π^o data to a t-value of $-3.0(GeV/c)^2$. The cross section was measured at 6, 12, and 18 GeV by observing the recoil proton with the SLAC 8(GeV/c) spectrometer. Again, only the sum of the π^o cross section and the Compton cross section is being determined. Unfortunately, since there is a 20% normalization discrepancy between these data and the earlier data by the Ritson group, the measured Compton data cannot be used directly to determine the π^o cross section. The authors(13), therefore, only quote cross sections at t-values where the Compton contribution is 20% or less of the total yield. The observed π^o cross section, multiplied by a factor 1.2, is

plotted in Fig. 2 versus t. For comparison, the previous data(11) are also shown. Apart from the question of normalization, the two experiments agree on both the t-dependence and the energy dependence. The most important feature, which is independent of both Compton subtraction and normalization uncertainties, is the decrease of the cross section beyond $t \simeq -1.2(\mathrm{GeV/c})^2$. As in the charged pion case, the cross section is decreasing nearly proportional to exp(3t). However the slope is not strictly independent of photon energy at least for $|t| \lesssim 2.0(\mathrm{GeV/c})^2$. More and better data at large t-values are needed for all charge states to help decide if a universal t dependence does indeed exist in these reactions or not.

In order to extract an effective trajectory $\alpha(t)$, the cross section data between 4 and 18 GeV have been fitted for fixed t to the form $d\sigma/dt = \beta(t)(s-M^2)^{2\alpha(t)-2}$. The $\alpha(t)$-values determined from this fit are plotted in Fig. 3 versus t. It is clear that $\alpha(t)$ is not equal to 0, i.e. the process does show some shrinkage for t between 0 and $-2.0(\mathrm{GeV/c})^2$. However, the points at high t-values are not in agreement with the expectations based on dominant ω-exchange, which predicts a trajectory $\alpha(t) \simeq .45 + .9t$. A fit to the SLAC data alone, assuming a linear trajectory $\alpha(t) = \alpha_o + \alpha' t$, leads to $\alpha_o = (.19 \pm .03)$ and $\alpha' = (.27 \pm .04)$. The extrapolation of this trajectory also passes through the Caltech point at $t = -2.0(\mathrm{GeV/c})^2$. However, there is no reason to assume a linear trajectory in the presence of strong absorptive effects and the data cannot exclude a

trajectory which has a large slope at small t-values and a small slope at larger t-values.

Measurements of π^o photoproduction from the proton with linearly polarized photons have been carried out at SLAC by Anderson et al.(11). Data were taken at incident energies of 4, 6, and 10 GeV for t-values between -0.2 and -1.4(GeV/c)^2. The photons from the π^o decay were detected by a pair of shower counters in coincidence with the recoil proton. This avoids the severe background problem caused by the contribution from unpolarized photons above the polarized spike. The asymmetry A is usually defined as:

$$A = \frac{\sigma_\perp - \sigma_{||}}{\sigma_\perp + \sigma_{||}}$$

Here $\sigma_\perp$ is the measured cross section for photons polarized normal to the reaction plane, and $\sigma_{||}$ is the cross section with the photon polarization vector in the reaction plane. Stichel(14) has shown for $s \to \infty$ that $\sigma_\perp$ only receives contributions from natural parity exchanges, whereas only trajectories with unnatural parity can contribute to $\sigma_{||}$. The values for A, as determined in this experiment, are plotted in Fig. 4 together with the earlier results from CEA(15). The two sets of data are in good agreement within the errors. The data show a large positive asymmetry over the whole t-region, and at large t-values the data are nearly consistent with purely natural parity exchange. The only structure observed is a small dip

around $t = -0.5(\mathrm{GeV/c})^2$. However even in the dip region the cross section is dominated by natural parity exchanges. The solid curve is the same for all energies and is only intended to make it easier to estimate the energy dependence. The results are clearly consistent with no energy dependence of the asymmetry.

The differential cross section for π° production at 6 GeV is plotted versus t in Fig. 5 for $\sigma_\perp$ and $\sigma_{||}$ separately. There is a prominent dip in the natural parity part whereas the unnatural parity part of the cross section is structureless within the large error bars. The dashed line represents a calculation by Gault et al.(16), using the Michigan model, the solid line is from the contribution by Kramer(17) using a fixed pole for the ρ-exchange(18) and keeping a NWS-zero for the ω-contribution. The dotted line is a prediction by Worden(19) using NWS-zeros for both ρ and ω-exchange, but including strong absorption. Comparing these sets of models with the data we see that Kramer's model has some difficulty in reproducing the secondary maximum around $t = -0.8(\mathrm{GeV/c})^2$. However, the fits by Gault et al. and Worden are in good agreement with data.

At the Liverpool Conference, Osborne et al. reported the first results on $\gamma n \to \pi^\circ n$ at high energies. Two groups, Braunschweig et al.(20) at DESY and Browman et al.(21) at Cornell, have submitted new results on this reaction. Both groups measure the ratio $R = (\gamma d \to (\pi^\circ n)p)/(\gamma d \to (\pi^\circ p)n)$ by detecting the recoil hadron in coincidence with both photons from

the π^0 decay. In this ratio most of the uncertainties due to the deuteron structure will cancel.

In the DESY experiment(20) data were taken at 4 GeV for values of t between -.2 and -1.2$(GeV/c)^2$. The measured values of R are plotted in Fig. 6a together with the earlier data from CEA. The two experiments are in good agreement and show that R is near to 1 except in the region around t = -.5$(GeV/c)^2$. Here the asymmetry dips down to about .6 corresponding to a lower limit on the isoscalar amplitude of about 15%.

In the Cornell experiment(21) data were taken at incident photon energies of 4.8 and 8 GeV and for t-values between -.2$(GeV/c)^2$ and -1.28$(GeV/c)^2$. The results for the two energies are plotted in Fig. 6b. The 8 GeV data are consistently higher than the 4.8 GeV data, however this might still be due to some small systematic error.

Comparing the data from the two groups shows the Cornell data to be systematically low with respect to the DESY data, with the largest discrepancy in the forward direction. The estimated systematic uncertainties, which are not shown, amount to 10% for the DESY data and 15% for the Cornell data. Although this is not enough to make the experiments agree, we should keep in mind that these are difficult experiments and that the results are only preliminary.

Representative Regge fits by Worden(19) and by Gault et al.(16) are shown in Fig. 6b. Although the absolute values differ, both models predict a dip around t = -.5$(GeV/c)^2$,

in general agreement with the DESY data.

The isoscalar part of the π^o cross section can be estimated from $\pi^+ n \to \omega p$ using the VDM and time-reversal invariance.

$$\frac{d\sigma}{dt}(\gamma p \to \pi^o p) = \left(\frac{\alpha\pi}{\gamma_\omega^2}\right)\frac{1}{2}(1 - \rho_{00})\frac{d\sigma}{dt}(\omega p \to \pi^+ n)$$

The data for $\pi^+ n \to \omega p$ were taken from the experiment(22) by Bari, Bologna, Firenze, and Orsay at 5.08 and scaled to 6 GeV. The $\omega - \gamma$ coupling constant $\gamma_\omega^2/4\pi$ was set equal to 7. in accordance with the values on the photon mass shell(23). However, since the relative isoscalar and isovector contributions to the different amplitudes are not known, we can only set limits on R. The lower limit on R is given by assuming that the isoscalar and isovector contributions are all in the same amplitude:

$$R_{min} = \frac{(I_V - I_S)^2}{(I_V + I_S)^2}$$

The result is shown as the dashed line marked R_{min} in Fig. 6a. A more reasonable guess for R might be:

$$R = \frac{(I_V - 1/3\, I_S)^2 + 4/9\, I_S^2}{(I_V + 1/3\, I_S)^2 + 4/9\, I_S^2}$$

This is roughly what we would expect assuming ω and ρ exchange with the commonly used values for the coupling constants(24). This result is plotted as the dotted line marked R in Fig. 6a.

The first results on π^o photoproduction from a polarized target have been reported by Booth et al.(25) working at Daresbury. Data were taken at 4 GeV and the process was identified by detecting the recoil proton with a magnetic spectrometer in coincidence with both the photons from the π^o decay. The authors determine, from measurements with a carbon target, that 85% of the observed counting rate with the butanol target is due to π^o production on the proton. The polarization of the target varied between 22% and 30%. In Fig. 7 the observed target asymmetry, defined as:

$$T = (1/P)(N_{\uparrow} - N_{\downarrow})/(N_{\uparrow} + N_{\downarrow})$$

is plotted versus t. Here $N_{\uparrow}$ and $N_{\downarrow}$ are the π^o rates with the target polarized "up" and "down", and P is the degree of target polarization. The data are consistent with a rather small asymmetry at low t-values, increasing to an average asymmetry of about 80% for t between $-0.45(GeV/c)^2$ and $-0.85(GeV/c)^2$, and then decreasing with increasing |t| again. The data are in good agreement with Kramer's predictions(17). The models by Gault et al.(16) and Worden(19) are in disagreement with the data, especially at low t-values.

The data on π^o photoproduction indicate that the process is very similar for small and large t-values. In both cases the cross section is smooth and structureless, the asymmetry with polarized photons is approaching 1 and the observed asymmetry

from a polarized target is small. Also R, the ratio of π^o production on neutrons and protons is the largest here. This is in contrast to the behavior at intermediate t-values, i.e. for t in the range from $-.3(GeV/c)^2$ to $-.9(GeV/c)^2$. In this t-region the differential cross section, the asymmetry with polarized photons and the neutron to proton ratio have dips. Also the asymmetry from a polarized target is the largest here.

The observed quantities can be expressed in terms of s-channel helicity amplitudes, $H^{\rho}_{\lambda\mu}$. Here ρ is the photon helicity, λ the final and μ the initial baryon helicity. A convenient(26) nomenclature for the four independent amplitudes is: $H^1_{--} = F_1$, $H^1_{+-} = D$, $H^1_{-+} = N$, $H^1_{++} = F_2$. The observed quantities can be written in terms of these amplitudes as:

Differential cross section: $$\frac{d\sigma}{dt} = |N|^2 + |F_1|^2 + |F_2|^2 + |D|^2$$

Polarized photon asymmetry: $$A = \frac{2Re(F_1F_2^* - ND^*)}{d\sigma/dt}$$

Polarized target asymmetry: $$T = \frac{2Im(N^*F_1 + D\,F^*_2)}{d\sigma/dt}$$

In the forward region, since A is approaching 1, $F_1 \simeq F_2$ and $N \simeq -D$. From angular momentum conservation, all the amplitudes, with the exception of N, must go to zero at t=0. From the observation that the cross section has a dip in the forward direction(27) we conclude that N and therefore D must be small, and $F_1 \simeq F_2$ are the dominant amplitudes. This will lead to a small target asymmetry as observed.

At large t-values $A \simeq 1$ so again $F_1 \simeq F_2$ and $N \simeq -D$. By analogy, we would again assume that $F_1 \simeq F_2$ are the large amplitudes and $D \simeq -N$ small. This is supported by the following observation: Assume ω and ρ exchange and no absorption. In this case, $F_1 = F_2$ and $N = -D$. However, at large t-values absorption or cuts are very important. To a good approximation F_1 still remains equal to F_2 in the presence of absorption, however N is no longer equal to -D. Since experimentally A is close to 1, N and D must be the small and $F_1 \simeq F_2$ the large amplitudes. This would again predict a small target asymmetry in agreement with the data(25). The π^o data therefore seem to indicate that the single flip amplitudes are approximately equal and much larger than the non-flip and double-flip amplitudes everywhere except around $t \simeq -.5(\text{GeV/c})^2$. If this is true, then the asymmetry from a polarized target should be equal to the recoil proton polarization(28) everywhere except around $t = -.5(\text{GeV/c})^2$. The observation that π^o photoproduction is dominated by the two

single flip amplitudes is consistent with the assumption that ω-exchange in the t-channel conserves the s-channel nucleon helicity.

η-Photoproduction

New data on η-photoproduction has been submitted to this conference by DeWire and collaborators(29) at Cornell. Data were taken at 4 GeV and 8 GeV for values of the momentum transfer squared between $-0.3(\text{GeV/c})^2$ to $-0.8(\text{GeV/c})^2$. In the experiment, both gamma rays from the η decay were detected in coincidence with the recoil proton. This eliminates most of the background observed in the earlier experiments where either the recoil proton or the two photons were detected. The cross section multiplied by $(s-m_p^2)^2$ is plotted in Fig. 8 versus t. Also shown are the earlier data from DESY(1) and SLAC(1). The new Cornell data are in good agreement with the earlier data, and they seem to prefer a slight shrinkage in accordance with the π^o data. The predictions by Worden(19) and by Gault et al.(16) are in reasonable agreement with the data. However a conventional Argonne model without strong absorption will predict a dip at $t = -.5(\text{GeV/c})^2$ in disagreement with the data.

$\gamma p \rightarrow \pi^+ n$

The measurements of $\gamma p \rightarrow \pi^+ n$ with linearly polarized photons have been extended up to 12 GeV by a SLAC-MIT collaboration(30). The low duty cycle of the SLAC accelerator made a coincidence experiment impossible and the process was identified by detecting only the π^+ in the SLAC 20(GeV/c) spectrometer. However, in this

case the photon energy is not uniquely determined and pions originating from photons in the polarized spike will only show up as a small step on a smoothly varying background. This makes it a very difficult experiment and puts stringent requirements on the stability of the beam and the detection apparatus. The measured asymmetry is plotted together with the older data at lower energy in Fig. 9a. The data show a large positive asymmetry, i.e. the reaction proceeds through positive parity exchange as observed at lower energies. In fact, a comparison between the new data and the older data shows that the observed asymmetry is consistent with being independent of energy between 3 and 12 GeV. Regge fits to the data are shown in Fig. 9b. Both the Michigan(24), and the Argonne(19) model give good fits to the data at small t-values, but fail to reproduce the large asymmetry at larger values of $|t|$.

The asymmetry in π^+ photoproduction from a polarized proton target has been measured at SLAC by a Berkeley-SLAC collaboration(31). The experimental apparatus, with the exception of the target, was similar to the one used by the Richter Group in the earlier photoproduction experiments. A butanol polarized-proton target was used and the process was identified by measuring only the π^+ yield. Typically 75% of the observed pions came from interactions with protons bound in carbon, and only 25% from the free protons.

Data were collected at 5 and 16 GeV for t between -.012 and $-1.0(\text{GeV/c})^2$ and the results are plotted versus t in Fig. 10.

The Regge fits to the data by Worden(19) and Kramer(17) are also shown. The observed asymmetry is large and negative at both energies. The data seems to show some energy dependence, although it is possible to find a single curve with an acceptable chi-square for both energies.

Models

The present data are still not sufficiently restrictive to distinguish between the two classes of models, i.e. to decide if NWS-zeros are present in the pole amplitude or not. However, we can compare the amplitudes evaluated from these models with the results from finite energy sum rule (FESR) calculations. This has been done by Worden(19). As an input to the FESR integral, he used the amplitudes from a recent dispersion calculation by Schwela and Weizel(32) up to an incident photon energy of 500 MeV. At higher energies, the phase shift analyses by Walker(33) were used. The sum rules are written in terms of the amplitudes $W_\lambda^\pm$. The $\pm$ superscripts label the exchanged parity and $\lambda = 0$ or 1 denotes the units of s-channel helicity flip of the nucleon. These amplitudes are related asymptotically to the s-channel helicity amplitudes as follows:

$$W_0^+ = F_1 + F_2$$

$$W_0^- = F_1 - F_2$$

$$W_1^+ = N - D$$

$$W_1^- = N + D$$

Worden compared the results of the FESR calculation with the amplitudes from four different Regge cut models, which all gave acceptable fits to the data. The results are shown in Fig. 11 for a model with NWS-zeros but strong absorption, and in Fig. 12 for the Michigan model(24). In the figure each column corresponds to fixed isospin and G-parity. The sum rules are labeled by the exchanged poles (and absorptive cuts) and by the s-channel helicity structure. For example, (π A_2,W_1^+), denotes the sum rule for the positive parity, nucleon spin flip amplitude W_1^+, to which A_2 plus cuts as well as pion cuts may contribute. There is good agreement (Fig. 11) between the FESR calculation and the model incorporating NWS-zeros. The Michigan model does fit the FESR for most amplitudes. However, as shown in Fig. 12 the model does not fit the sum rules with ρ or ω quantum numbers. The most striking disagreement is in the amplitude which dominates π^0 photoproduction, W_0^+. Since the relative sign of the ω,ρ amplitudes is fixed by VDM and the absolute sign of the ρ amplitude by the π^+/π^- ratio, this discrepancy cannot be cured by changing the sign of the ω amplitude. The strong absorption, which causes the sign of the full amplitude to be different from the sign of the pole contribution, is necessary in order to reproduce the dip at $t = -0.5(\mathrm{GeV/c})^2$.

Conclusion: On the whole both classes of models achieve reasonable fits to the photoproduction data. The Michigan model is in some disagreement with FESR computations, whereas models with NWS-zeros satisfy FESR. It would be more satisfying if the

models could be separated on the basis of high energy measurements only. This should be possible by doing more complex experiments involving polarized beam and target and thus being able to determine the amplitudes directly as emphasized by Berger and Fox(26).

$\underline{\gamma p \rightarrow \pi\Delta}$

The reaction $\gamma p \rightarrow \pi^- \Delta^{++}$ has previously been studied in bubble chambers(34,35) up to 6 GeV and with counter techniques(36) between 5 and 16 GeV. New data on this reaction are reported by two groups(37,38).

In a collaboration between SLAC, Tel-Aviv University and the Weizmann Institute(37) the $\pi^- \Delta^{++}$ cross section has been measured between 4.3 and 7.5 GeV using the SLAC-40" chamber in the positron annihilation beam. The qualitative features of the data can be explained by the gauge invariant extension of the one pion exchange model (GIOPE) by Stichel and Scholz(39) when absorptive corrections are included. However, quantitatively the data show that other exchanges besides pion exchange must be present.

The SLAC-Berkeley-Tufts (SBT) collaboration(38), using the fairly monochromatic and highly polarized photon beam from back scattering of laser light on electrons, has measured the cross section for $\gamma p \rightarrow \pi^- \Delta^{++}$ at 2.8 and 4.7 GeV. In this experiment the contributions from natural and unnatural parity exchange can be separated. The measured asymmetry A is plotted in Fig. 13 versus $\sqrt{-t}$. Pure pion exchange would correspond to A = -1 in disagreement with the experiment. However the observed asymmetry

is in qualitative agreement with a prediction by Harari(2). The argument leading to this prediction is straight forward. The observed cross section is the sum of the natural and unnatural parity exchanges. i.e. $\sigma = \sigma_{\perp} + \sigma_{\parallel}$ and furthermore from conservation of angular momentum $\sigma_{\perp} = \sigma_{\parallel}$ at t=0. The $\pi^{-}\Delta^{++}$ cross section dips sharply at $|t| \lesssim m_{\pi}^2$ and since only π exchange can cause such a rapid variation for $|t| \lesssim m_{\pi}^2$ this dip will be in the $\sigma_{\parallel}$ part whereas $\sigma_{\perp}$ will remain nearly constant. Therefore, at small values of t, $\sigma_{\parallel}$ will be larger than $\sigma_{\perp}$ corresponding to a negative asymmetry as observed. A SLAC-MIT collaboration(31) has measured the reaction $\gamma p \rightarrow \pi^{+}\Delta^{o}$ with polarized photons at 12 GeV. The results for the asymmetry are plotted in Fig. 13. The data seem to be slightly positive at larger t, corresponding to more natural than unnatural parity exchange. The cross section for $\gamma p \rightarrow \pi^{+}\Delta^{o}$ is not well known at small t-values, and we can therefore not predict the asymmetry with any confidence.

An interesting result related to $\pi^{-}\Delta^{++}$ production near threshold has recently been obtained by Lüke and Söding(40). Fig. 14 gives the energy dependence of $\sigma_{\pi^{-}\Delta^{++}}$. One of the main questions here was whether the rapid rise above threshold is caused by the contact graph, or comes from the P_{11} (1470) excitation in the s-channel. A detailed analysis of the DESY-Bubble chamber data(34) showed that P_{11}(1470) excitation is weak and that the production and decay characteristics of the Δ^{++} are quantitatively explained by the D_{13} amplitude due to the contact term. The decisive piece of information came from the

density matrix elements in the helicity system. Pure P_{11} (1470) excitation leads to $\rho^H_{33} = \mathrm{Re}\ \rho^H_{3-1} = \mathrm{Re}\ \rho^H_{31} = 0$ in strong disagreement with the data (see Fig. 15) whereas the GIOPE(39) prediction is in agreement with the data. Also the contribution from the D_{13} (1520) resonance is small, in particular it fails to explain the rapid raise of the cross section near threshold.

Assuming only I=1 exchange, the ratio of $\left[(\gamma p \to \pi^+\Delta^0) + (\gamma n \to \pi^+\Delta^-)\right] / (\gamma p \to \pi^+\Delta^0)$ should equal 4. Experimentally(41) the observed ratio is more like 3 or less for $|t|$ larger than $0.1(\mathrm{GeV/c})^2$, i.e. I=2 exchanges contribute at least 16% to the amplitude. Several authors(42) including the experimenters(41) have attributed this large I=2 amplitude to double exchanges. In this case the I=2 amplitudes should become increasingly important at lower energies. Unfortunately there are no measurements at lower energies.

$\pi^- p \to \rho^0 n$

The Vector Dominance Model (VDM) directly relates charged pion photoproduction to the reaction $\pi^- p \to V^0 n$, where V^0 is a mixture of ρ, ω, and Φ. In the sum of π^+ and π^- photoproduction the isoscalar-isovector interference term cancels and the isoscalar term only makes a contribution of a few percent and can be neglected. The VDM then predicts:

$$\frac{1}{2}\left[\frac{d\sigma}{dt}(\gamma p \to \pi^+ n) + \frac{d\sigma}{dt}(\gamma n \to \pi^- p)\right] = \left(\frac{|k_\gamma|^2}{|k_\pi|^2}\right)_{c.m.} \cdot \left(\frac{\pi\alpha}{\gamma_\rho^2}\right) \cdot \left[\rho^H_{11} \cdot \frac{d\sigma}{dt}(\pi^- p \to \rho^0 n)\right]$$

Here ρ^H_{11} is the density matrix element in the helicity frame which

projects out the transversely polarized ρ's. By replacing ρ^H_{11} with $(\rho^H_{11} + \rho^H_{1-1})$ or $(\rho^H_{11} - \rho^H_{1+1})$ the cross section corresponding to photons polarized normal to or parallel to the reaction plane can be projected out.

At the time of the last photon conference(1,3) the agreement for the unpolarized cross section was quite good, whereas the relationship involving the polarized data was not satisfied. However this could, at least partially, be blamed on the poorly known density matrix elements, in particular the ρ^H_{1-1} element. Furthermore, due to a lack of rho data, no test was possible in the interesting region around $|t| \simeq m_\pi^2$.

Data on the reaction $\pi^- p \to \rho^o n$ for $|t| \lesssim .3(\text{GeV/c})^2$ are now available from an experiment at SLAC by Bulos et al.(43). The experiment was done for an incident pion momentum of 15 GeV/c using a wire spark chamber spectrometer.

The authors fitted the $\pi^+\pi^-$ data assuming s and p wave. They conclude from the quality of the fit that higher partial waves are not present, but they do find evidence for a strong s-wave. In order to extract the ρ^H_{11} element the s-wave contribution must be known. Independent information on ρ^S_{00} can be obtained from the existing data(44) on $\pi^- p \to \pi^o\pi^o n$ assuming this reaction to be a pure s-wave. Unfortunately the $\pi^o\pi^o$ data are not sufficient to determine the shape of the differential cross section and the shape as predicted from an absorptive one pion exchange model was used. The values of ρ^H_{0S} and ρ^H_{11} determined from $\pi^- p \to \pi^o\pi^o n$ are consistent with the limits on ρ^H_{0S} and $\rho^H_{\|}$ imposed by the Schwartz inequalities.

The density matrix elements for the ρ^o in the helicity frame is shown in Fig. 16. Note the strong peaking of ρ^H_{11} for $|t| \lesssim m_\pi^2$ whereas ρ^H_{1-1} remains rather constant. The authors note that a 30% decrease in the s-wave cross section would result in a 30% increase in the transverse ρ cross section for $.1 \lesssim (|t|)^{1/2} \lesssim .2(\text{GeV/c})^2$.

Fig. 17 shows a detailed comparison between these data and the photoproduction data using $\gamma_\rho^2/4\pi = .5$. For this comparison the polarized photon data(45) at lower energies were combined with the unpolarized cross section data(46) at 16 GeV. In the case of the unpolarized cross section plotted in Fig. 17a the agreement is reasonable at large t, but the strong interaction data falls off more steeply at small t than the photoproductions data. In Fig. 17b the cross sections corresponding to photons polarized normal to the reaction plane are compared. Since $(\rho^H_{11} + \rho^H_{1-1})$ is invariant under rotations normal to the reaction plane this comparison is independent of frame ambiguities caused by the finite ρ mass. Except for the extreme forward direction, the data have a similar shape but the strong interaction data are roughly a factor of 2 below the photon data. In Fig. 17c the data corresponding to photons polarized in the reaction plane are compared. The agreement is excellent. In Fig. 17d the ratio of ρ_{1-1}/ρ_{11} is compared. This ratio is independent of the normalization of the two data sets as well as the value of $\gamma_\rho^2/4\pi$.

The predictions from the VDM are well fulfilled for $|t| \lesssim 2m_\pi^2$, but there is some disagreement at larger t-values. It

is clear from this comparison that the ρ data display the same structure as observed in single pion production, although there are discrepancies between the strong and electromagnetic data which cannot be resolved by altering the value of $\gamma_\rho^2/4\pi$. However we should bear in mind that the error shown in Fig. 17 are only the statistical error. In addition to these errors we have possible errors due to the assumed ρ-shape, the separation of s and p wave and uncertainties in $\gamma_\rho^2/4\pi$. Furthermore, ρ-ω interference effects in the observed $\pi^+\pi^-$ spectrum have been neglected.

PHOTON INDUCED INCLUSIVE REACTIONS

Although the production of multiparticle states has been subject to much work(47), both from the experimental and the theoretical side, our understanding of such processes has progressed rather slowly. This can be blamed to some extent on the variety and complexity of the final states, which makes it difficult to single out the relevant kinematical quantities of the problem.

The situation changed abruptly when it became clear that reactions of the type a + b → c + "anything", where we measure only the properties of one particle and sum over all the others, still contain interesting physics. These inclusive(48) reactions are quasi two-body reactions and are therefore completely determined by the momentum $\underset{\sim}{p}$ and the mass μ of the detected particle c together with s, the total center of mass energy squared. It is common to use these variables to define a Lorentz

invariant cross section for an inclusive reaction as:

$$d^3\sigma = \left(\frac{d^3p}{E}\right) \cdot \rho\,(p,s)$$

Here E is the energy and ρ the distribution function of the particle c.

The energy and momentum dependence of the distribution function have been studied for several reactions involving hadrons(47) and in five papers submitted to this conference corresponding data using photons has become available. The kinematical regions covered by these experiments are listed in Table 1. A comparison between the photon data and the hadron data will show if the photon behaves like a hadron in many-body reactions, as it seems to do in two-body process. If the photon indeed behaves like a hadron it can be used as an extra hadron to check various predictions like scaling or projectile independence(49). Furthermore, the use of a polarized photon beam gives us the first opportunity to learn something about spin correlations(50) in inclusive reactions.

The SLAC Streamer Chamber Group(51) has measured the cross section for $\gamma + p \rightarrow \pi^- +$ "anything" in the target fragmentation region. In this experiment a Bremsstrahlung beam with an end-point energy of 18 GeV was passed through a pressurized hydrogen gas target located inside the chamber. The 3, 5, 7, and 9-prong topologies were used and the events were binned into four energy intervals between 5 and 18 GeV. All negative tracks were

used and no attempts were made to exclude K^- production. However, the authors estimate this to cause an error of only 5%. The main difficulty in analyzing the experiment is due to the continuous Bremsstrahlung spectrum, which makes it impossible to determine the photon energy for an event with missing neutrals. The authors discuss how to correct for this in their paper.

The SLAC-Berkeley-Tufts (SBT) collaboration(52) working with the SLAC 82" bubble chamber, avoids this difficulty by using the highly polarized and relatively monochromatic photon beam resulting from the back scattering of laser light on a high energy electron beam. This group reports results for $\gamma + p \rightarrow \pi^- +$ "anything" at 2.8, 4.7, and 9.3 GeV. Here also the 3, 5, 7, and 9-prong topologies were used. Events with strange particles were excluded from the analysis.

Using the DESY Streamer Chamber, the Aachen-Hamburg Heidelberg-Munich collaboration(53) has measured the cross section for $\gamma + p \rightarrow \pi^- +$ "anything" between 3 and 6.5 GeV using a tagged photon beam with a width of 60 MeV. The 3, 5, and 7-prong events (excluding elastic ρ-events) were used in the analysis. The K^- events were not separated but again the authors estimate this to be only a 5% correction.

Whereas these experiments only have information on the π^--distributions, the experiment by Boyarski and collaborators(54) also measures the distributions for π^+, K^+, and K^- in addition to the π^--distribution. The experiment was done using the SLAC 20 GeV/c spectrometer with the same detection

equipment as used in the earlier photoproduction experiments by the Richter group. By subtracting yield curves, usually taken at end-point energies of 19 and 17 GeV, data can be quoted for a fixed photon energy of (18 ± 1) GeV. Data were mainly collected at large values of $p_\perp$ and mainly positive values of x, where x is defined as $x = 2p_{\parallel}^{c.m.}/\sqrt{s}$. The available data points are shown in Fig. 18.

Gladding et al.(55) using a tagged photon beam at CEA have measured the spectrum of recoil protons for incident photon energies between 2.4 and 5 GeV. The missing mass varied between .5 and 1.1 GeV and the t-value for the proton from $-.15(GeV/c)^2$ to $-1.0(GeV/c)^2$.

The general features of an inclusive reaction are shown in Fig. 19. The Bubble Chamber data at 9.3 GeV are plotted versus x and $p_{\parallel}$ in the laboratory. The solid lines represent the phase space boundaries and the dotted curve indicates a constant transverse momentum. The few events outside the phase space boundary is caused by the finite width of the photon beam. On the plot the number of events per bin are written as a number up to 9; from there on letters are used, i.e. A stands for 10 events, V for 31 or more. It is clear from the plot that the events cluster along lines of small transverse momenta. Furthermore, there is a clustering of events for small x centered around x=0. These qualitative features agree well with what is observed in hadronic reactions.

Multiplicities and Topological Cross Sections

The various topological cross sections are plotted versus s in Fig. 20. It is seen that the cross section for 3-prong events peak at low energies and have already decreased substantially at 9.3 GeV. The cross section for 5-prong events is rapidly rising at low energies and seem to have reached a broad maximum around $s \simeq 20\ GeV^2$. The 7-prong cross section increases monotonically in this energy range and the 9-prong cross section is only measurable at 9.3 GeV. The cross section for strange particle production is plotted in the same figure and is roughly 10% of the total cross section. The same low ratio of kaons to pions is also observed in hadron initiated reactions. There it seems to persist even at the center of mass energies available at the ISR(56).

The average multiplicity minus the charge in the initial state is plotted versus $\ell n(s)$ in Fig. 21. The data are consistent with a straight line, i.e. the average multiplicity seems to increase proportional to $\ell n(s)$ as predicted by most models. The average multiplicity in hadronic reactions also increases proportional to $\ell n(s)$ as seen in Fig. 21 for πp and pp reactions. The "net" charged multiplicity is higher in photon than in purely hadronic reactions by about 1. However, the total cross section remains nearly constant despite the rapid increase with energy of the topological cross sections with high multiplicities. We would therefore expect the individual topological cross sections with low multiplicity to start to

decrease at a much lower energy in photon-induced reactions. This is shown more clearly in Fig. 22 where the 3-prong cross section for γp and the 4-prong cross section for $\pi^- p$ is plotted versus s. The 3-prong cross section has already decreased substantially and a measurement at 100 GeV at NAL would indeed help decide if the topological cross sections drop as low as required by the multiperipheral models or stay up as permitted by the limiting fragmentation models.

The Transverse Momentum Distribution

An important feature of the inclusive reactions is the distribution of the transverse momenta, which seems to be limited to a few hundred MeV/c nearly independent of energy. This is shown in Fig. 23 where the SLAC streamer chamber data(51), integrated over small longitudinal momenta, are plotted versus $p_\perp^2$ for events in the target fragmentation region. The distribution is seen to be nearly independent of energy between 5 and 18 GeV and the bulk of the events have transverse momenta less than about 300 MeV/c.

In Fig.24 the cross section for $\gamma + p \to \pi^- +$ "anything" as measured by the DESY streamer chamber collaboration(52) is plotted versus $p_\perp^2$ for photon energies between 3 and 6.3 GeV. Plotted is the cross section integrated over all longitudinal momenta less than .5(GeV/c). It is clear that even between 3 and 6 GeV the $p_\perp^2$ distributions is constant independent of energy. Chen et al.(57) have collected data from the following reactions:

(a) $\pi^+ + p \rightarrow \pi^- +$ "anything" at 7 GeV/c

(b) $p + p \rightarrow \pi^- +$ "anything" at 28.5 GeV/c

(c) $K^+ + p \rightarrow \pi^- +$ "anything" at 12.7 GeV/c

(d) $\pi^- + p \rightarrow \pi^- +$ "anything" at 24.8 GeV/c

The various cross sections for these reactions normalized to the asymptotic values of their total cross sections are also plotted in Fig. 24. Based on arguments by Mueller(58), the inclusive reaction a + b → c + "anything" can be related, through a generalized optical theorem to the imaginary part of the three particle $a\bar{c}b \rightarrow a\bar{c}b$ scattering amplitude. Using duality Chan et al.(59) argue that when the quantum numbers of the $a\bar{c}b$ system are exotic, limiting behavior should occur at a relatively low energy. Of the shown reactions $p + p \rightarrow \pi^- +$ "anything", $K^+ + p \rightarrow \pi^- +$ "anything" and $\pi^+ + p \rightarrow \pi^- +$ "anything" are exotic in this sense while, $\pi^- + p \rightarrow \pi^- +$ "anything" is not. The exotic reactions seem to cluster together whereas the cross section for the non-exotic reaction is about 50% higher. The photon data seem to fall in between these two groups, however remember that these data are normalized to the total γp cross section between 3 to 6.3 GeV. If we normalize the photon data to the asymptotic cross section, then the photon points will move upward by $\sim 30\%$ into good agreement with the non-exotic $\pi^- + p \rightarrow \pi^- +$ "anything". We

conclude that the photon, at least in this process, behaves like a hadron.

The next question is: "What happens at large $p_\perp^2$ and do different secondaries have the same behavior as a function of $p_\perp^2$?" The invariant cross sections as measured by Boyarski et al.(54) are plotted versus $p_\perp^2$ in Fig. 25 for x = .2. The π^+ and π^- distributions are very similar over the whole range of transverse momenta, whereas the K^+ cross section is about a factor of two larger than the K^- cross section. At small |t|-values the pion yield decreases proportional to $e^{-8p_\perp^2}$ as compared to $e^{-4.4p_\perp^2}$ for the kaons. This corresponds to an average transverse momentum for a kaon about twice that for a pion. Note that when plotted against $p_\perp^2$, the ratio of pions to kaons is about 15 at small values of $p_\perp^2$ and that the slope is continually changing. In Fig. 26 the π/K ratios are plotted versus $m_\perp^2 = (p_\perp^2 + \mu^2)$, the transverse mass squared(60). Here μ is the mass of the detected particle. Plotted against this variable the π/K ratio is not very large even at small values of $m_\perp^2$ and seems to approach 1 at large values of $m_\perp^2$.

Since the cross section depends so differently on the longitudinal and transverse momenta, it has been speculated that the cross section might be factorized into a product of two functions, one depending only on the transverse momentum, the other only on the longitudinal momentum. Whereas this approach has met with some success in $p+p \rightarrow \pi^- +$"anything"(61), it fails in other reactions(62). To look for the same feature in

$\gamma + p \to \pi^-$ "anything", the cross section as measured in the Bubble Chamber experiment is plotted versus $p_\perp^2$ for different values of x in Fig. 27. The solid lines are just an eyeball fit to the distribution for $0 \leqslant x \leqslant .1$ normalized at small values of $p_\perp^2$. It is clear that this is not a good representation of all the data, i.e. the transverse distribution does indeed depend on the longitudinal momentum.

Scaling and Limiting Behavior

In general the structure function depends on the momentum of the detected particle as well as the total center of mass energy squared. However, several models predict a very simple form for the structure function at high energies. In fact, as is well known, this already follows from the multi-peripheral model of Amati, Bertocchi, Fubini, Stanghellini, and Tonin(63). Expressed in terms of the rapidity variable $y = \ln((E+p_\parallel)/m_\perp)$, deTar(64) has written these predictions as follows:

(1) For events in the target fragmentation region i.e. $y \leqslant \Delta$.

$$\rho(p_\perp, y, s) \xrightarrow[s\to\infty]{} \rho_T(p_\perp, y)$$

Furthermore the distribution of the events should be independent of the nature of the projectile in this region.

(2) For events in the projectile fragmentation region:

$(y_{max} - y) \leqslant \Delta$

$$\rho(p_\perp, y, s) \xrightarrow[s\to\infty]{} \rho_p(p_\perp, y)$$

(3) As the energy increases the width of the distribution will increase proportional to $\ell n(s)$ and a plateau should develop.

$$\rho(p_\perp, y, s) \xrightarrow[s \to \infty]{} \rho_{pI}(p_\perp)$$

i.e. events in this region are independent of both the target and the projectile.

Similar predictions has been made by Feynman(48) in terms of $p_\perp$ and $x = 2p_{||}^{c.m.}/\sqrt{s}$. He predicts:

$$\left(\frac{2E}{\pi\sqrt{s}}\right)\frac{d^2\sigma}{dx \cdot dp_\perp^2} = \rho(x, p_\perp^2, s) \xrightarrow[s \to \infty]{} \rho_\infty(x, p_\perp^2)$$

Furthermore, if scaling occurs then the structure function for events in the target or beam fragmentation region should satisfy the relation $\rho(x,t) = (1-|x|)^{1-2\alpha|t|}$. Here $\alpha(t)$ represents the highest trajectory which can carry off the quantum numbers at the $\gamma \to \pi$ or the p-π vertex.

Based on the droplet model, Benecke, Chan, Yang and Yen(65) suggested that the spectra of low energy particles, that is particles associated with the target, should become independent of energy when viewed in the laboratory frame. They also predicted limiting behavior in the projectile fragmentation region when viewed in the frame of the projectile.

All these predictions are strictly true only at asymptotic energies, and there they give the same results. At lower energies the predictions differ, and one must test to see if any

of them are valid at present energies. This has been done by the SBT collaboration(52), who have plotted their data in different frames. They found 10-30% deviations from scaling both in the rapidity frame and in the laboratory frame. However using Feynman's variable x, scaling seems to be valid for large values of |x|. In Fig. 28, F(x), defined as $F(x) = \int_0^\infty \left(\frac{2E}{\pi\sqrt{s}}\right) \cdot \frac{d^2}{dx dp_\perp^2}\, dp_\perp^2$, is plotted versus x for incident energies of 2.8, 4.7 and 9.3 GeV. The agreement between the different energies is quite good, especially for events in the target fragmentation region $x \ll -.1$ or in the beam fragmentation region i.e. $x \gg .1$. To be able to judge the energy dependence better, F(x) is plotted versus s for different cuts on x in Fig. 29. The data are remarkably independent of energy in the beam or target fragmentation region, whereas for x=0 the cross section does depend upon the incident energy. To see what happens around x=0, i.e. if we also have pionization, the data are plotted in Fig. 30 against y. In this variable we should see a flat top develop with increasing energy. No flat top is seen, and the data are compatible with a Gaussian having a width which increases logarithmically with energy. This is not very surprising since no such flat top has been seen in hadron reactions at higher energies.

Since scaling seems to be nearly valid at large values of |x| the distribution function should show the expected Regge behavior. This is shown in Fig. 31 where the values for $\alpha(t)$ is plotted versus t. The values for $\alpha(t)$ in the target

fragmentation region are quite low compared to the leading Regge trajectory which is the Δ, but similar to those obtained from other inclusive experiments(66). The observed trajectory in the forward direction is compatible with a Regge trajectory of slope 1 GeV^{-2} and intercept of 0. Note that such a strong shrinkage is not seen in forward two-body reactions.

All the predictions of scaling and limiting behavior are derived for high energies, and it is important to estimate how these limits are being approached. This has been done recently by Abarbanel(67) and by Chan et al.(49) using the observation by Mueller(48) that the total cross section for $a + b \to c +$ "anything" can be related to the elastic 3-body scattering amplitude $a + b + \bar{c} \to a + b + \bar{c}$. As sketched in Fig. 32 this follows intuitively from writing $a + b \to c +$ "anything" as $a + b + \bar{c} \to$ "anything", i.e. the total cross section initiated by the 3-body collisions $a + b + \bar{c}$. From a "generalized" optical theorem the imaginary part of this elastic amplitude is then related to the total cross section. This observation provides a very convenient language for the inclusive reactions and allows us to introduce the Regge picture, which has been reasonably successful in dealing with two-body processes. One can distinguish between two different Regge limits for this amplitude as also shown in Fig. 32. In the first limit the mass of one of the two subsystems, i.e. $(a\ \bar{c})$ in the projectile fragmentation region or $(b\ \bar{c})$ in the target fragmentation region is kept small and constant as the energy increases. Assume now that the

amplitude is dominated by the usual Regge singularities(59), the Pomeranchuk trajectory with $\alpha_P(0)=1$ and the meson trajectories with $\alpha_m(0) \simeq .5$. In this case the cross section will approach the limiting behavior as $A(p,p_\perp) + B(p,p_\perp) \cdot 1/\sqrt{s}$. This is shown in Fig. 33 where the cross section(52), integrated over all transverse momenta, is plotted versus $1/\sqrt{s}$ for different values of $p_\parallel$. Since there are only 3 points available, it is impossible to make a strong statement, but the data are certainly consistent with a straight line. Note that for events in the target fragmentation region the curve is going through 0, corresponding to a negligible Pomeron exchange.

The second limit in Fig. 32 corresponds to the pionization limit. In this case we require both subenergies (a $\bar{c}$) and (b $\bar{c}$) to be large; and by the same argument as above(59,67), we would expect to approach this limit as $1/(s)^{1/4}$. Therefore this limit will be reached very slowly, so perhaps it is understandable that we do not see any sign of pionization at these energies.

Comparison with the Hadronic Reactions

According to the multipheripheral model(63) the distribution of a particle c in the target fragmentation region is independent of the nature of the incident particle--i.e. two different reactions $a_1 + b \rightarrow c + x$ and $a_2 + b \rightarrow c + x$ will be related formally as:

$$\frac{1}{\sigma_T(a_1 b)} \cdot \rho(b \xrightarrow{a_1} c) = \frac{1}{\sigma_T(a_2 b)} \rho(b \xrightarrow{a_2} c)$$

Here $\sigma_T(a_1 b)$ and $\sigma_T(a_2 b)$ are the asymptotic values for the total cross sections. This relationship is valid in the scaling region under the assumption that the Pomeron factorizes. The DESY data(53), integrated over transverse momenta, are plotted in Fig. 34 versus the longitudinal momentum in the laboratory. The various curves correspond to different hadronic reactions(57), as labeled on the figure. Note that the reactions where $(ab\bar{c})$ are exotic tend to cluster together about 50% lower than $\pi^- + p \rightarrow \pi^- +$"anything" which is nonexotic. The photon data seem to be bracketed by these two groups. However remember that the photon data are again normalized to the total γp cross section between 3 and 6.3 GeV, whereas the strong interaction data are normalized to the asymptotic values.

In Fig. 35, the Bubble Chamber data at 9.3 GeV are compared with $\pi^+ + p \rightarrow \pi^- +$"anything" and $\pi^- + p \rightarrow \pi^- +$"anything" both(68) at 18.5 GeV. In this comparison the values for the total cross section at the corresponding energies have been used. The agreement between $\pi^- + p \rightarrow \pi^- +$"anything" and $\gamma + p \rightarrow \pi^- +$ "anything" is rather good for events in the target fragmentation region. This might be taken as evidence for factorization of the Pomeron, since the data are scaling in this region.

Swanson and collaborators(69) have compared $\gamma + p \rightarrow \pi^- +$"anything" at an average energy of 10.5 GeV with $K^+ + p \rightarrow \pi^- +$"anything" at 11.8 GeV. They compare the cross sections, normalized to asymptotic values of the respective total

cross sections, and integrated over all longitudinal momenta less than +.5 GeV/c and over all transverse momenta. The value for the photon induced cross section is (.45 ± .06) as compared to (.17 ± .02) for the $K^+ + p \rightarrow \pi^- +$ "anything" case.

Relative Particle Yields

In Fig. 36 the structure function as measured by Boyarski et al.(54) at 18 GeV is plotted against x for various values of the transverse momentum. The cross sections for pion and kaon production are becoming more similar with increasing transverse momentum, independent of x. Also the ratios π^+/π^- and K^+/K^- are independent of $P_\perp$ over the present range in x-values. Fig. 37 shows the π^+/π^- ratio together with the K^+/K^- ratio plotted versus x for $p_\perp$ = 1 GeV/c. The corresponding missing mass for kaons are shown in the parentheses. The π^+/π^- ratio is close to 1 except at the largest x-values where it seems to approach 2. The K^+/K^- ratio is consistent with 2 from x=0 to about x=.5. For larger values of x, corresponding to events in the projectile fragmentation region, the K^+/K^- ratio is rapidly increasing with x reaching a value of 5 at x=.78. The recoiling mass in the case of K^- has the quantum numbers of an exotic particle. In the absence of exotic states the threshold for K^- production would be at 1433 MeV ($m_K + m_p$) as compared with 1116 MeV(Λ) in the case of K^+ production. The lowest missing mass observed in this experiment, however, is at 2.3 GeV which is well above the threshold.

In the scaling limit, the Mueller model would predict the K^+/K^- ratio to be 1 for events in the projectile fragmentation region. To explain the observed K^+/K^- ratio we have to assume that the process is very far from the scaling limit and that trajectories with opposite charge conjugation add in the K^+ case and subtract in the K^- case. It would therefore be very interesting to measure the yield of kaons at lower energies to see if scaling is indeed badly violated in the projectile fragmentation region, in apparent disagreement with the results on $\gamma + p \rightarrow \pi^- +$"anything".

On the basis of a simple Drell model the K^+/K^- ratio is given by $\sigma_T(K^-p)/\sigma_T(K^+p)$. The ratio of these cross sections is about 2 at these values of missing mass. However since we are rather far off the mass shell at this value of $p_\perp^2$ it is not a priori clear that this is a meaningful comparison.

Asymmetry with Polarized Photons

To search for a correlation between the azimuthal angle of a pion and the polarization vector φ of the incident photon the SBT collaboration have plotted their 9.3 GeV data integrated over all transverse momenta as a function of φ. Here φ is defined as $\varphi = \tan^{-1}\left(\frac{(\hat{K} \times \underline{\epsilon})p_\perp}{\epsilon \cdot p_\perp}\right)$ and $\hat{K}$ is a unit vector along the direction of the incident photon. The results with the elastic ρ removed are shown in Fig. 39 for different values of x. They find no statistically significant correlations between the π^- and the polarization vector for $x \lesssim .3$. However, some correlation might be present at larger values of x.

Abarbanel and Gross(50) interpret the lack of any correlation in the target fragmentation region as proof that the residues of the photon and target vertices factorize.

Conclusions

Although much more data are needed, especially for kaons at all energies and for pions above 10 GeV, it is tempting to summarize the results of these first experiments as follows:

(1) Photons behave like hadrons also in inclusive reactions.

(2) The π^--distribution from $\gamma + p \to \pi^- +$"anything" shows evidence for scaling in the target and beam fragmentation region already at 9 GeV.

(3) In the laboratory frame, the cross section $d\sigma/dp_{\parallel}^{L}$ approaches the scaling limit as $1/\sqrt{s}$.

(4) The average transverse momentum for a kaon is twice that of a pion.

(5) The K^+/K^- ratio is very different from 1 in the projectile fragmentation region.

ACKNOWLEDGEMENTS

I wish to thank Prof. F. Gilman and Prof. A. Schwimmer for many discussions. I'm very indebted to Dr. E. C. Loh and Mr. J. Eickmeyer for all the help I received during the preparation of the talk.

FIGURE CAPTIONS

Fig. 1: The differential cross section(11) for π^0 photoproduction on the proton is plotted versus t for incident photon energies of 6, 9, 12, and 15 GeV. The dashed lines are only connecting data points at the same energy.

Fig. 2: The differential cross section for π^0 photoproduction on the proton is plotted versus t for incident photon energies of 6, 12, and 18 GeV. Shown are the data at large t-values by Gomez et al.(13) multiplied by a factor 1.2. The earlier SLAC data are represented by the dashed line.

Fig. 3: The effective trajectory $\alpha(t)$ for the reaction $\gamma p \rightarrow \pi^0 p$ is plotted versus t. $\alpha(t)$ was determined from a fit of the form $d\sigma/dt(s,t)=\beta(t)(s-m^2)^{2\alpha(t)-2}$ to the data(11,13).

Fig. 4: The asymmetry A in π^0 photoproduction on the proton with linearly polarized photons is plotted versus t for incident photon energies of 4, 6, and 10 GeV. The data are from the experiment by Anderson et al.(11). The older results by Bellinger et al.(1) at 3 GeV are also shown. To help judge the energy dependence the identical curve is shown at the three energies.

Fig. 5: The differential cross section(11) for π^0 photoproduction on the proton at 6 GeV is plotted for photons polarized normal and parallel to the reaction plane. The solid line is from a fit by Kramer(17), the dotted line is from a fit by Worden(19) and the dashed line is from a fit by Gault et al(16).

Fig.6a: The ratio $R = (\gamma d \rightarrow (\pi^{o}n)p)/(\gamma d \rightarrow (\pi^{o}p)n)$ as measured by Braunschweig et al.(20) is plotted versus t for an incident energy of 4 GeV. For comparison the older data by Bolon et al.(1) are also shown. The dotted lines indicate different estimates of R using the VDM to relate $\pi^{+}n \rightarrow \omega p$ to the isoscalar part of $\gamma p \rightarrow \pi^{o} p$.

Fig.6b: The ratio $R = \frac{\gamma d \rightarrow (\pi^{o}n)p}{\gamma d \rightarrow (\pi^{o}p)n}$ as measured by Browman et al.(21) is plotted versus t for incident energies of 4.8 and 8 GeV. The Regge fits by Worden(19) and Gault et al.(16) are also shown.

Fig. 7: The Daresbury data(25) on the asymmetry T in π^{o} photoproduction from a polarized target is plotted versus t. The lines show representative Regge fits (16,17,19) to the data.

Fig. 8: The new Cornell data on $\gamma p \rightarrow \eta p$ are plotted versus t for incident photon energies of 4 and 8 GeV. The earlier results by Bonn-DESY and SLAC are also shown. The dashed line is from the fit by Gault et al.(16) and the dotted line is from the fit by Worden(19).

Fig.9a: The asymmetry A in π^{+} photoproduction with linearly polarized photons is plotted versus $\sqrt{-t}$ for the new SLAC-MIT(30) data at 12 GeV. The older data from CEA(1) and DESY(1) at lower energies are also shown.

Fig.9b: The asymmetry A in π^{+} photoproduction on the proton(30) is compared with two representative Regge calculations by Kane et al.(24) and by Worden(19).

Fig.10: The asymmetry T, in π^+ photoproduction on a polarized proton target is plotted versus t for incident photon energies of 5 and 16 GeV. The data are from the Berkeley-SLAC collaboration(31). Representative Regge fits are shown(17,19).

Fig.11: Finite Energy Sum Rules, as evaluated by Worden(19), are plotted as a function of momentum transfer t between t=0 and t=-1.0(GeV/c)^2. Columns refer to the t-channel quantum numbers ($I^G = 1^+$, 1^- and 0) and rows refer to the s-channel helicity structure. The amplitudes are defined in the text. The results are shown for a model with NWS-zeros but strong absorption(19).

Fig.12: The Finite Energy Sum Rules(19) are compared with the results of the Michigan model(24). Note the strong discrepancy in the (ω, W_0^+) amplitude. The nomenclature is the same as in Fig. 11.

Fig.13: The asymmetry A with linearly polarized photons are plotted versus $\sqrt{-t}$ for the reactions $\gamma p \longrightarrow \pi^- \Delta^{++}(30)$ and $\gamma p \rightarrow \pi^+ \Delta^0(34)$.

Fig.14: The total cross sections(34) for $\gamma p \rightarrow \pi^- \pi^+ p$, $\gamma p \rightarrow \rho^0 p$, $\gamma p \rightarrow \pi^+ \Delta^0$, $\gamma p \rightarrow \pi^- \Delta^{++}$ are plotted versus energy.

Fig.15: Helicity density matrix elements of the Δ^{++} from the reaction $\gamma p \rightarrow \pi^- \Delta^{++}$ are plotted as a function of the cosine of the C. of M. production angle. The solid line is the result of a fit(40) including the Born terms and the s-channel resonance contribution.

Fig.16: The various spin-density-matrix elements in the helicity frame for the ρ^0 from the reaction $\pi^- p \rightarrow \rho^0 n$. The

contribution due to the s-wave in the measured $\pi^+ \pi^-$ spectrum has been removed.

Fig.17: Comparison between forward charged pion photoproduction and ρ^o production in $\pi^- p \rightarrow \rho^o n$.

a) The unpolarized cross section.

b) The natural parity cross section.

c) The unnatural parity cross section.

d) The asymmetry $A^{\pm} = (\sigma_{\perp}^{\pm} - \sigma_{\parallel}^{\pm})/(\sigma_{\perp}^{\pm} + \sigma_{\parallel}^{\pm})$. Here, $\sigma_{\perp}^{\pm}$ stands for the differential cross section for $\gamma p \rightarrow \pi^+ n$ with photons polarized normal to the reaction plane.

Fig.18: C. of M. plot of the data points taken by Boyarski et al.(56) on the inclusive reactions $\gamma + p \rightarrow \pi^{\pm} +$"anything" and $\gamma + p \rightarrow K^{\pm} +$"anything" at 18 GeV.

Fig.19: The number of π^- events from the reaction $\gamma + p \rightarrow \pi^- +$"anything" at 9.3 GeV is plotted versus $x = 2P_{\parallel}^{c.m.}/\sqrt{s}$ and $P_{\parallel}^{L}$. On the plot the number of events in each bin are written as a number up to 9; from here on letters are used, i.e. A stands for 10 events and V for 31 or more. Curves of constant transverse momentum are shown as solid lines.

Fig.20: The various charged topological cross sections(52) are plotted as a function of s.

Fig.21: The average charged multiplicity minus the initial charge is plotted versus s.

Fig.22: The 3-prong cross section in $\gamma + p \rightarrow \pi^- +$"anything" and the 4-prong cross section in $\gamma + p \rightarrow \pi^- +$"anything" are plotted versus s. Note that ρ^o production, shown as the dotted line,

only accounts for a small fraction of the 3-prong cross section at these energies.

Fig.23: The differential cross section(51) for $\gamma+p \rightarrow \pi^-+$"anything" integrated over longitudinal momenta in the laboratory between -.3 and +.3(GeV/c) is plotted versus $P_\perp^2$ for four different energy intervals.

Fig.24: The differential cross section(53) for $\gamma+p \rightarrow \pi^-+$"anything" is plotted versus P_L for energies between 3 and 6.3 GeV and $P_L \lesssim .5$ GeV/c. Note that this cross section is normalized to the average value of the total γp cross section between 3 and 6.3 GeV For comparison the differential cross sections for(57) $\pi^-+p \rightarrow \pi^-+$"anything" at 24.8 GeV ---, $\pi^++p \rightarrow \pi^-+$"anything" at 7 GeV and $K^++p \rightarrow \pi^-+$"anything" at 12.7 GeV —.—.—., and $p+p \rightarrow \pi^-+$"anything" at 28.5 GeV— — are also shown. Note these cross sections are normalized to the asymptotic value of the various total cross sections.

Fig.25: The invariant cross sections(54) for $\gamma+p \rightarrow \pi^\pm+$"anything"and $\gamma+p \rightarrow K^\pm+$"anything" are plotted versus $P_\perp^2$ for incident photon energy of 18 GeV and x = .2. For comparison the cross section for $\gamma+p \rightarrow \pi^-+$"anything" at 9.3 GeV is also shown(52).

Fig.26: The ratio π^-/K^- and π^+/K^+ at 18 GeV and x = .2 are plotted versus the transverse mass squared m_T^2. The transverse mass is defined as $m_T = (p_\perp^2 + \mu^2)^{1/2}$ where μ is the mass of the detected particle.

Fig.27: The distribution function(52) for $\gamma+p \rightarrow \pi^{-}_{+}$"anything" at 9.3 GeV is plotted versus $P_{\perp}^2$ for different values of x. The solid line is an eyeball fit to the cross section for $0 \lesssim x \lesssim .1$, normalized at small values of $P_{\perp}^2$. It is clear that the $P_{\perp}^2$ distributions are dependent on P_L.

Fig.28: Plotted is F(x), the invariant cross section integrated over all transverse momenta, for the reaction $\gamma + p \rightarrow \pi^{-}_{+}$"anything" at three energies 2.8, 4.7, and 9.3 GeV(52).

Fig.29: F(x) for $\gamma+p \rightarrow \pi^{-}_{+}$"anything" is plotted versus s for different cuts on x. The data(52) are consistent with scaling in the target or the beam fragmentation regions. The data however do not scale for $x \approx 0$.

Fig.30: The cross section(52) for the reaction $\gamma+p \rightarrow \pi^{-}_{+}$"anything" is plotted versus the rapidity y for the three energies 2.8, 4.7, and 9.3 GeV.

Fig.31: The effective trajectories(52) $\alpha(t)$ for the π^- from the target fragmentation region (a), or from the beam fragmentation region (b), are plotted versus t.

Fig.32: a. The analogy in an inclusive reaction to the optical theorem in the two-body case. b. Single Regge limit for an inclusive reaction. Either subenergy($a\bar{c}$) or ($b\bar{c}$) is small compared to the total energy. c. Double Regge limit (pionization) for an inclusive reaction. Here both subenergies ($a\bar{c}$) and ($b\bar{c}$) are large.

Fig.33: $d\sigma/dp$ (52) for the reaction $\gamma+p \rightarrow \pi^{-}_{+}$"anything" plotted versus $s^{-1/2}$. Note that a straight line through the data

points in the target fragmentation region extrapolates through 0.

Fig.34: Longitudinal momentum distribution(53) of the π^- in the laboratory for photon energies between 3 and 6.3 GeV. The curves, as defined in the figure, are from fits to the data collected by Chen et al.(57).

Fig.35: The distribution function(52) for $\gamma+p\rightarrow\pi^-+$"anything" at 9.3 GeV, normalized to the total cross section, is plotted versus x. For comparison the data(56) on $\pi^-+p\rightarrow\pi^-+$"anything" and $\pi^+ + p\rightarrow\pi^-+$"anything" at 18.5 GeV are also shown.

Fig.36: The distribution function(54) for $\gamma+p\rightarrow\pi^{\pm}_{+}$"anything" and $\gamma+p\rightarrow K^{\pm}_{+}$"anything" at 18 GeV is plotted versus x for different values of the transverse momentum.

Fig.37: The π^+/π^- and K^+/K^- ratios(54) at 18 GeV and $P_\perp = 1.0(\mathrm{GeV/c})^2$ are plotted as a function of x. The number in the parentheses gives the missing mass for the K.

Fig.38: The differential cross section $d\sigma/d\phi$ plotted against the azimuthal angle ϕ between the outgoing pion and the polarization vector of the photon, for various cuts on x. Data(52) are from the reaction $\gamma + p \rightarrow \pi^- +$ "anything" at 9.3 GeV.

REFERENCES

1. K. Lübelsmeyer, in "Proceedings of the Fourth International Symposium on Electron and Photon Interactions at High Energies, Daresbury Laboratory, Liverpool, England (1969).

2. H. Harari, in "Proceedings of the Fourth International Symposium on Electron and Photon Interactions at High Energies, Daresbury Laboratory, Liverpool, England (1969).

3. R. Diebold, in "Proceedings of the Boulder Conference on High Energy Physics", Boulder, Colorado (1969).

4. R.C.E. Devenish, W. J. Leigh, and D. H. Lyth, University of Lancaster Preprint (June 1970);

I. Barbour, W. Malone, and R. G. Moorhouse, UCRL-20635 and contribution to this conference.

5. R. C. Arnold and M. L. Blackmon, Phys. Rev. 176, 2082 (1968).

6. F. S. Henyey, G. L. Kane, J. Pumplin, and M. H. Ross, Phys. Rev. 182, 1579 (1969).

7. The most important failures of the Argonne model is perhaps in the non-flip amplitudes. i.e. no crossover at the right t-value in elastic scattering. It also predicts dips in various reactions like $\gamma p \rightarrow \eta p$ where none are seen.

The Michigan Model fails to fit the polarization data in $\pi^{\pm} p \rightarrow \pi^{\pm} p$ and would most naturally predict dips in $\pi^- p \rightarrow \eta^o n$, $\pi^+ p \rightarrow \eta \Delta^{++}$, $K^- p \rightarrow K^o n$ and $K^+ n \rightarrow K^o p$ where none are seen.

8. A. P. Contogouris, in the DESY Summer School on Photon-Hadron Interactions (1971).

9. H. Harari, Phys. Rev. Letters 26, 1400 (1971).

10. R. L. Anderson, D. Gustavson, J. Johnson, D. Ritson, B. H. Wiik, W. G. Jones, D. Kreinick, F. Murphy, and R. Weinstein, Phys. Rev. D1, 27, (1970).

11. R. L. Anderson, D. B. Gustavson, J. R. Johnson, I. D. Overman, D. M. Ritson, B. H. Wiik, and D. Worcester, SLAC-PUB-925. Contribution to the conference.

12. R. L. Anderson, D. Gustavson, J. Johnson, I. Overman, D. M. Ritson, B. H. Wiik, R. Talman, J. K. Walker, and D. Worcester, Phys. Rev. Letters 25, 1218 (1970).

13. R. Gomez, et al. contribution to this conference.

14. P. Stichel, Zeitschift f. Physik 180, 170 (1964).

15. D. Bellenger, R. Bordelon, K. Cohen, S. B. Deutsch, W. Lobar, D. Luckey, L. S. Osborne, E. Pothier, and R. Schwitters, Phys. Rev. Letters 23, 540 (1969).

16. F. D. Gault, A. D. Martin, and G. L. Kane, University of Durham Preprint. Submitted to this conference.

17. G. Kramer, DESY Report 71/27.

18. C. B. Chiu and S. Matsuda, Physics Letters 31B, 455 (1970).

19. R. Worden, CALT-68-313. Contribution to this conference.

20. W. Braunschweig, H. Dinter, W. Erlewein, H. Frese, K. Lübelsmeyer, H. Meyer-Wachsmuth, C. C. Moorhouse, D. Schmitz, A. Schultz v.Dratzig, and G. Wessels, contribution to this conference.

21. A. Browman, K. Hanson, T. Meyer, A. Osborne, A. Silverman, F. Taylor, N. Horwitz, contribution to this conference.

22. Bari, Bologna, Firenze, and Orsay collaboration, Nuovo Cimento 65A, 637 (1970).

23. H. J. Behrend, C. K. Lee, F. Lobkowicz, E. H. Thorndike, M. E. Nordberg,Jr., and A. A. Wehmann, Phys. Rev. Letters 27, 61 (1971). Using the value for $\gamma_\omega^2/4\pi$ as measured on the ω mass shell would reduce the computed value for R.

24. See for example: G. L. Kane, F. Henyey, D. R. Richards, M. Ross, and G. Williamson, Phys. Rev. Letters 25, 1519 (1970).

25. P. S. L. Booth, G. R. Court, B. Craven, P. J. Hayman, J. R. Holt, A. P. Hufton, J. N. Jackson, and J. H. Norem. Contribution to this conference.

26. E. L. Berger and G. Fox, Phys. Rev. Letters 25, 1783 (1970).

27. M. Braunschweig, W. Braunschweig, D. Husmann, K. Lübelsmeyer, and D. Schmitz, Nuclear Physics B20, 191 (1970).

28. Measurements of the proton recoil polarization in π^0 photoproduction is now being carried out at Cornell by M. Deutsch and collaborators.

29. J. DeWire, B. Gittelman, R. Loe, E. C. Loh, D. J. Ritchie, and R. A. Lewis. Contribution to this conference.

30. R. F. Schwitters, J. Leong, D. Luckey, L. S. Osborne, A. M. Boyarski, S. D. Ecklund, R. Siemann, and B. Richter, Phys. Rev. Letters 27, 120 (1971).

31. C. C. Morehouse, M. Borghini, O. Chamberlain, R. Fuzesy, W. Gorn, T. Powell, P. Robrish, S. Rock, S. Shannon, G. Shapiro, H. Weisberg, A. Boyarski, S. Ecklund, Y. Murata, B. Richter, R. Siemann, and R. Diebold, Phys. Rev. Letters 25, 835 (1970).

32. D. Schwela and R. Weizel, Zeitschrift f. Physik 221, 71 (1969).

33. R. L. Walker, Phys. Rev. 182, 1729 (1969).

34. Aachen-Berlin-Bonn-Hamburg-Heidelberg-München collaboration, Phys. Letters 23, 707 (1966) and Phys. Rev. 175, 1669 (1968).

35. Cambridge Bubble Chamber Group, Phys. Rev. 163, 1510 (1967).

36. A. M. Boyarski, R. Diebold, S. D. Ecklund, G. E. Fischer, Y. Murata, R. Richter, W.S.C. Williams, Phys. Rev. Letters 22, 148 (1969).

37. J. Ballam, G. B. Chadwick, M. M. Menke, P. Seyboth, Y. Eisenberg, B. Haber, E. E. Ronat, A. Shapira, Y. Stahl, G. Yekutieli, S. Dagan, and A. Levy, SLAC, Tel-Aviv University and Weizmann Institute. Contribution to this conference.

38. J. Ballam, G. B. Chadwick, R. Gearhart, Z.G.T. Guiragossian, J. J. Murray, P. Seyboth, C. K. Sinclair, I. O. Skillicorn, H. Spitzer, G. Wolf, H. H. Bingham, W. B. Fretter, K. C. Moffeit, W. J. Podolsky, M. S. Rabin, A. H. Rosenfeld, R. Windmolders, and R. H. Milburn. Contribution to this conference.

39. P. Stichel and M. Scholz, Nuovo Cimento 34, 1381 (1964).

40. D. Lüke and P. Söding, Springer Tracts in Modern Physics (Springer-Verlag, New York, 1971); Vol. 59, p. 39.

41. A. M. Boyarski, R. Diebold, S. D. Ecklund, G. E. Fischer, Y. Murata, B. Richter, and M. Sands, Phys. Rev. Letters 25, 695 (1970).

42. C. Quigg, UCRL-20032, University of California, Berkeley.

H. Harari, Phys. Rev. Letters 26, 1079 (1971).

F. S. Henyey, G. L. Kane, and J.J.G. Scanio, Phys. Rev. Letters 27, 350 (1970).

43. F. Bulos, R. K. Carnegie, G. E. Fischer, E. E. Kluge, D.W.G.S. Leith, H. L. Lynch, B. Ratcliff, B. Richter, H. H. Williams, S. H. Williams, M. Beniston, Phys. Rev. Letters 26, 1453 (1971) and Phys. Rev. Letters 26, 1457 (1971).

44. P. Sonderegger and P. Bonamy, in "Proceedings of the Fifth International Conference on Elementary Particles" Lund, Sweden (1969). E. I. Shibata, D. H. Frisch, and M. A. Wahlig, Phys. Rev. Letters 25, 1227 (1970).

45. H. Burfeindt, G. Buschhorn, C. Geweniger, P. Heide, R. Kotthaus, H. Wahl, and K. Wegener, Phys. Letters 33B, 509 (1970). Note that these data agree with the measured(30) asymmetry at 12 GeV.

46. A. M. Boyarski, F. Bulos, W. Busza, R. Diebold, S. D. Ecklund, G. E. Fischer, J. R. Rees, and B. Richter, Phys. Rev. Letters 20, 300 (1968).

A. M. Boyarski, R. Diebold, S. D. Ecklund, G. E. Fischer, Y. Murata, B.Richter, and W.S.C. Williams, Phys. Rev. Letters 21, 1767 (1968).

47. See for example: D. Horn, Invited talk presented at the International Conference on Duality and Symmetry in Hadron Physics, Tel-Aviv (1971). L. Van Hove, Physics Report 1C, 349 (1971).

48. R. P. Feynman, Phys. Rev. Letters 23, 1415 (1969), and "Proceedings of the Third Topical Conference on High Energy Collisions of Hadrons, Stony Brook, New York (1969).

49. H. Satz and D. Schildknecht, CERN-Report T.H. 1332 and contribution to this conference.

50. H. D. I. Abarbanel and D. J. Gross, Phys. Rev. Letters 26, 732 (1971).

51. W. P. Swanson, M. Davier, I. Derado, D. C. Fries, F. F. Liu, R. F. Mozley, A. C. Odian, J. Park, F. Villa, and D. E. Young. Contribution to this conference.

52. J. Ballam, G. B. Chadwick, M. Della-Negra, R. Gearhart, K. C. Moffeit, J. J. Murray, P.Seyboth, C. K. Sinclair, I. O. Skillicorn, H. Spitzer, G. Wolf, H. H. Bingham, W. B. Fretter, W. J. Podolsky, M. Rabin, A. H. Rosenfeld and R. H. Milburn. Contribution to this conference.

53. W. Struczinski, I. Derado, P. Dittmann, V. Eckardt, G. Hentschel, V. Heynen, P. Joos, G. Knies, J. Knobloch, G. Kronseder, A. Ladage, E. Maier, H. Meyer, B. Naroska, D. Notz,

E. Rabe, P. Schacht, P. Söding, S. Wolff. Contribution to this conference.

54. A. M. Boyarski, D. Coward, S. Ecklund, B. Richter, D. Sherden, R. Siemann, and C. Sinclair. Contribution to this conference.

55. G. E. Gladding, J. J. Russel, M. J. Tannenbaum, J. M. Weiss, and G. B. Thomsop. Contribution to this conference.

56. L. G. Ratner, R. J. Ellis, G. Vannini, B. A. Babcock, A. D. Krisch, and J. B. Roberts, Phys. Rev. Letters 27, 68 (1971).

57. M. S. Chen, R. R. Kinsey, T. W. Morris, R. S. Panvini, L. L. Wang, T. F. Wong, S. L. Stone, T. Ferbel, P. Slattery, B. Werner, J. W. Elbert, and A. R. Erwin, Phys. Rev. Letters 26, 1585 (1971).

58. A. H. Mueller, Phys. Rev. D2, 2963 (1970).

59. Chan Hong-Mo, C. S. Hsue, C. Quigg, and Jiunn-Ming Wang, Phys. Rev. Letters 26, 672 (1971).

60. R. C. Arnold and E. L. Berger suggest that the particle mass μ only will show up in the combination $(\mu^2 + p_\perp^2)$. ANL/HWP-7131, 1971.

61. N. F. Bali, Lowell S. Brown, R. D. Peccei, and A. Pignotti, Phys. Rev. Letters 25, 557 (1970).

62. N. N. Biswas, N. M. Cason, V. P. Kenney, J. X. Powers, W. D. Shephard, and D. W. Thomas, Phys. Rev. Letters 26, 1589 (1971).

W. Ko and R. L. Lander, Phys. Rev. Letters 26, 1064 (1971).

63. L. Bertocchi, S. Fubini, and M. Tonin, Nuovo Cimento 25, 626 (1962).

D. Amati, A. Stanghellini, and S. Fubini, Nuovo Cimento 26, 896 (1962).

64. C. E. DeTar, Phys. Rev. D3, 128 (1971).

65. J. Benecke, T. T. Chou, C. N. Yang and E. Yen, Phys. Rev. 188, 2159 (1969).

66. L. Caneschi and A. Pignotti, Phys. Rev. Letters 22, 1219 (1969).

C. Risk UCRL-20841.

67. H. D. I. Abarbanel, Phys. Letters 34B, 69 (1971).

68. W. D. Shephard, J. T. Powers, N. N. Biswas, N. M. Cason, V. P. Kenney, R. R. Riley, D. W. Thomas, J. W. Elbert, and A. R. Erwin, University of Wisconsin, Preprint (1971).

69. W. P. Swanson, W. Ko, R. L. Lander, and C. Risk. Contribution to this confernce.

Table I

Available Data on Inclusive Reactions

Experiment	Detected Particle	Photon energy (GeV)	Longitudinal Momentum $P_{\parallel}^{L}$ GeV/c	Max. Transverse Momentum $P_{\perp}$ (GeV/c)
SLAC Streamer Chamber[41]	π^-	5 - 18	less than |.5|	.8
SLAC Bubble Chamber[42]	π^-	2.8, 4.7, 9.3	all	1.0
DESY Streamer Chamber[43]	π^-	3 - 6.3	less than |1.5|	.5
SLAC Group C[44]	$\pi^{\pm}$, $K^{\pm}$	18	see Fig. 18	see Fig. 18
CEA[45]	p	2.4 - 4.8	less than 1.0	1.

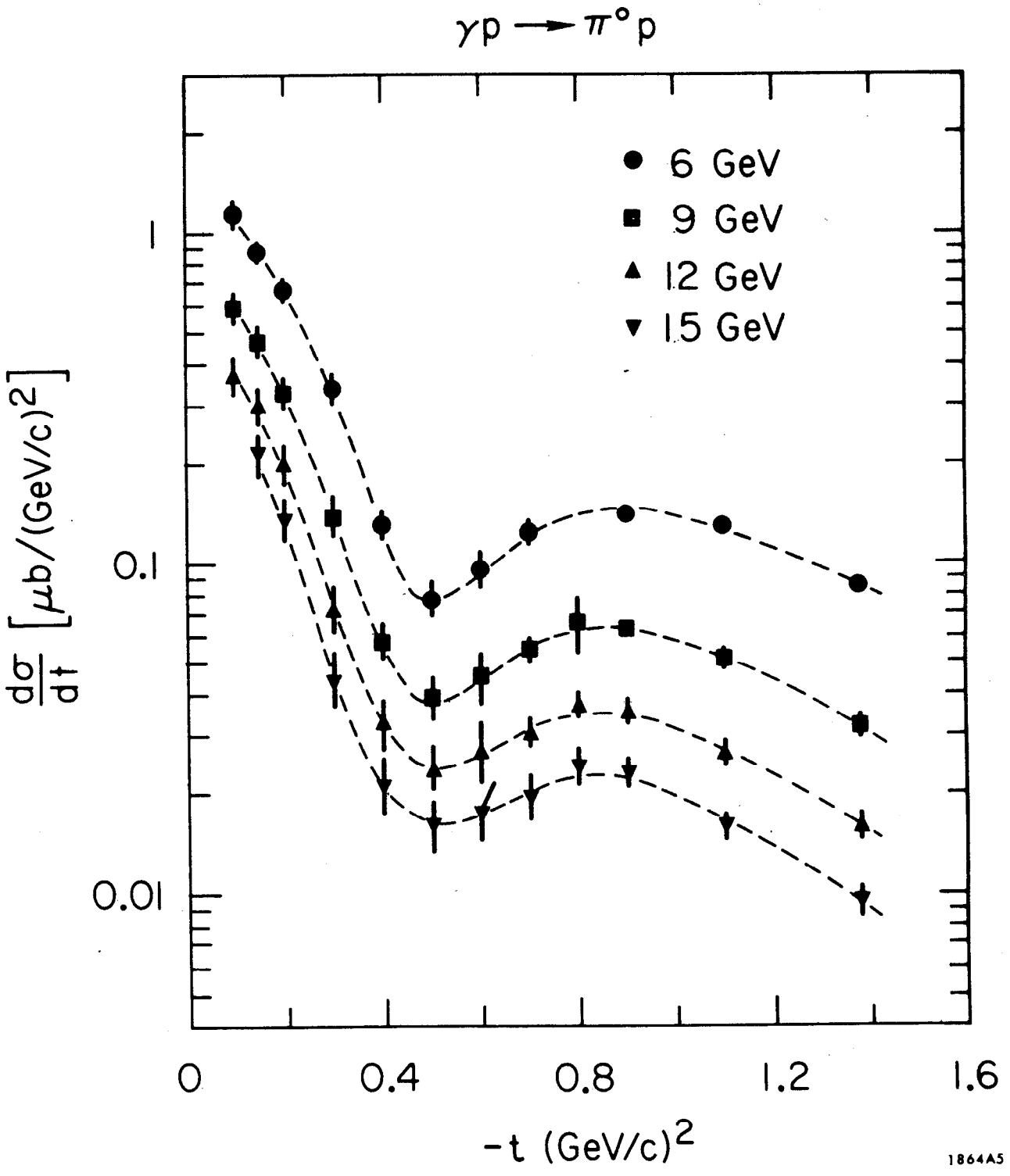
γp → π°p
6 GeV
9 GeV
12 GeV
15 GeV
dσ/dt [μb/(GeV/c)²]
1
0.1
0.01
0
0.4
0.8
1.2
1.6
-t (GeV/c)²
1864A5

Fig. 1

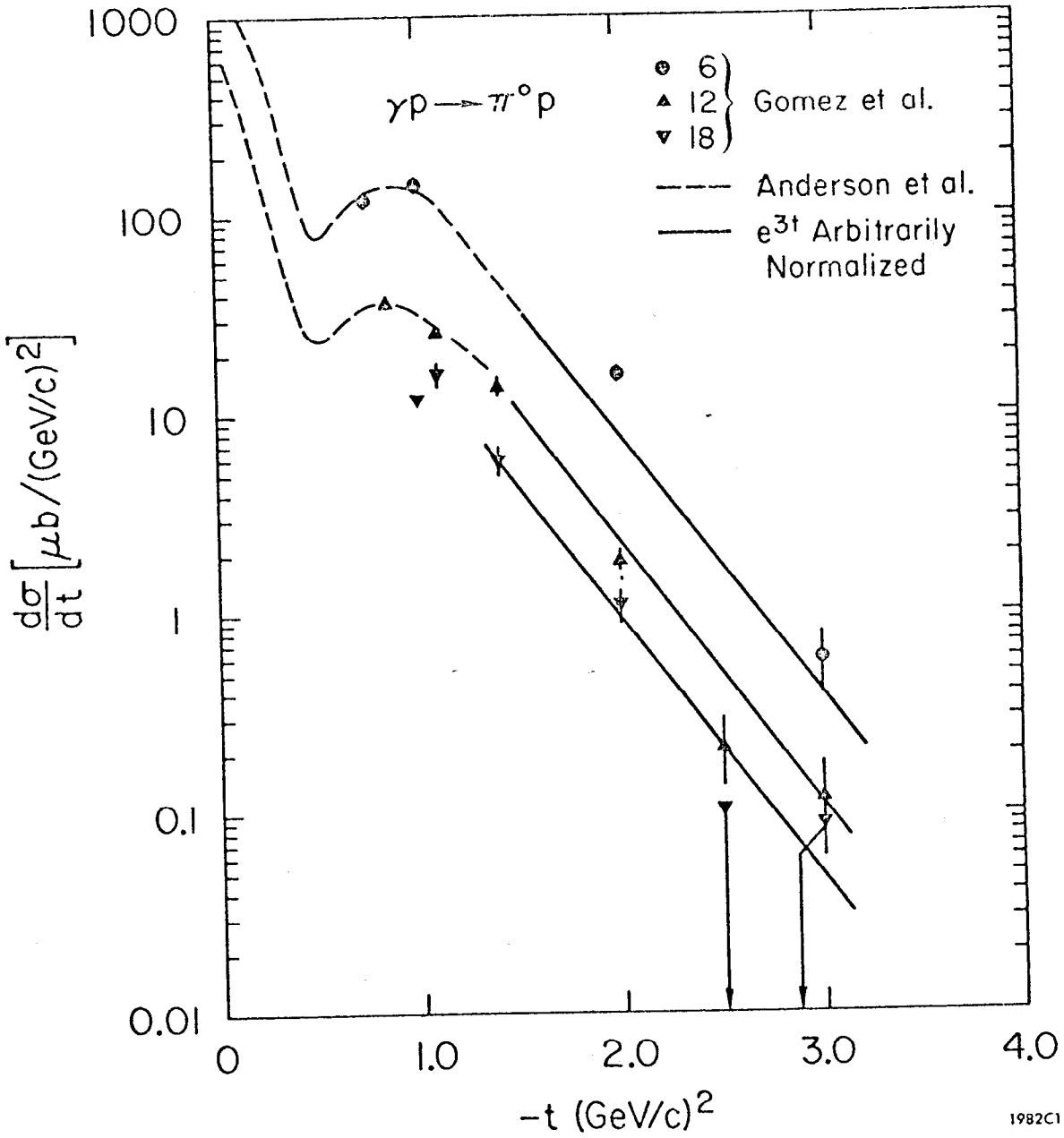
1000
100
10
1
0.1
0.01
$\frac{d\sigma}{dt}\left[\mu b/(GeV/c)^2\right]$
$\gamma p \rightarrow \pi^0 p$
6
12
18
Gomez et al.
Anderson et al.
e^{3t} Arbitrarily Normalized
0
1.0
2.0
3.0
4.0
$-t\ (GeV/c)^2$
1982C1

Fig. 2

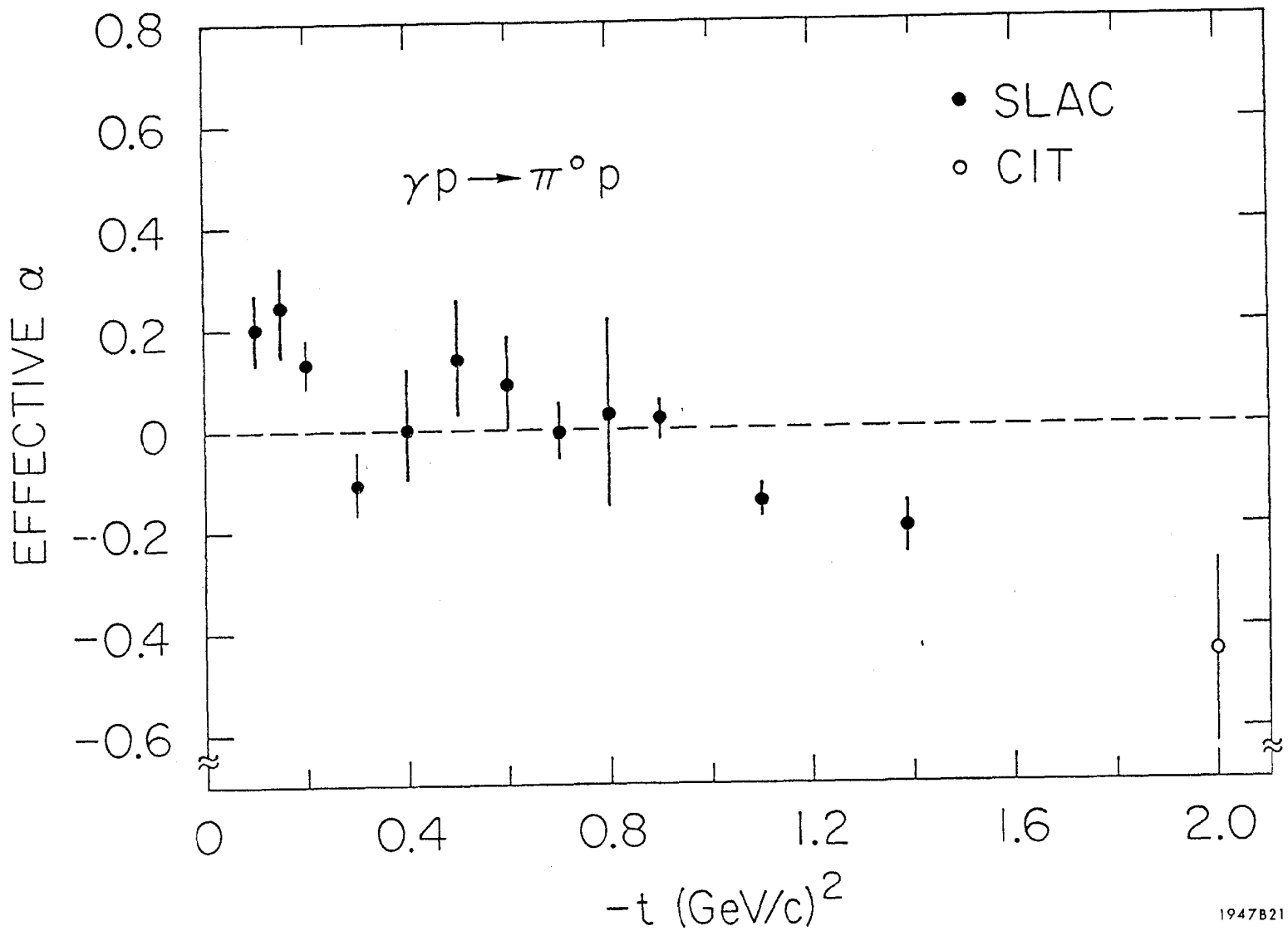
0.8
0.6
0.4
0.2
0
-0.2
-0.4
-0.6
EFFECTIVE α
γp → π°p
• SLAC
○ CIT
0
0.4
0.8
1.2
1.6
2.0
-t (GeV/c)²
1947B21

Fig. 3

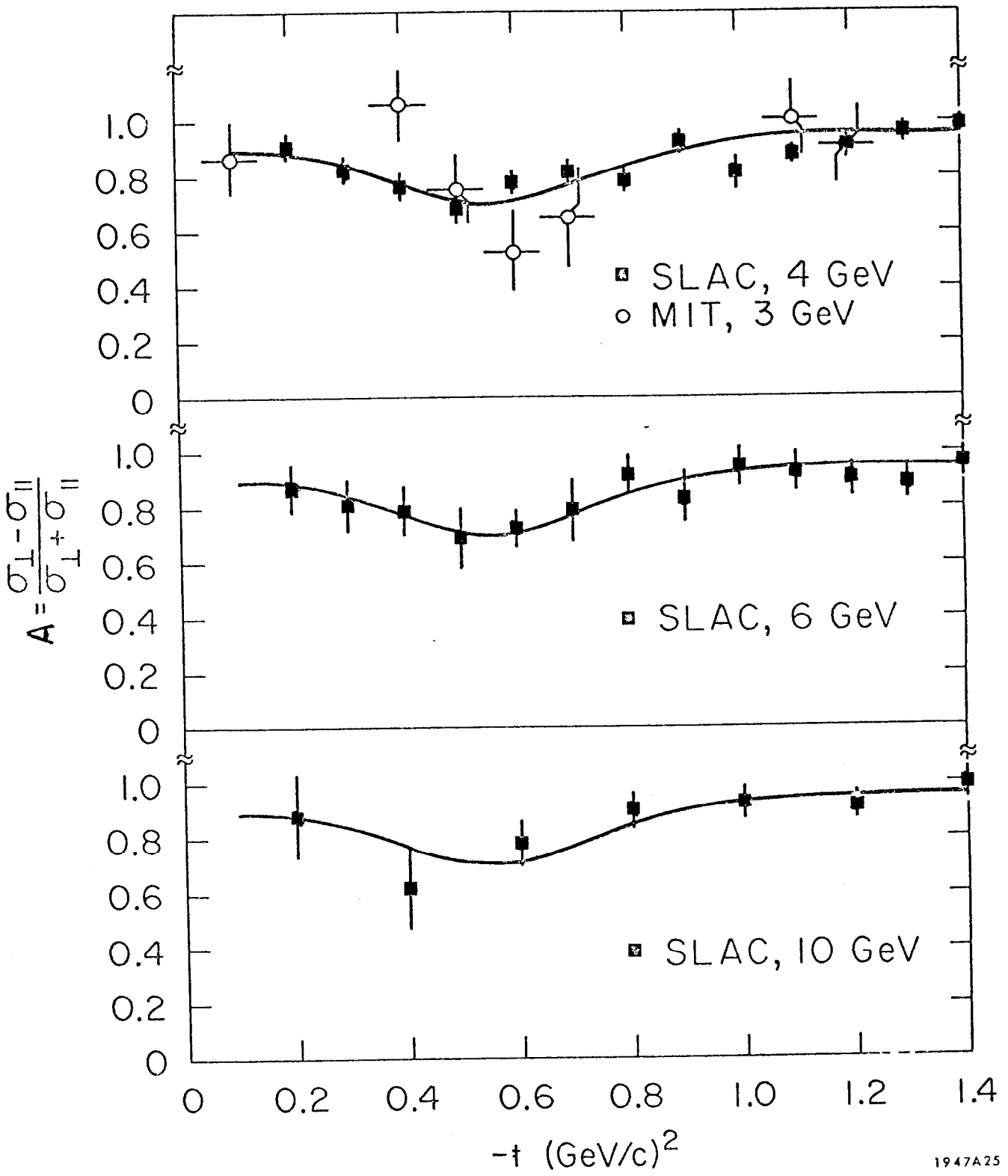
$A = \frac{\sigma_T - \sigma_=}{\sigma_T + \sigma_=}$
1.0
0.8
0.6
0.4
0.2
0
SLAC, 4 GeV
MIT, 3 GeV
SLAC, 6 GeV
SLAC, 10 GeV
0
0.2
0.4
0.6
0.8
1.0
1.2
1.4
$-t$ (GeV/c)^2
1947A25

Fig. 4

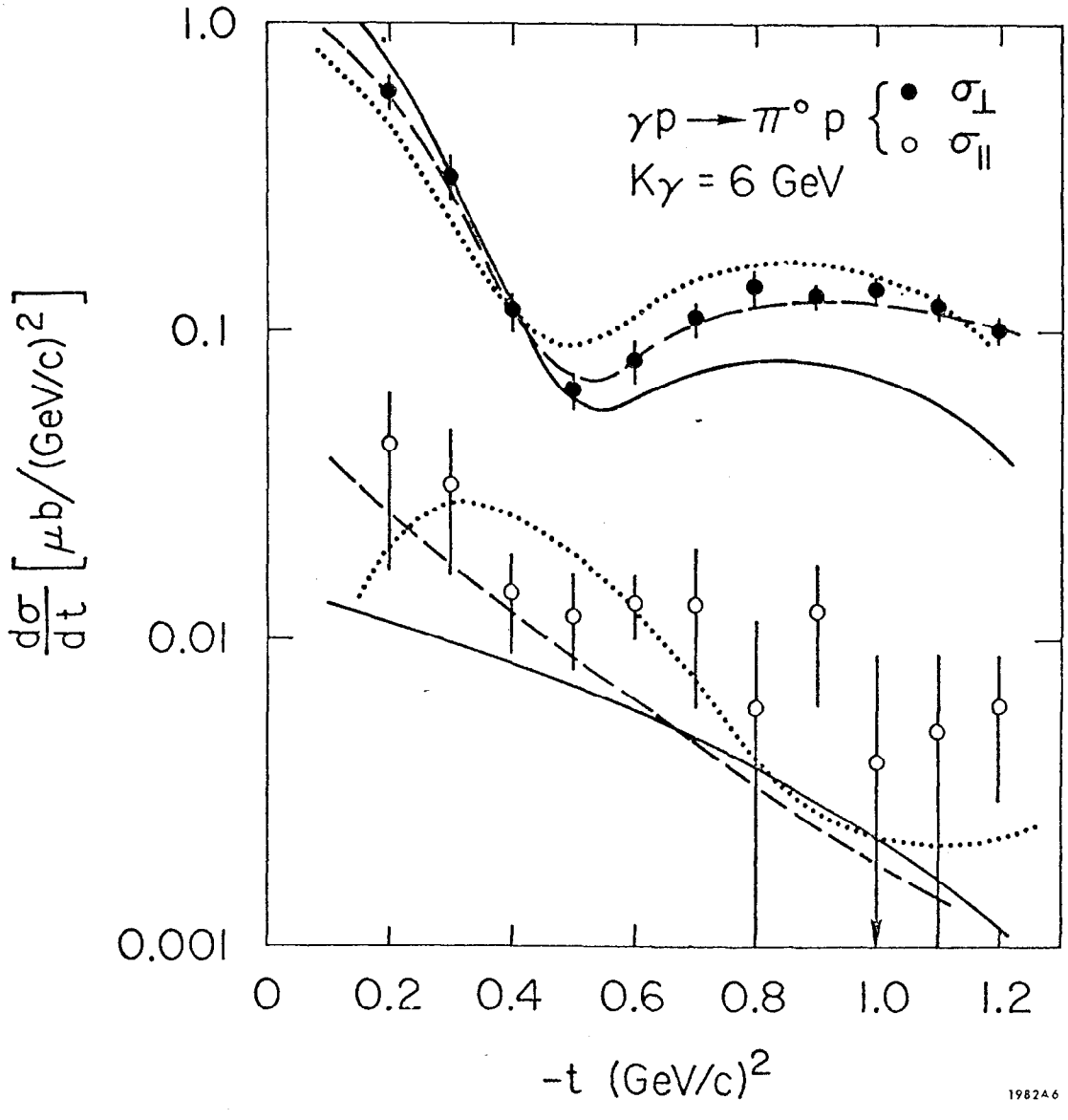
1.0
0.1
0.01
0.001
0
0.2
0.4
0.6
0.8
1.0
1.2
$\gamma p \rightarrow \pi^\circ p$
$K\gamma$ = 6 GeV
$\sigma_\perp$
$\sigma_{||}$
$\frac{d\sigma}{dt}$ [μb/(GeV/c)^2]
$-t$ (GeV/c)^2
198246

Fig. 5

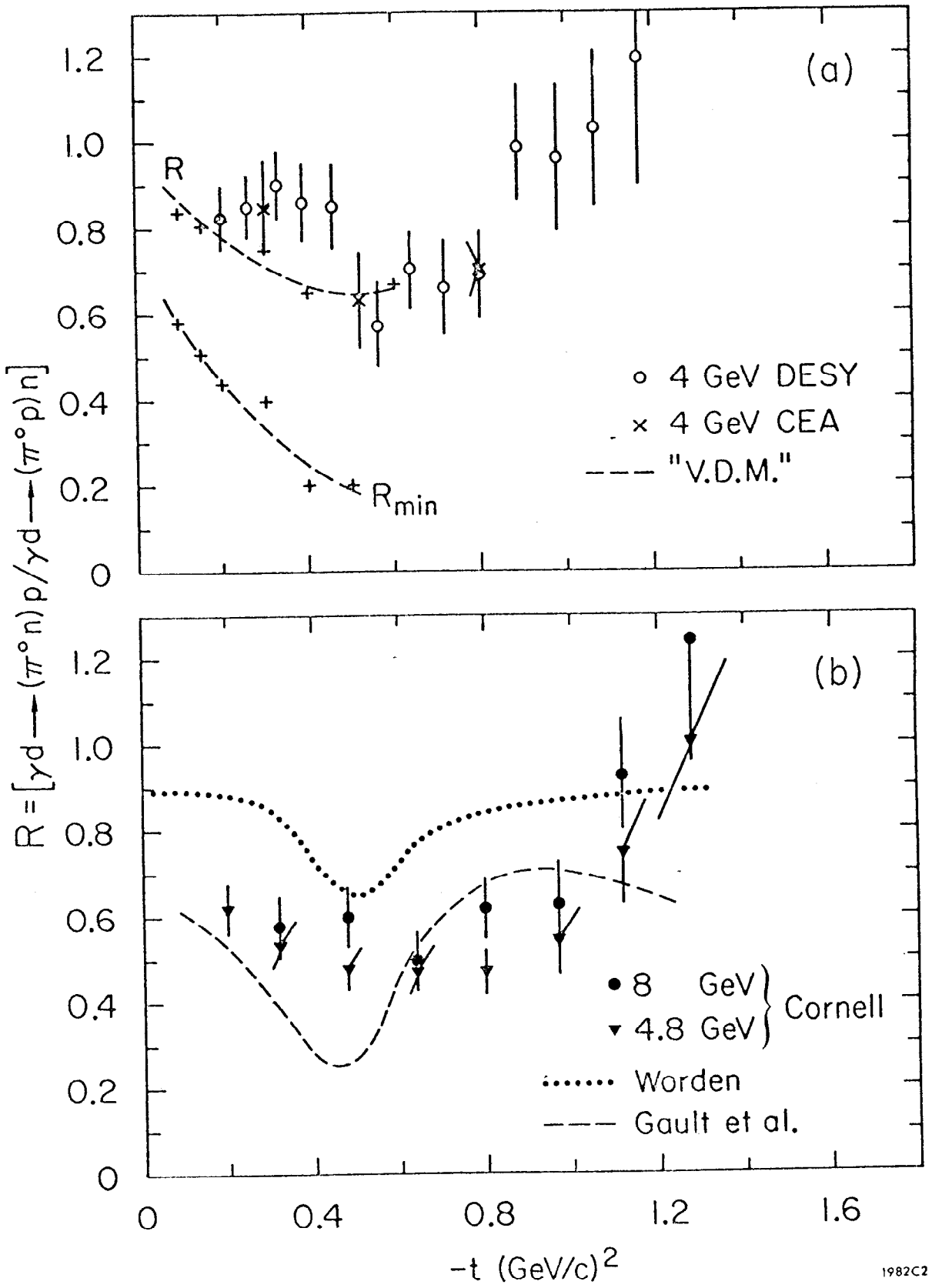
(a)
R
R_{min}
o 4 GeV DESY
× 4 GeV CEA
--- "V.D.M."
(b)
• 8 GeV
▾ 4.8 GeV
Cornell
····· Worden
---- Gault et al.
$R = [\gamma d \to (\pi^\circ n) p / \gamma d \to (\pi^\circ p) n]$
$-t\ (GeV/c)^2$
0
0.2
0.4
0.6
0.8
1.0
1.2
1.6
1982C2

Fig. 6

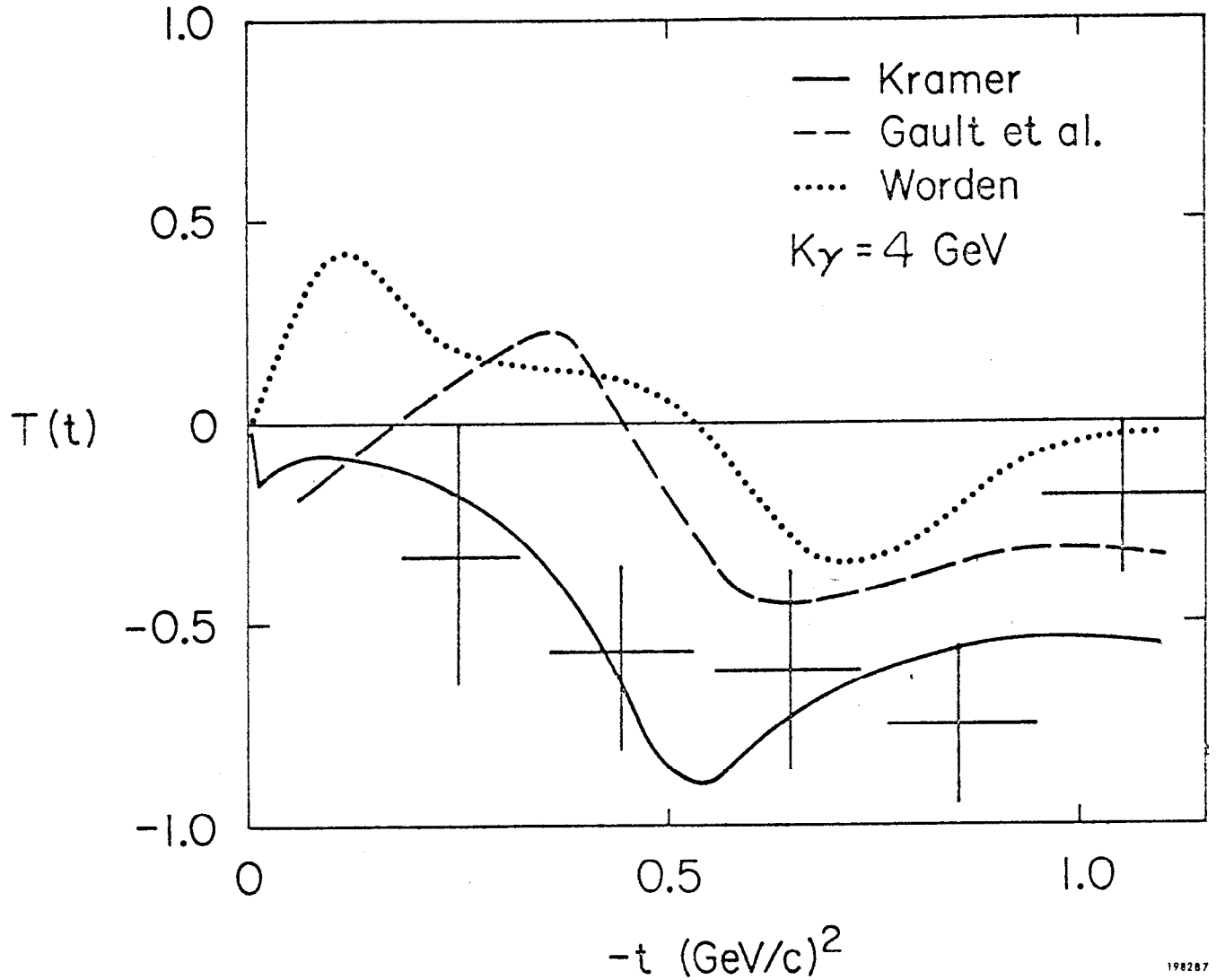
1.0
0.5
0
-0.5
-1.0
T(t)
0
0.5
1.0
-t (GeV/c)^2
Kramer
Gault et al.
Worden
Kγ = 4 GeV
198287

Fig. 7

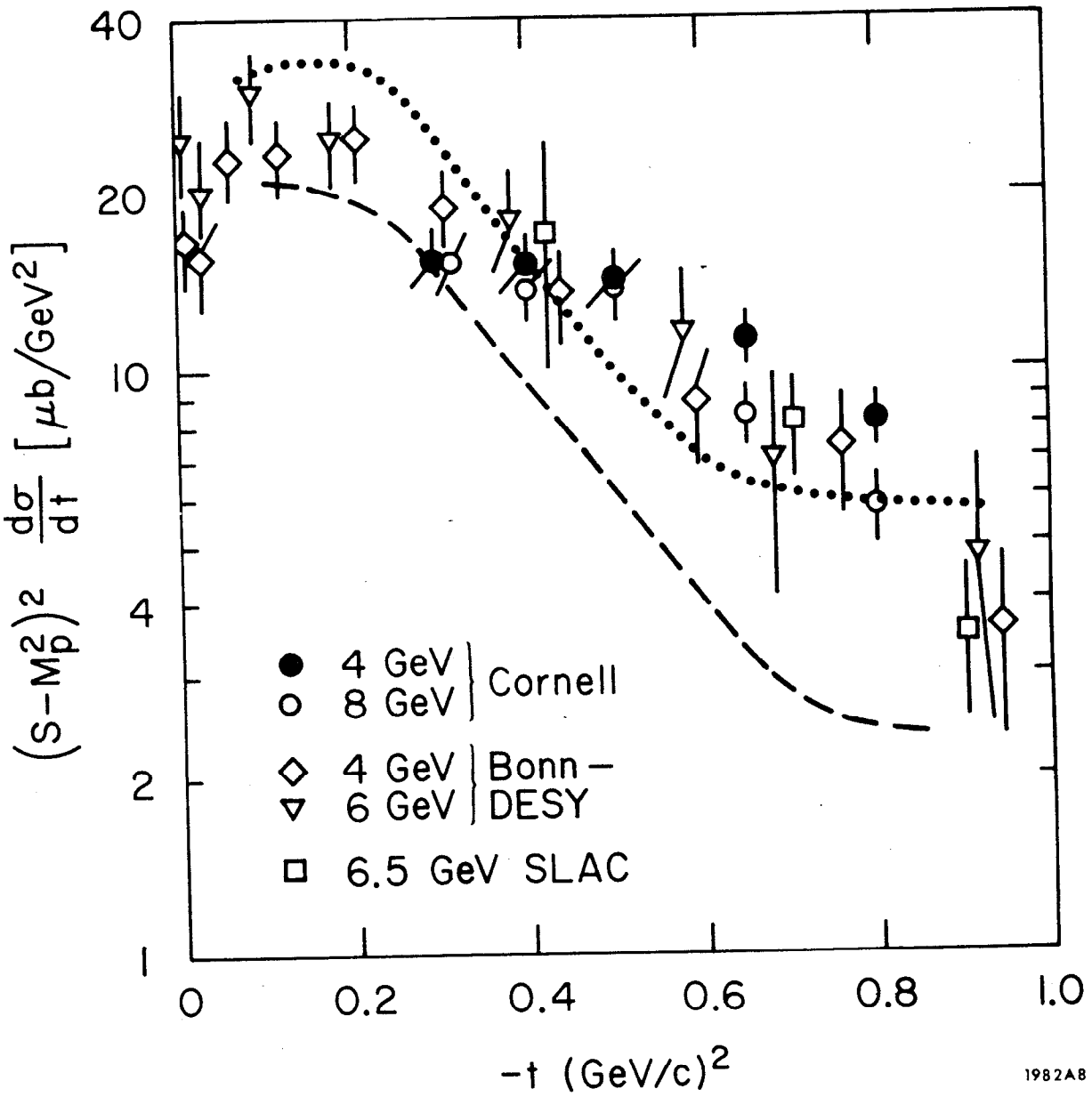
40
20
10
4
2
1
0
0.2
0.4
0.6
0.8
1.0
$(S-M_p^2)^2 \frac{d\sigma}{dt}$ [μb/GeV^2]
-t (GeV/c)^2
4 GeV | Cornell
8 GeV |
4 GeV | Bonn –
6 GeV | DESY
6.5 GeV SLAC
1982A8

Fig. 8

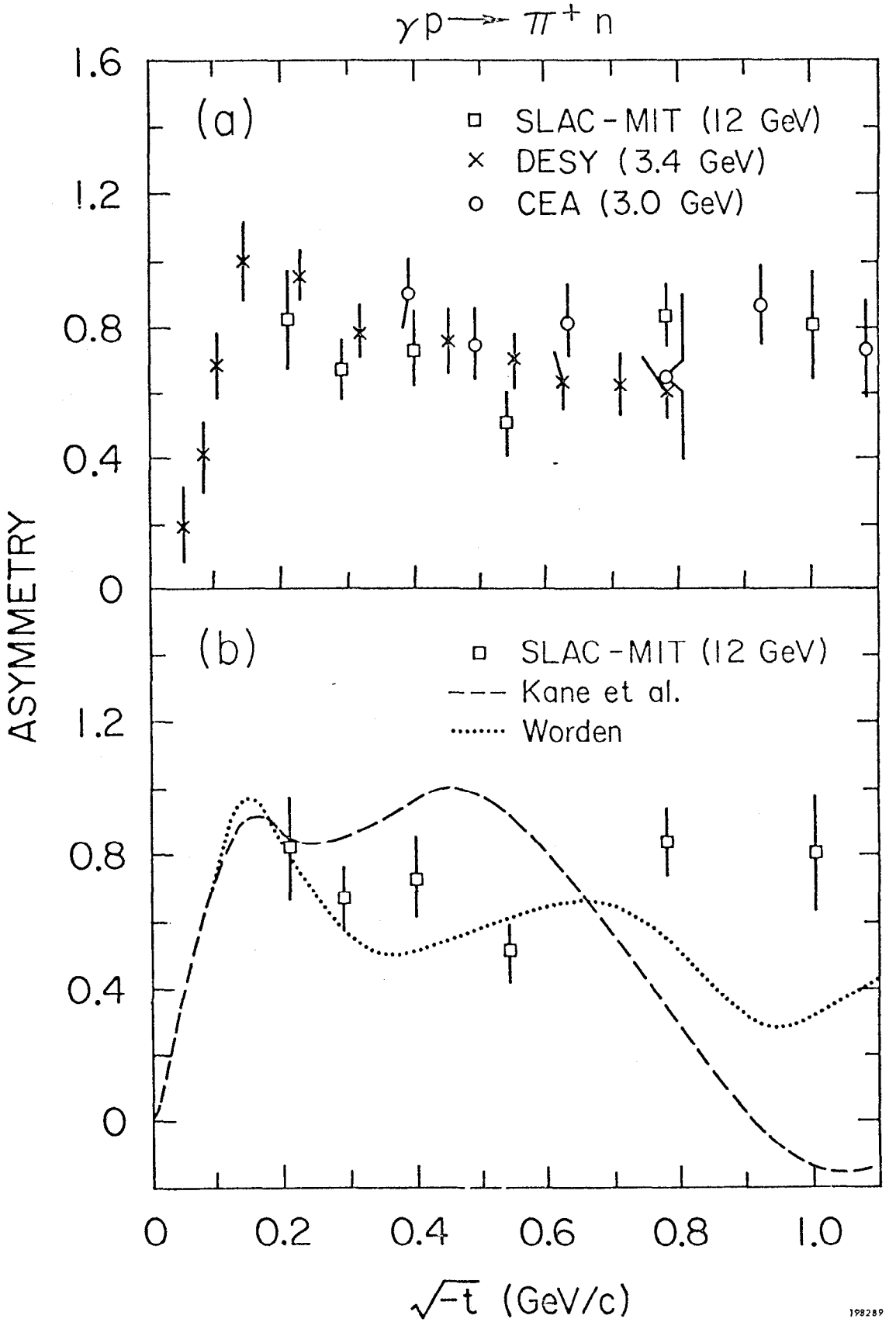
γp → π⁺n
(a)
SLAC-MIT (12 GeV)
DESY (3.4 GeV)
CEA (3.0 GeV)
(b)
SLAC-MIT (12 GeV)
Kane et al.
Worden
ASYMMETRY
1.6
1.2
0.8
0.4
0
0
0.2
0.4
0.6
0.8
1.0
√-t (GeV/c)
198289

Fig. 9

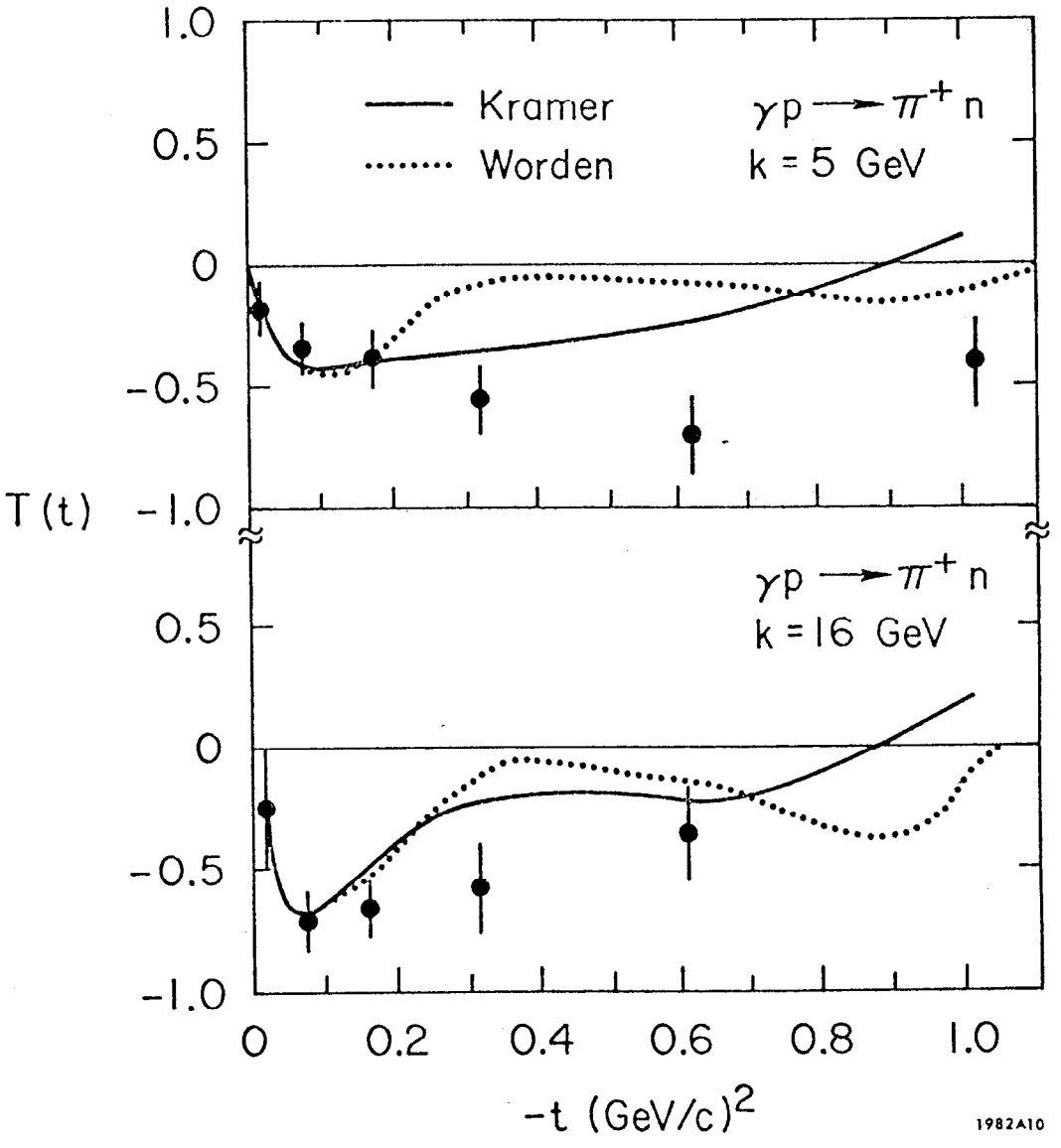
1.0
0.5
0
-0.5
-1.0
T(t)
Kramer
Worden
γp → π+ n
k = 5 GeV
γp → π+ n
k = 16 GeV
0
0.2
0.4
0.6
0.8
1.0
-t (GeV/c)2
1982A10

Fig. 10

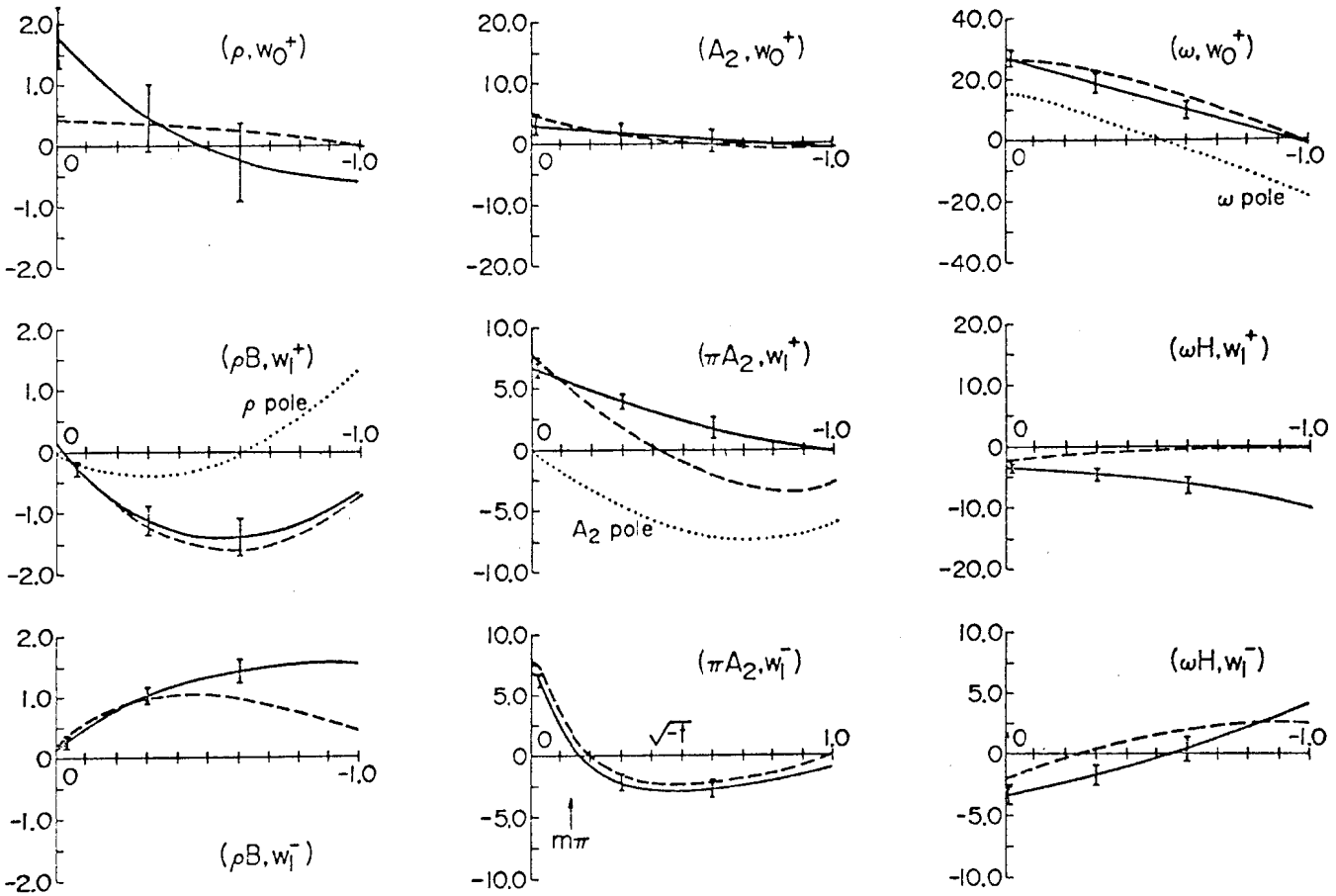

—I— FESR

– – – Square cut fit

Plotted as functions of momentum transfer, t, except where indicated.

1947A40

Fig. 11

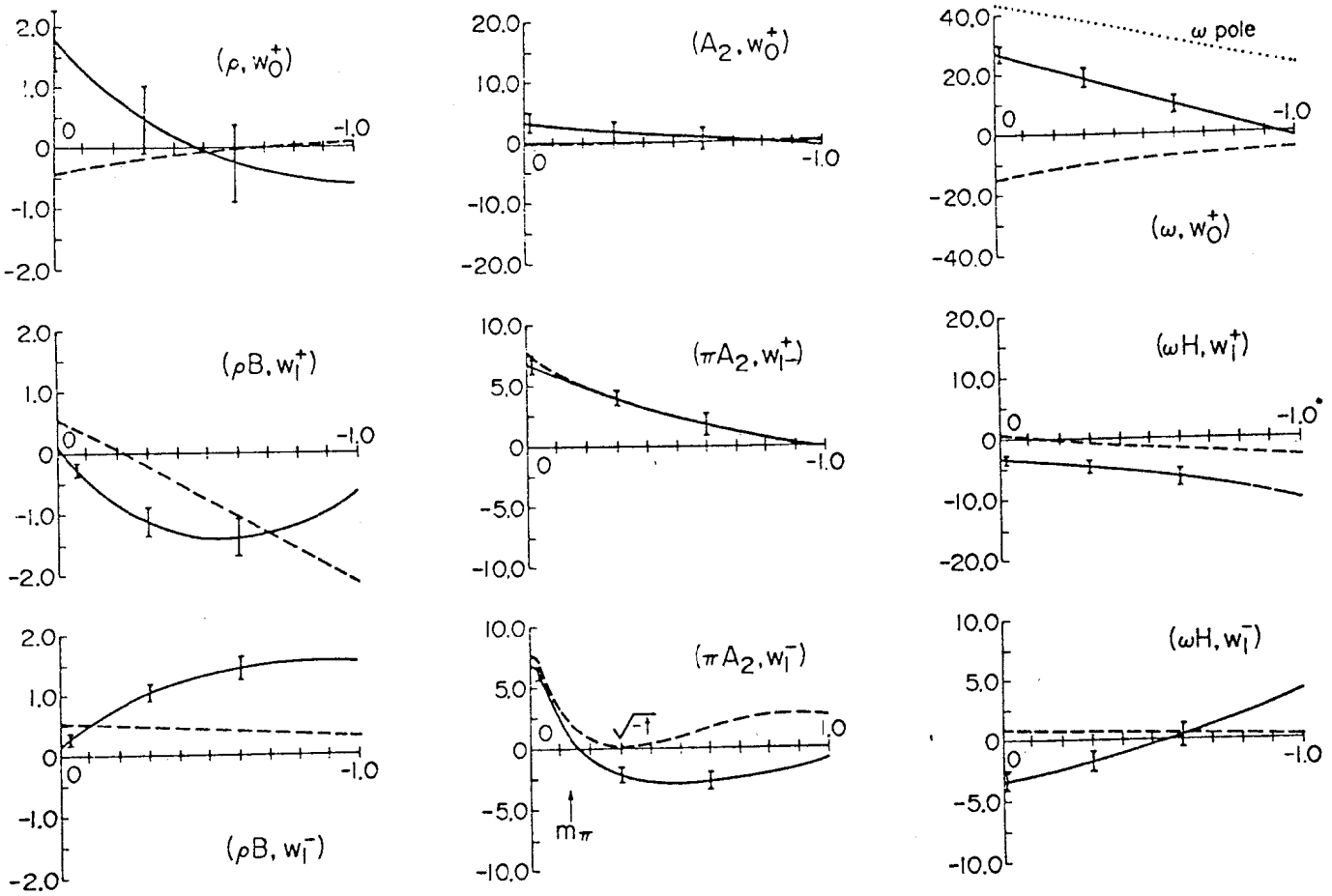
(ρ, w_0^+)
(A_2, w_0^+)
ω pole
(ω, w_0^+)
$(\rho B, w_1^+)$
$(\pi A_2, w_{1-}^+)$
$(\omega H, w_1^+)$
$(\rho B, w_1^-)$
$(\pi A_2, w_1^-)$
$(\omega H, w_1^-)$
$\sqrt{-t}$
m_π
FESR
SCRAM fit
Plotted as functions of momentum transfer, t, except where indicated.
1947A39

Fig. 12

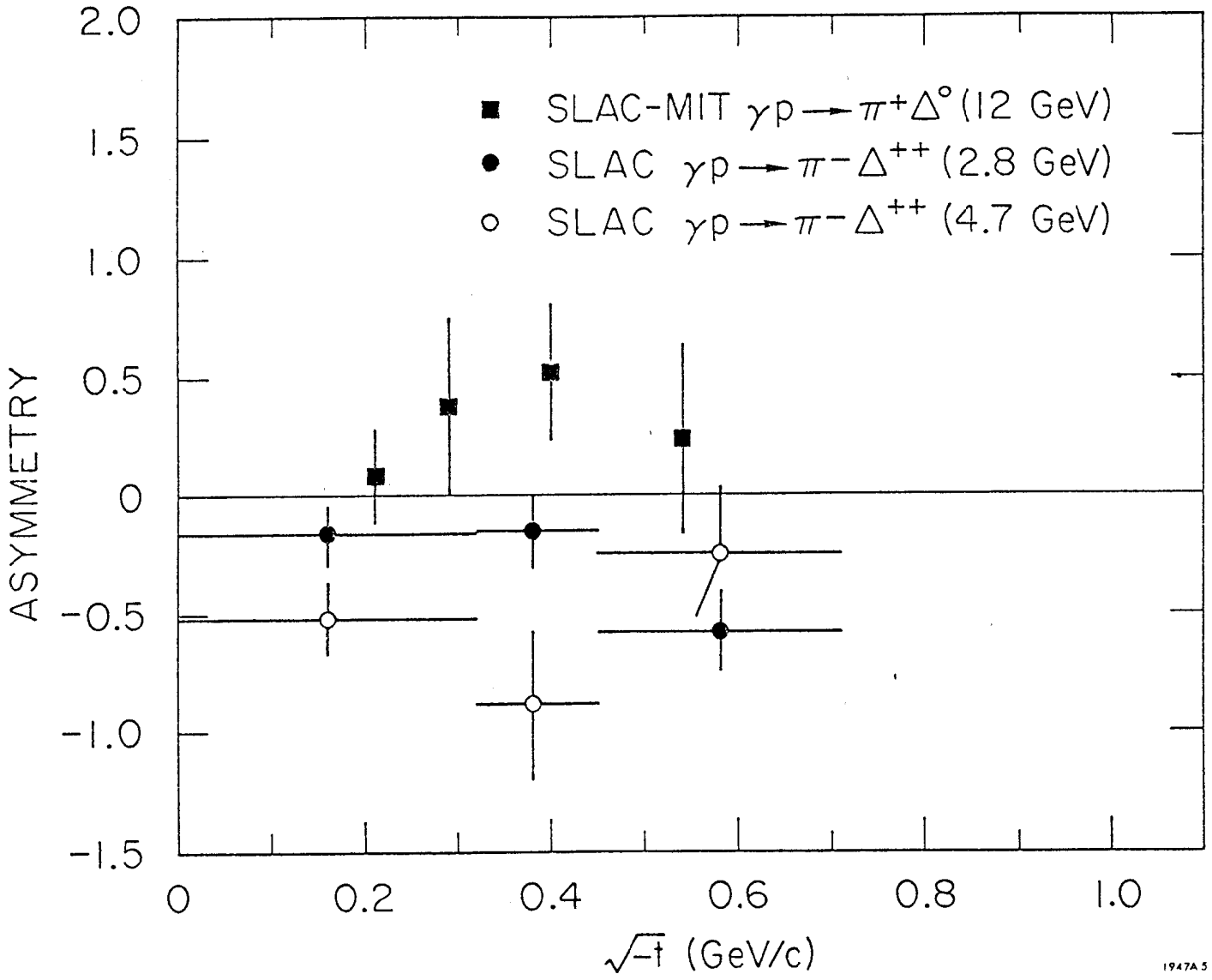
SLAC-MIT γp → π+Δ°(12 GeV)
SLAC γp → π−Δ++(2.8 GeV)
SLAC γp → π−Δ++(4.7 GeV)
ASYMMETRY
2.0
1.5
1.0
0.5
0
−0.5
−1.0
−1.5
0
0.2
0.4
0.6
0.8
1.0
√−t (GeV/c)
1947A5

Fig. 13

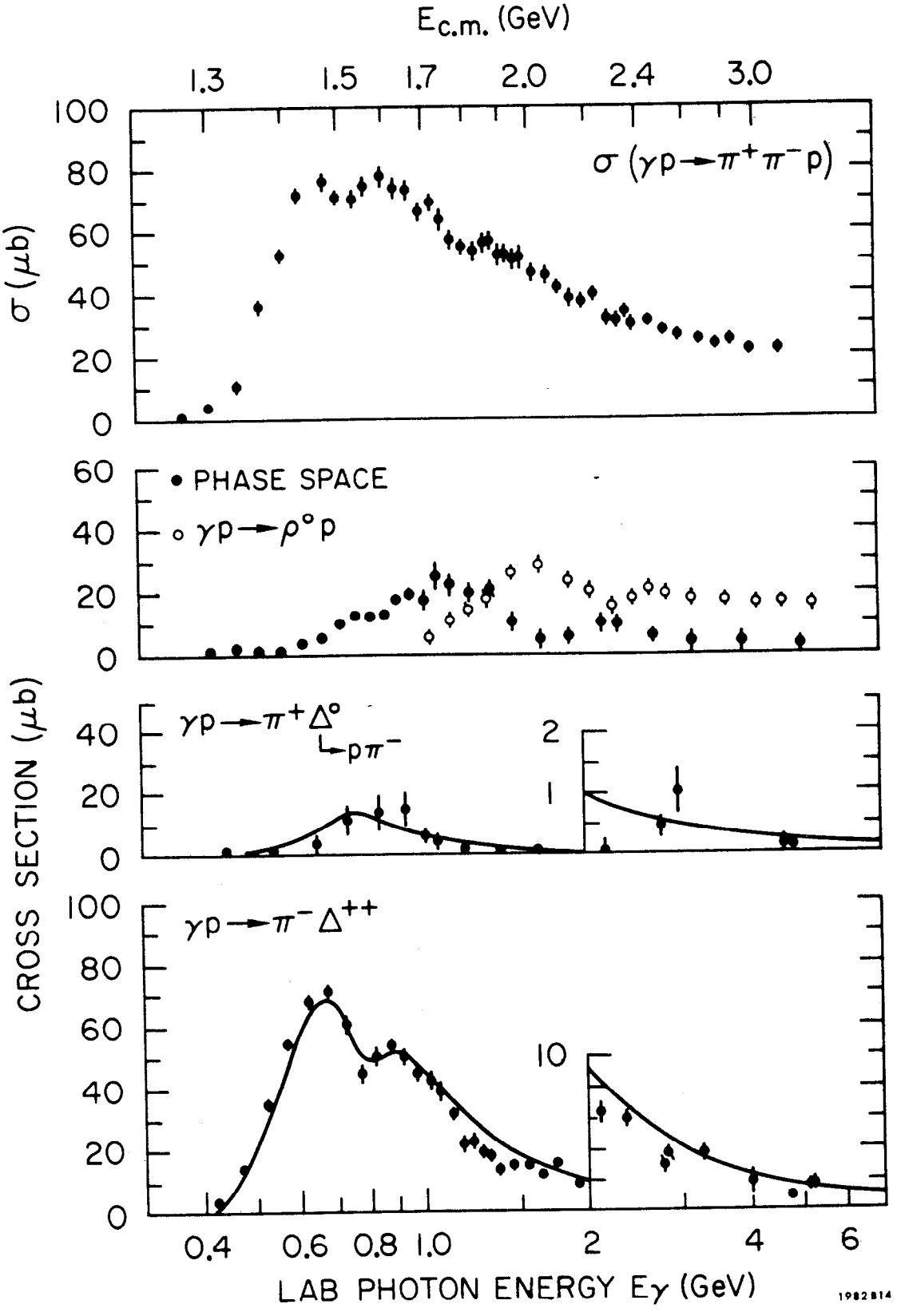
E c.m. (GeV)
1.3
1.5
1.7
2.0
2.4
3.0
σ (μb)
σ (γp→π⁺π⁻p)
• PHASE SPACE
∘ γp→ρ°p
γp→π⁺Δ°
↳pπ⁻
γp→π⁻Δ⁺⁺
CROSS SECTION (μb)
LAB PHOTON ENERGY Eγ (GeV)
1982B14

Fig. 14

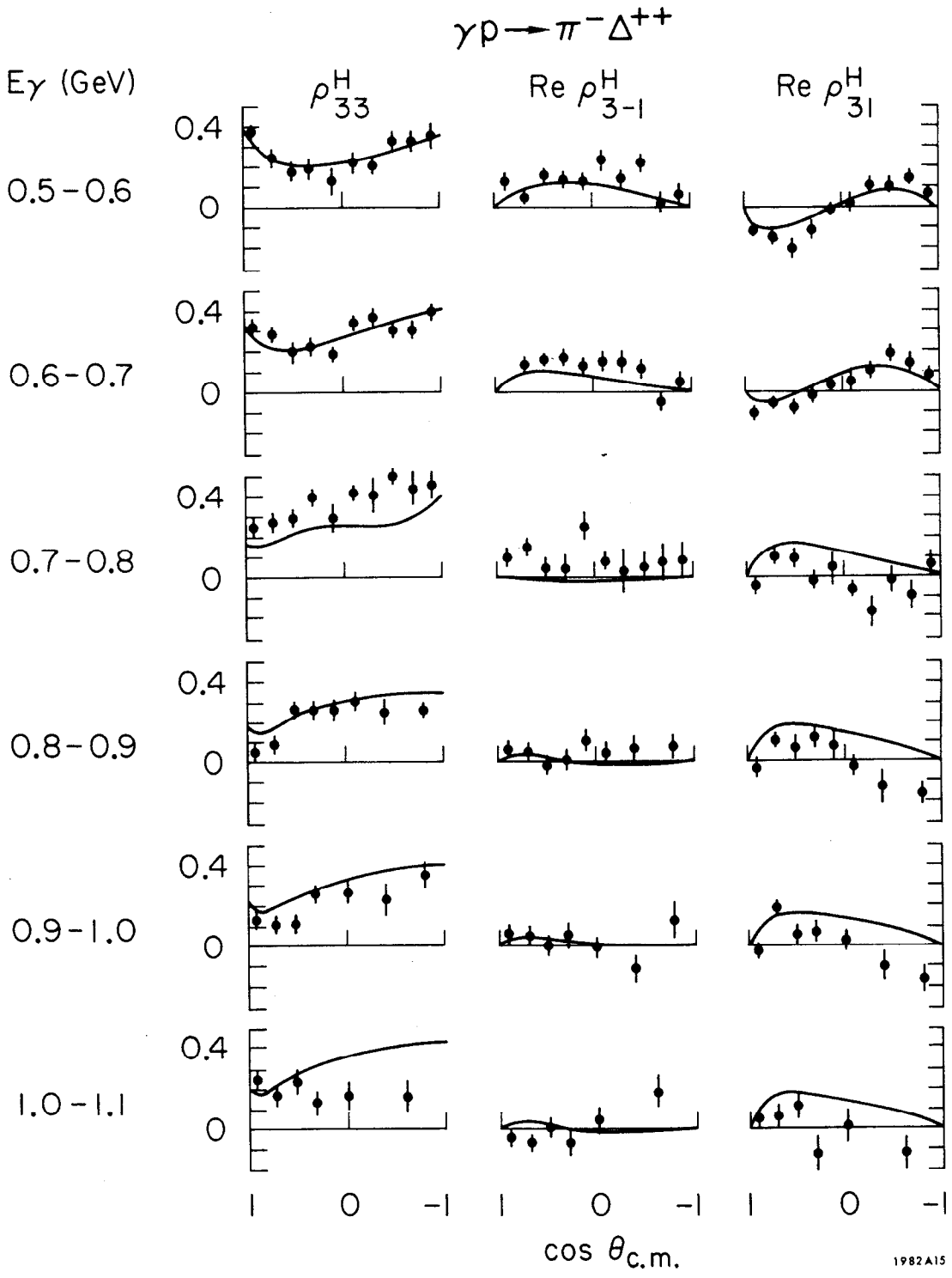
γp → π⁻Δ⁺⁺
Eγ (GeV)
ρ^H_{33}
Re ρ^H_{3-1}
Re ρ^H_{31}
0.5 - 0.6
0.6 - 0.7
0.7 - 0.8
0.8 - 0.9
0.9 - 1.0
1.0 - 1.1
0.4
0
1
0
-1
cos $\theta_{c.m.}$
1982A15

Fig. 15

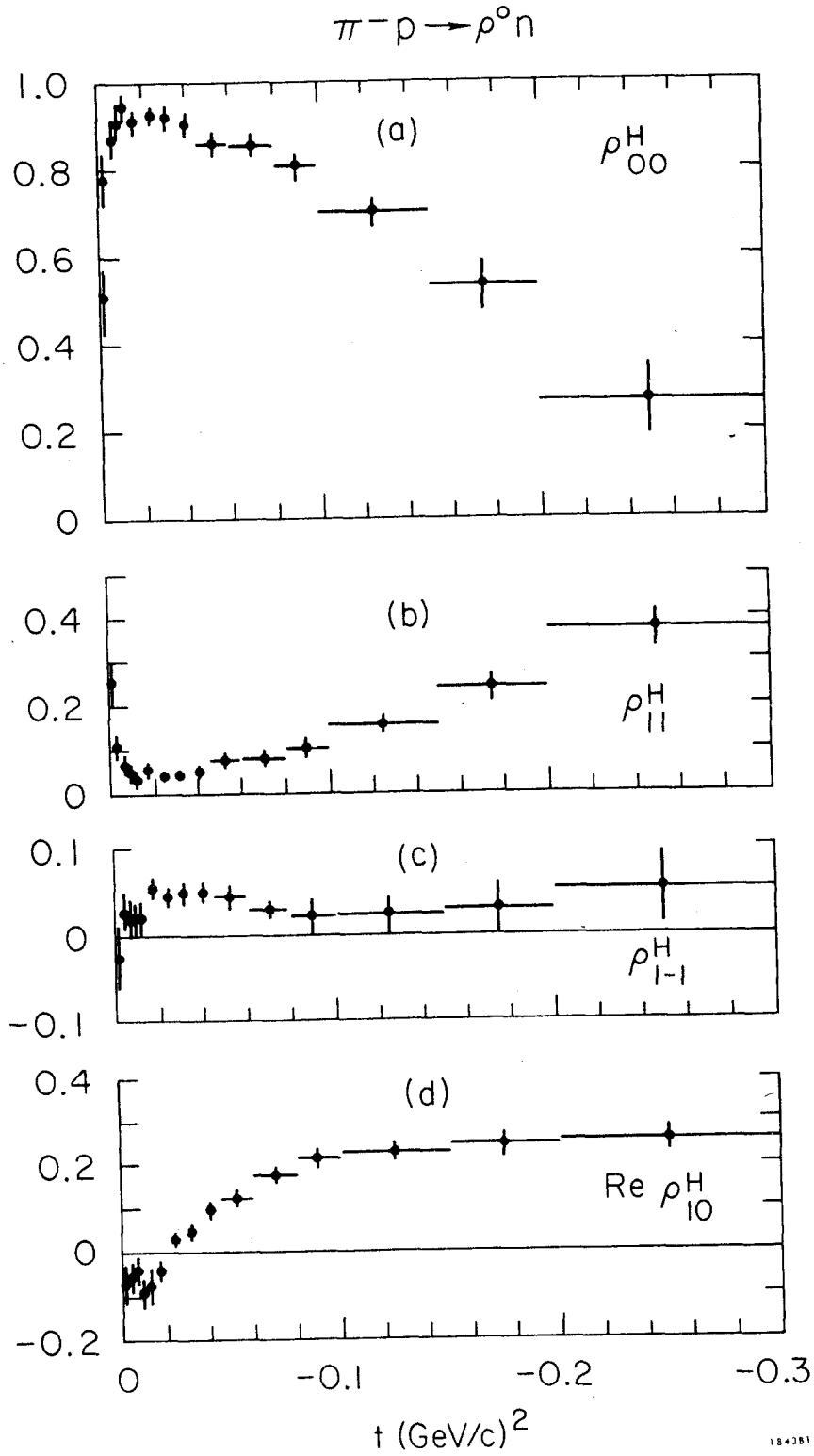
$\pi^- p \to \rho^0 n$
(a)
ρ^H_{00}
(b)
ρ^H_{11}
(c)
ρ^H_{1-1}
(d)
Re ρ^H_{10}
1.0
0.8
0.6
0.4
0.2
0
0.4
0.2
0
0.1
0
-0.1
0.4
0.2
0
-0.2
0
-0.1
-0.2
-0.3
t (GeV/c)^2
184381

Fig. 16

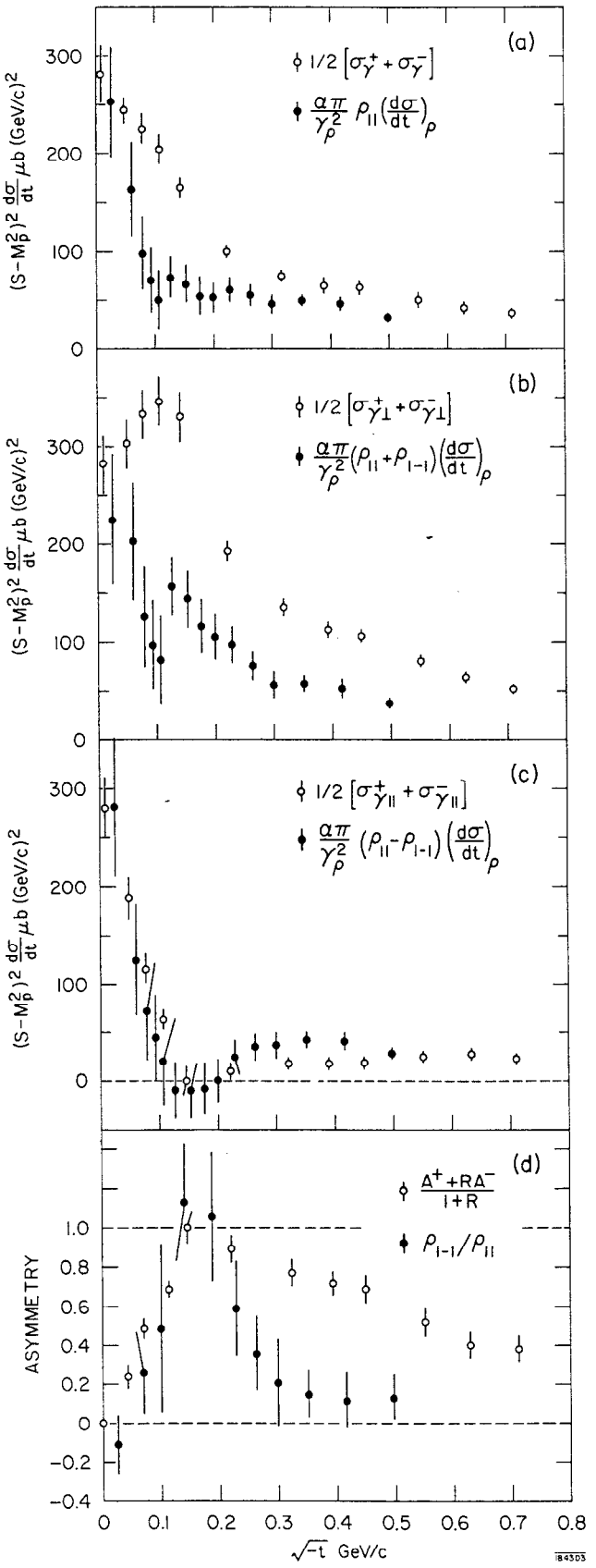
(a)
(b)
(c)
(d)
$\frac{1}{2}[\sigma^{+}_{\gamma} + \sigma^{-}_{\gamma}]$
$\frac{\alpha\pi}{\gamma_\rho^2}\rho_{11}\left(\frac{d\sigma}{dt}\right)_\rho$
$\frac{1}{2}[\sigma^{+}_{\gamma\perp} + \sigma^{-}_{\gamma\perp}]$
$\frac{\alpha\pi}{\gamma_\rho^2}(\rho_{11}+\rho_{1-1})\left(\frac{d\sigma}{dt}\right)_\rho$
$\frac{1}{2}[\sigma^{+}_{\gamma\parallel} + \sigma^{-}_{\gamma\parallel}]$
$\frac{\alpha\pi}{\gamma_\rho^2}(\rho_{11}-\rho_{1-1})\left(\frac{d\sigma}{dt}\right)_\rho$
$(S-M_p^2)^2\frac{d\sigma}{dt}\mu b\,(GeV/c)^2$
$\frac{A^{+}+RA^{-}}{1+R}$
ρ_{1-1}/ρ_{11}
ASYMMETRY
$\sqrt{-t}$ GeV/c
184303

Fig. 17

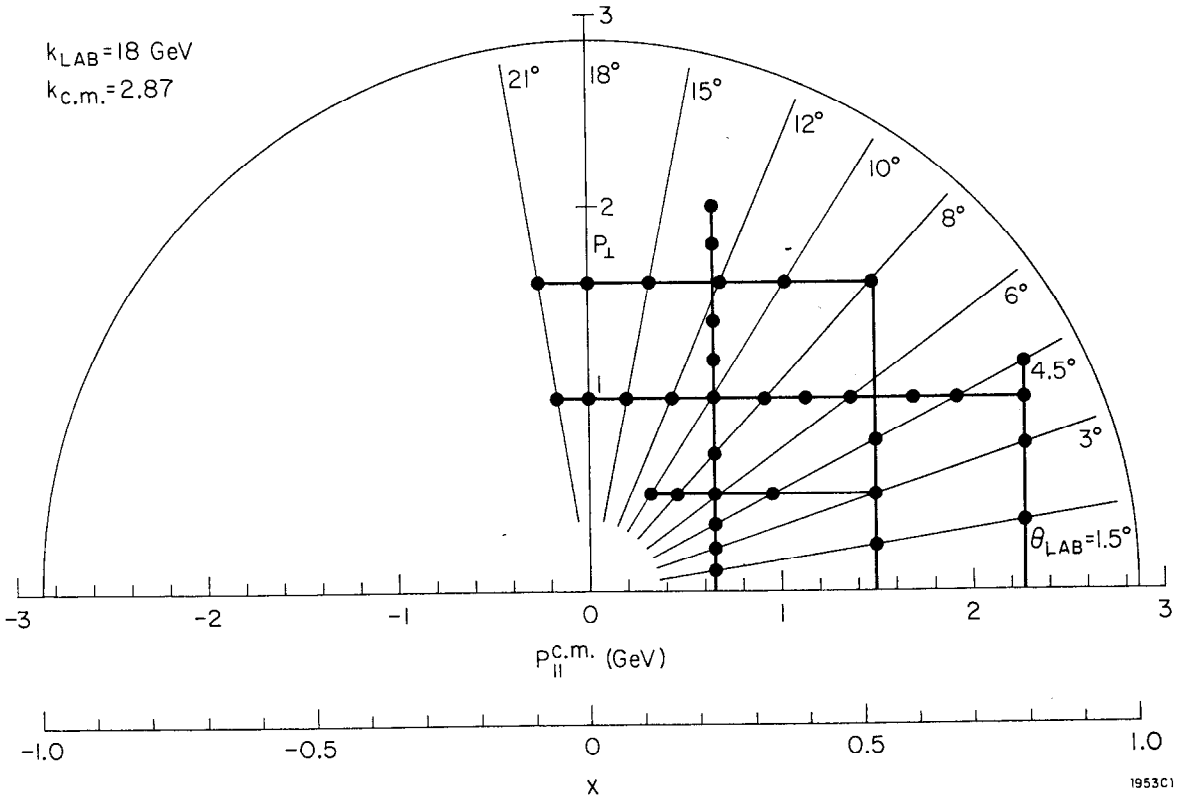
k_{LAB}=18 GeV
$k_{c.m.}$=2.87
21°
18°
15°
12°
10°
8°
6°
4.5°
3°
θ_{LAB}=1.5°
3
2
$P_\perp$
1
-3
-2
-1
0
1
2
3
$P_{||}^{c.m.}$ (GeV)
-1.0
-0.5
0
0.5
1.0
X
1953C1

Fig. 18

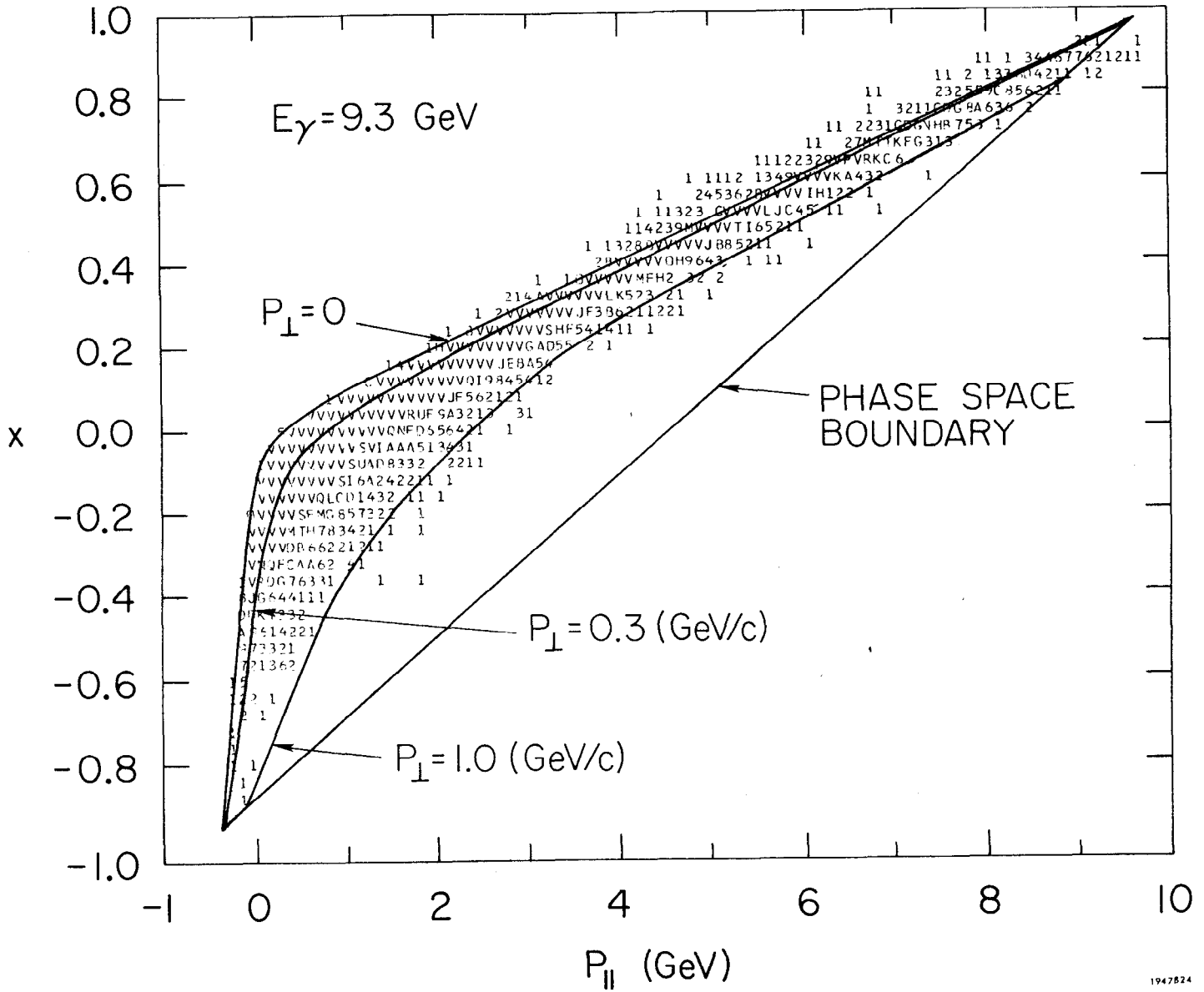
1.0
0.8
0.6
0.4
0.2
0.0
-0.2
-0.4
-0.6
-0.8
-1.0
x
-1
0
2
4
6
8
10
$P_{||}$ (GeV)
E_γ = 9.3 GeV
$P_\perp$ = 0
$P_\perp$ = 0.3 (GeV/c)
$P_\perp$ = 1.0 (GeV/c)
PHASE SPACE BOUNDARY
1947824

Fig. 19

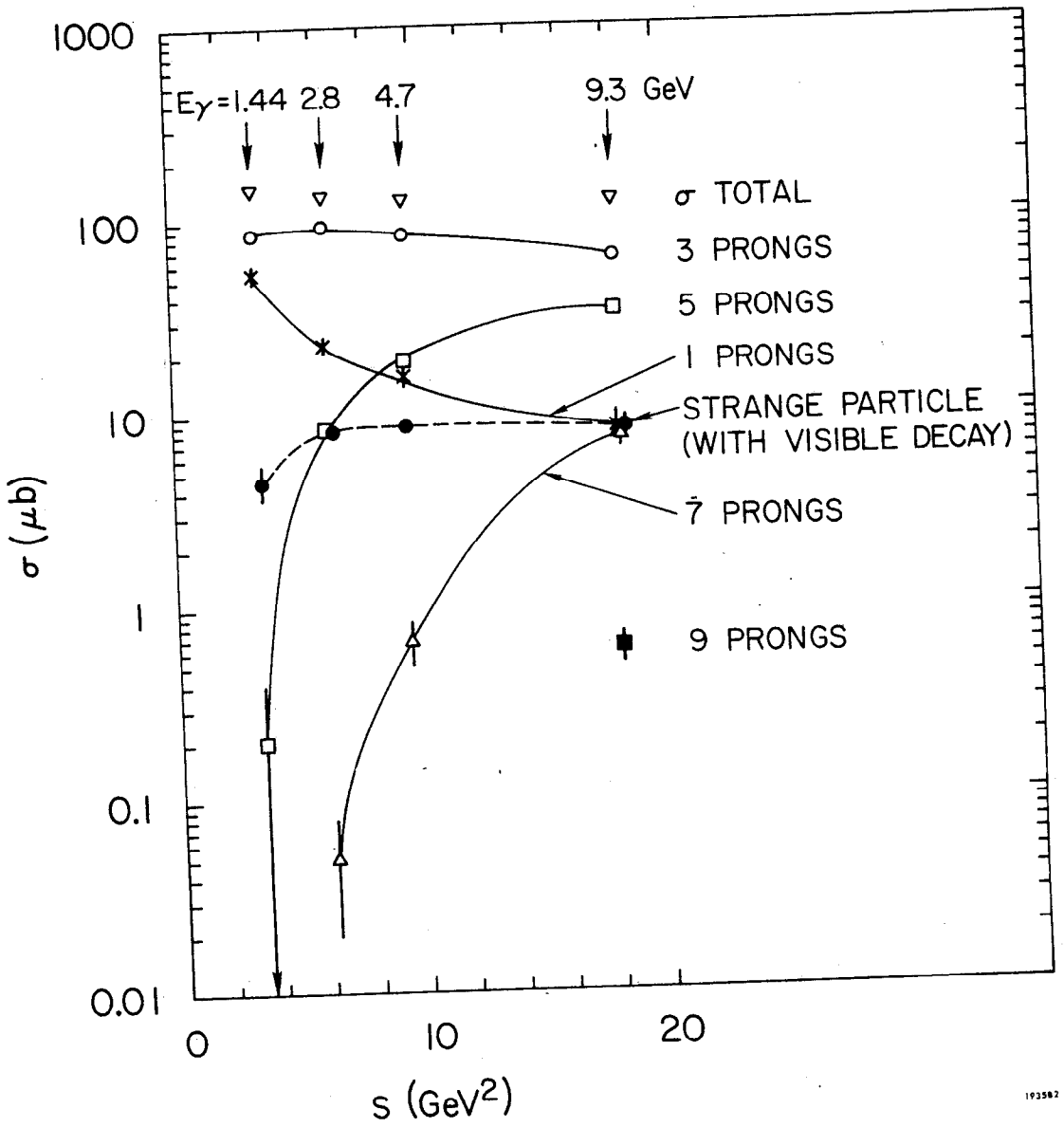
1000
100
10
1
0.1
0.01
σ (μb)
Eγ=1.44 2.8 4.7
9.3 GeV
σ TOTAL
3 PRONGS
5 PRONGS
1 PRONGS
STRANGE PARTICLE
(WITH VISIBLE DECAY)
7̄ PRONGS
9 PRONGS
0
10
20
s (GeV²)
193582

Fig. 20

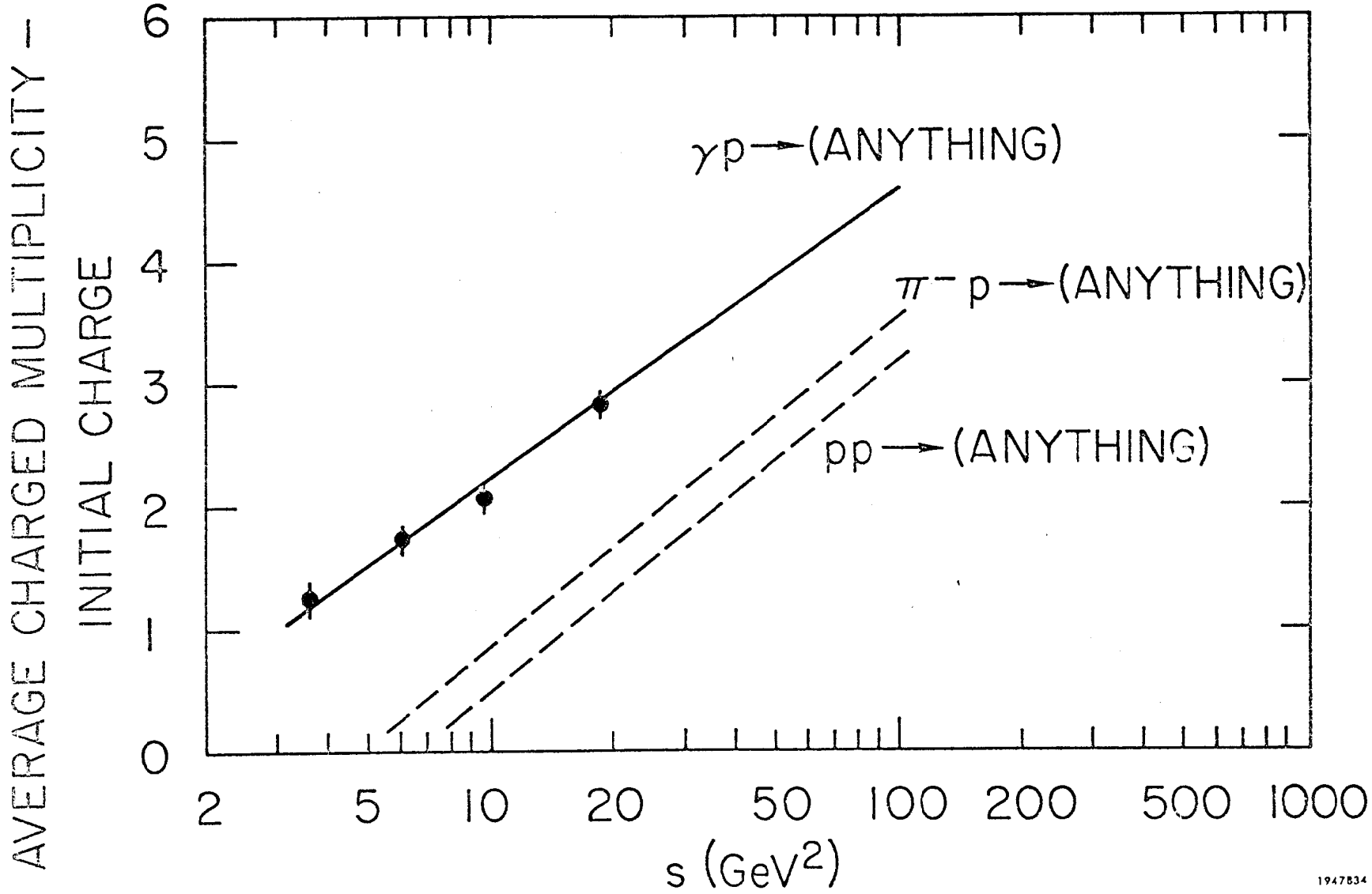
AVERAGE CHARGED MULTIPLICITY - INITIAL CHARGE
0
1
2
3
4
5
6
2
5
10
20
50
100
200
500
1000
s (GeV²)
γp → (ANYTHING)
π⁻p → (ANYTHING)
pp → (ANYTHING)
1947B34

Fig. 21

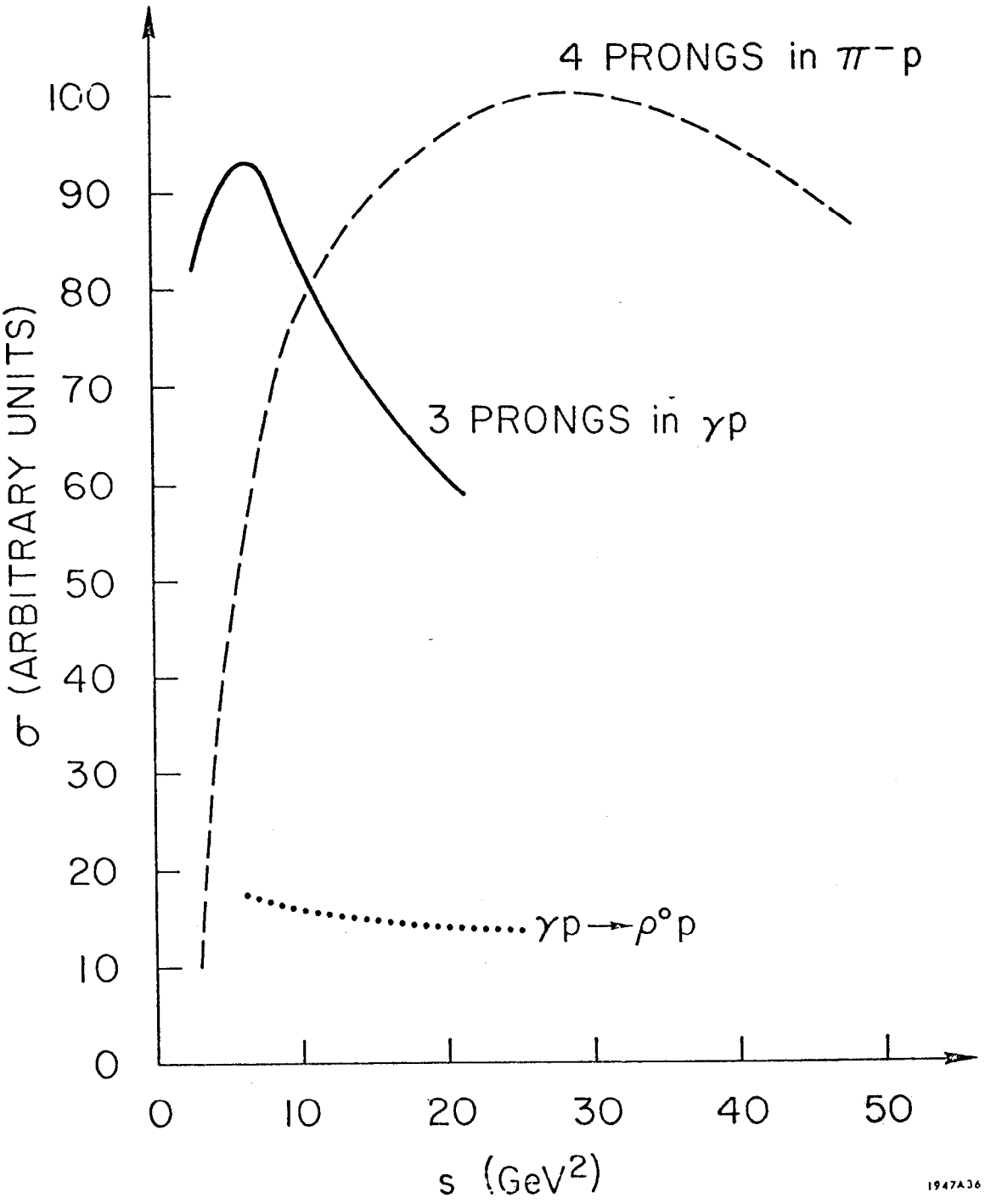
4 PRONGS in π^-p
3 PRONGS in γp
γp → ρ^0p
σ (ARBITRARY UNITS)
s (GeV²)
0
10
20
30
40
50
60
70
80
90
100
1947A36

Fig. 22

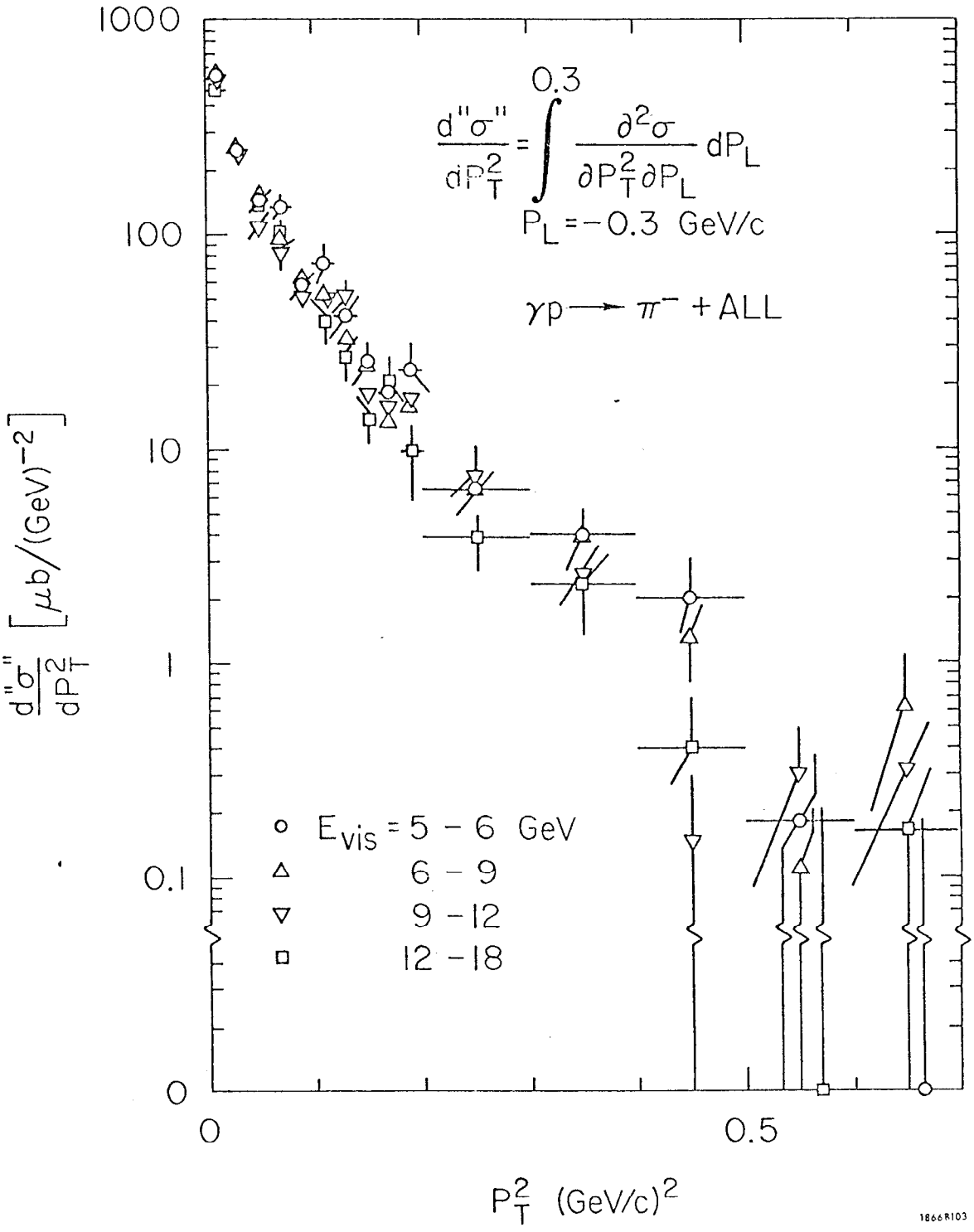
1000
100
10
1
0.1
0
0
0.5
$\frac{d''\sigma''}{dP_T^2}$ [μb/(GeV)$^{-2}$]
P_T^2 (GeV/c)^2
$\frac{d''\sigma''}{dP_T^2} = \int_{P_L=-0.3\ GeV/c}^{0.3} \frac{\partial^2\sigma}{\partial P_T^2 \partial P_L} dP_L$
$\gamma p \rightarrow \pi^- + ALL$
E_{vis} = 5 - 6 GeV
6 - 9
9 - 12
12 - 18
1866R103

Fig. 23

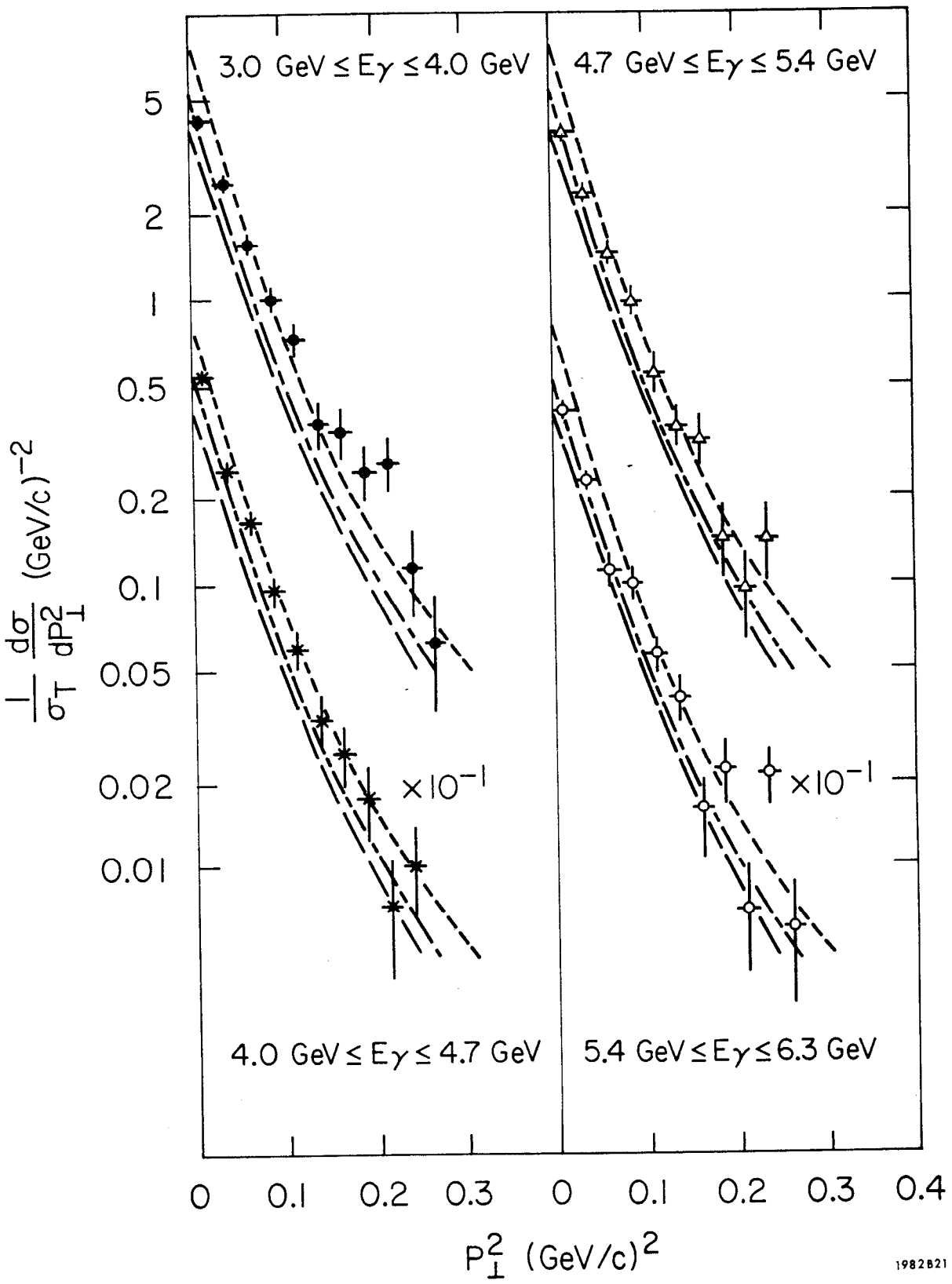
3.0 GeV ≤ Eγ ≤ 4.0 GeV
4.7 GeV ≤ Eγ ≤ 5.4 GeV
4.0 GeV ≤ Eγ ≤ 4.7 GeV
5.4 GeV ≤ Eγ ≤ 6.3 GeV
×10⁻¹
×10⁻¹
1/σT dσ/dP²⊥ (GeV/c)⁻²
P²⊥ (GeV/c)²
5
2
1
0.5
0.2
0.1
0.05
0.02
0.01
0
0.1
0.2
0.3
0
0.1
0.2
0.3
0.4
1982B21

Fig. 24

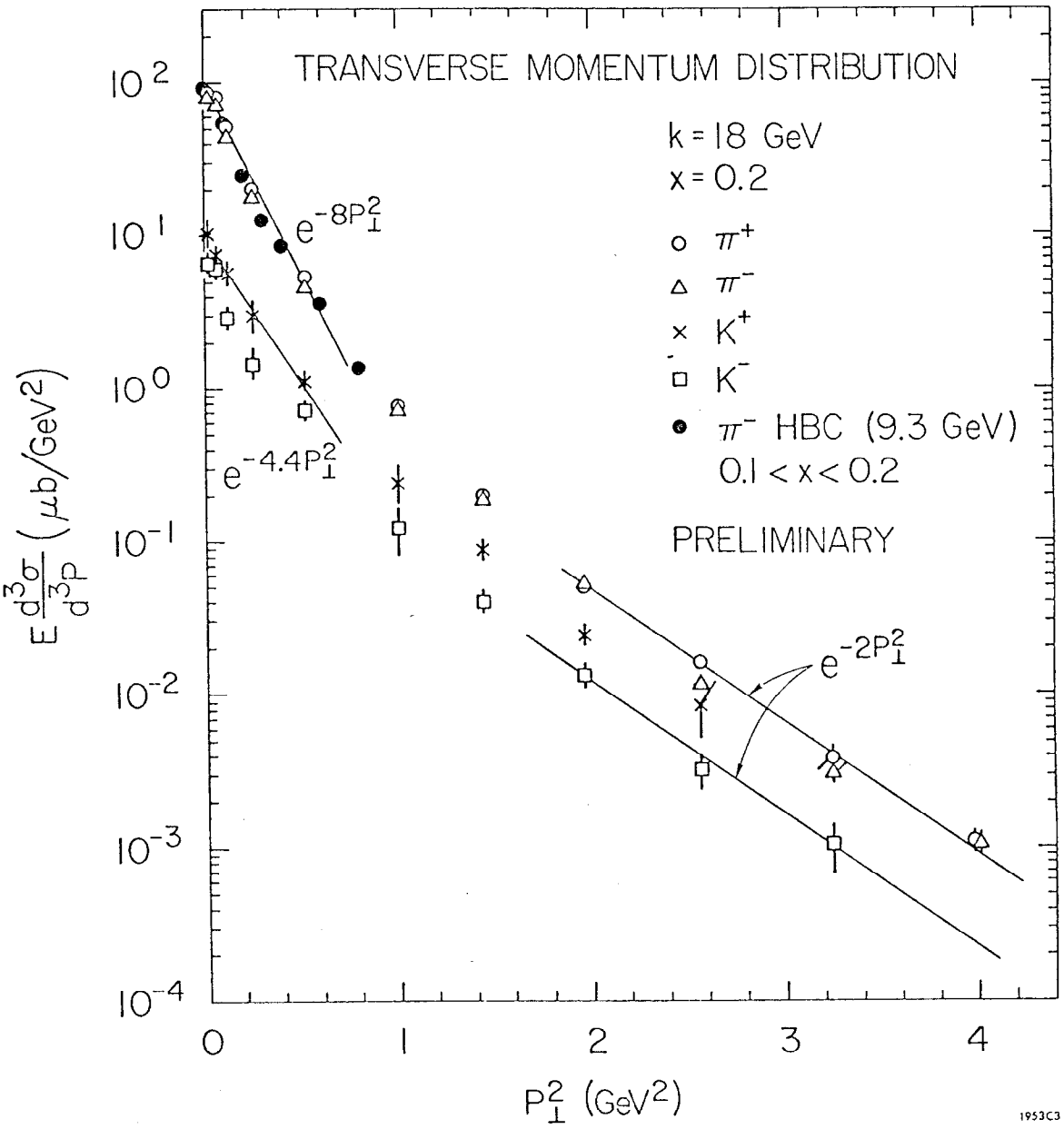
TRANSVERSE MOMENTUM DISTRIBUTION
k = 18 GeV
x = 0.2
π+
π−
K+
K−
π− HBC (9.3 GeV)
0.1 < x < 0.2
PRELIMINARY
e^-8P⊥²
e^-4.4P⊥²
e^-2P⊥²
E d³σ/d³p (μb/GeV²)
P⊥² (GeV²)
10²
10¹
10⁰
10⁻¹
10⁻²
10⁻³
10⁻⁴
0
1
2
3
4
1953C3

Fig. 25

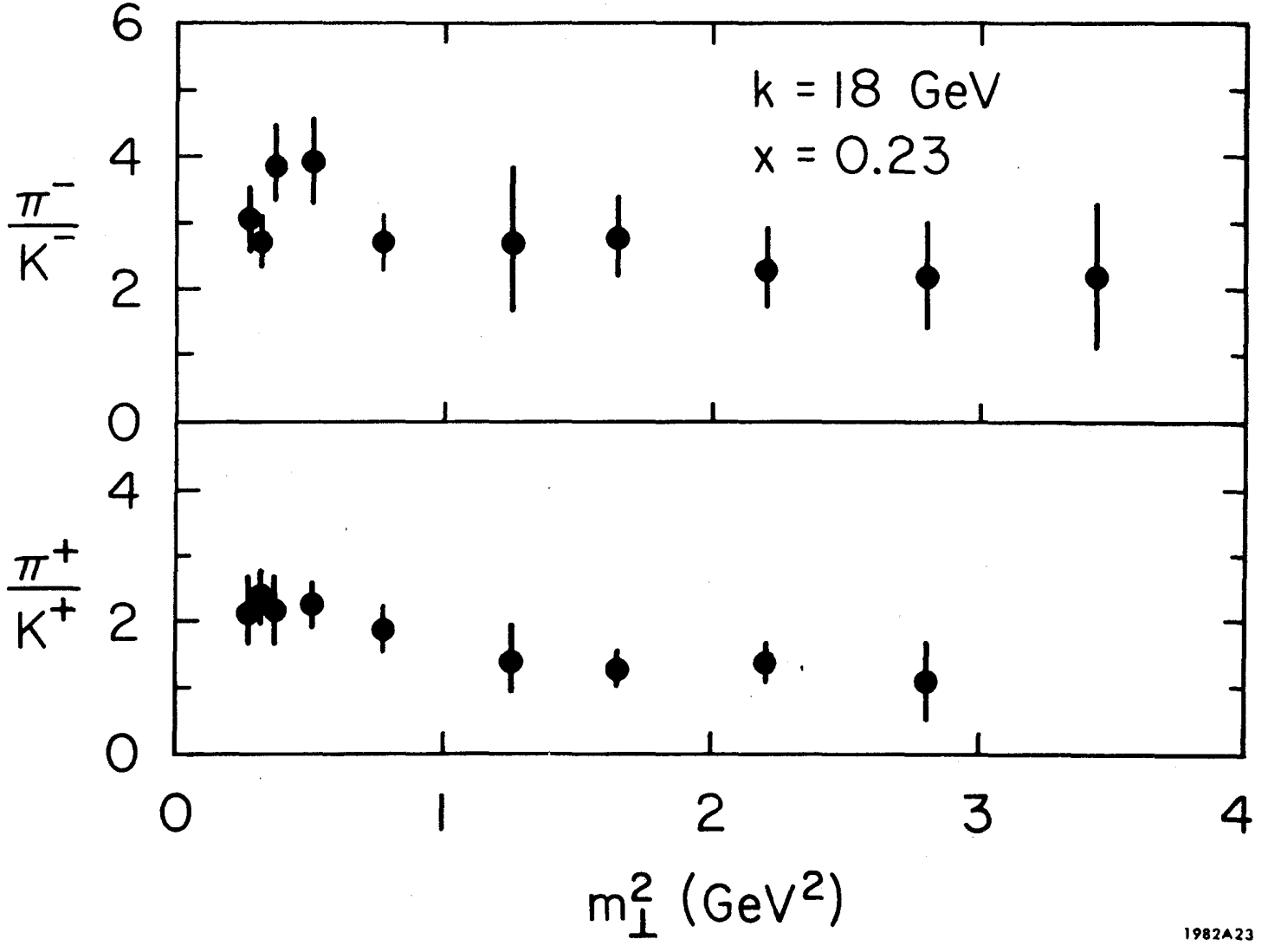
k = 18 GeV
x = 0.23
$\frac{\pi^-}{K^-}$
$\frac{\pi^+}{K^+}$
6
4
2
0
4
2
0
0
1
2
3
4
$m_\perp^2$ (GeV^2)
1982A23

Fig. 26

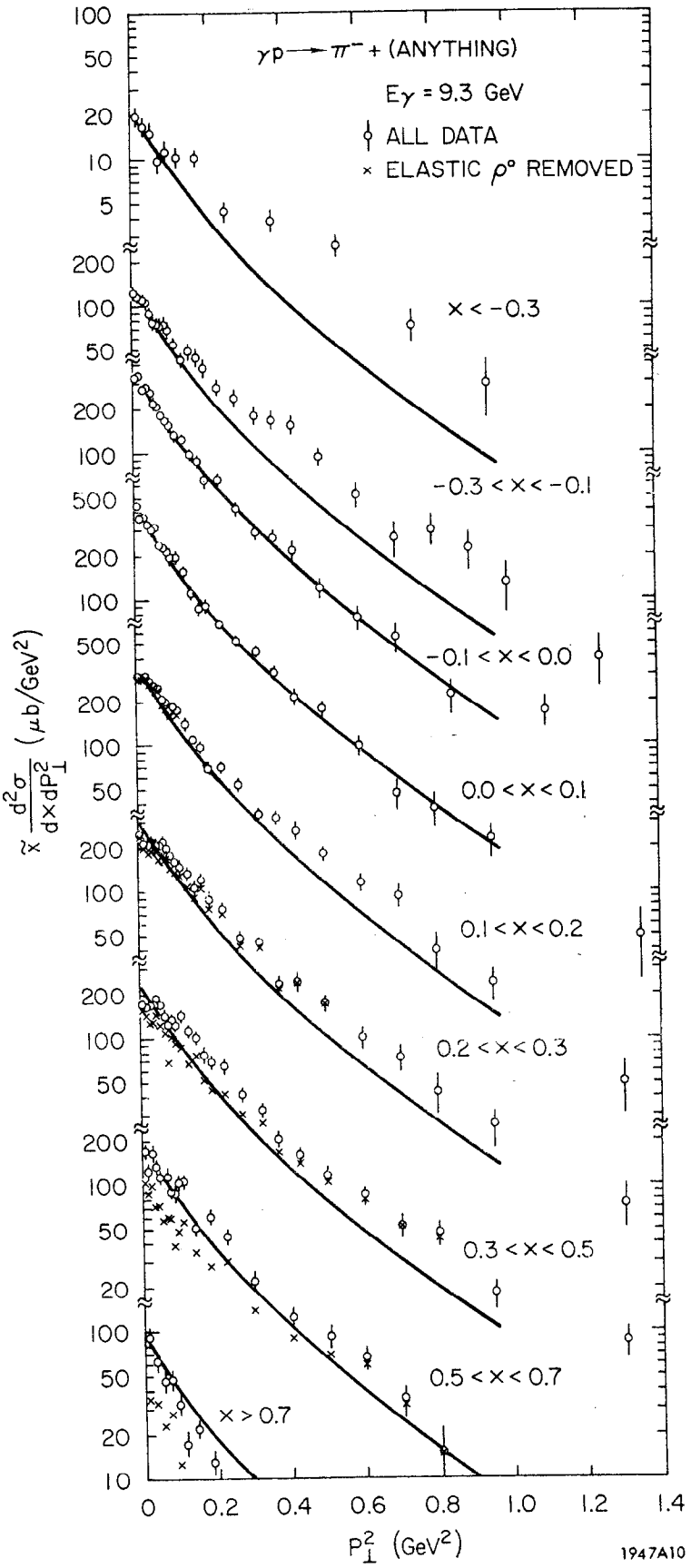
γp → π⁻ + (ANYTHING)
Eγ = 9.3 GeV
ALL DATA
× ELASTIC ρ° REMOVED
x < −0.3
−0.3 < x < −0.1
−0.1 < x < 0.0
0.0 < x < 0.1
0.1 < x < 0.2
0.2 < x < 0.3
0.3 < x < 0.5
0.5 < x < 0.7
x > 0.7
$\tilde{x}\frac{d^2\sigma}{dx\,dP_T^2}$ (μb/GeV²)
P_T^2 (GeV²)
1947A10

Fig. 27

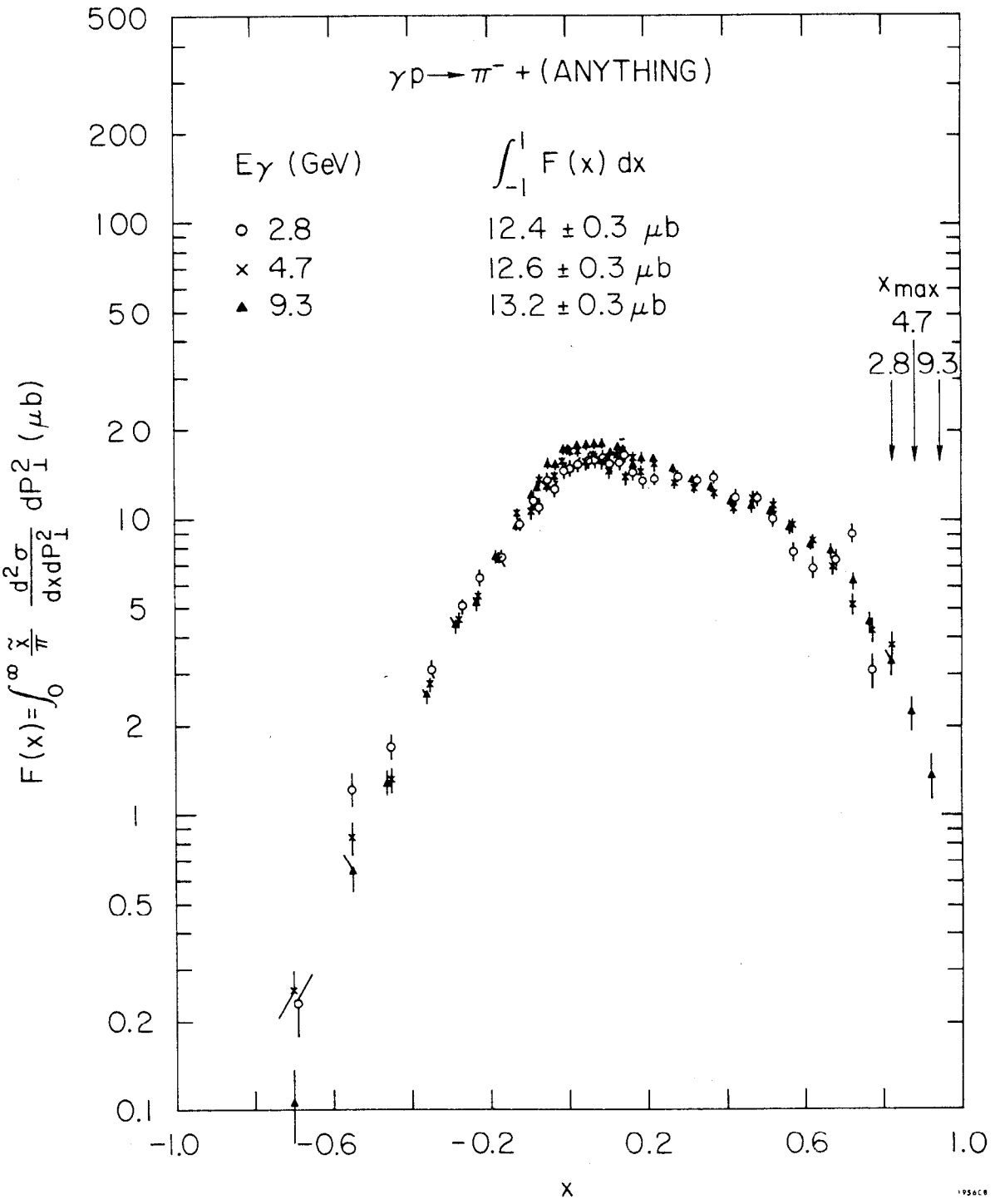
γp → π⁻ + (ANYTHING)
Eγ (GeV)
∫ F(x) dx
o 2.8
12.4 ± 0.3 μb
× 4.7
12.6 ± 0.3 μb
▲ 9.3
13.2 ± 0.3 μb
x max
4.7
2.8 9.3
F(x)=∫ x̃/π d²σ/dxdP²⊥ dP²⊥ (μb)
500
200
100
50
20
10
5
2
1
0.5
0.2
0.1
-1.0
-0.6
-0.2
0.2
0.6
1.0
x

Fig. 28

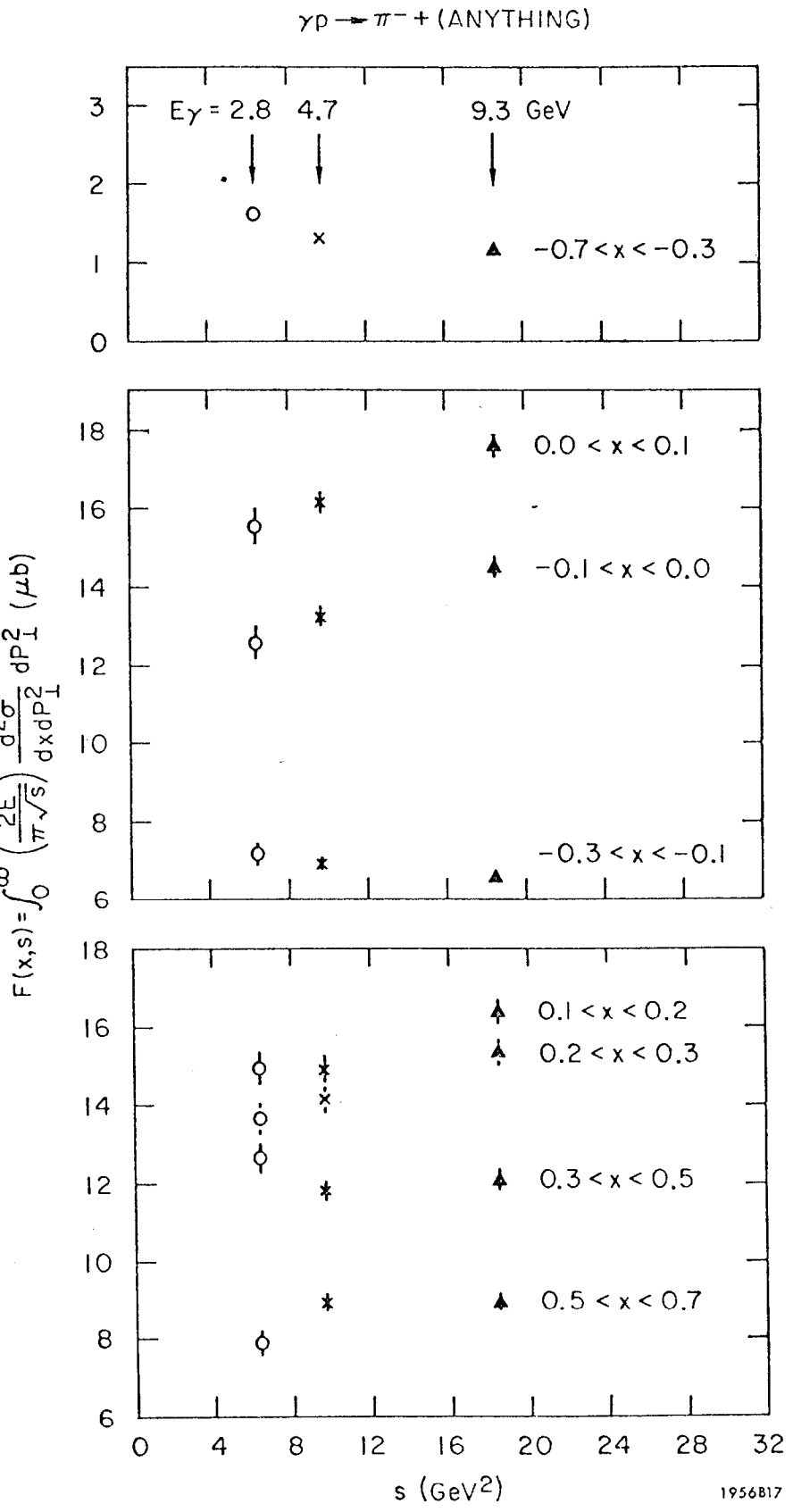
γp → π⁻ + (ANYTHING)
Eγ = 2.8
4.7
9.3 GeV
−0.7 < x < −0.3
0.0 < x < 0.1
−0.1 < x < 0.0
−0.3 < x < −0.1
0.1 < x < 0.2
0.2 < x < 0.3
0.3 < x < 0.5
0.5 < x < 0.7
F(x,s) = ∫₀^∞ (2E/π√s) d²σ/dx dP_T² dP_T² (μb)
s (GeV²)
1956B17

Fig. 29

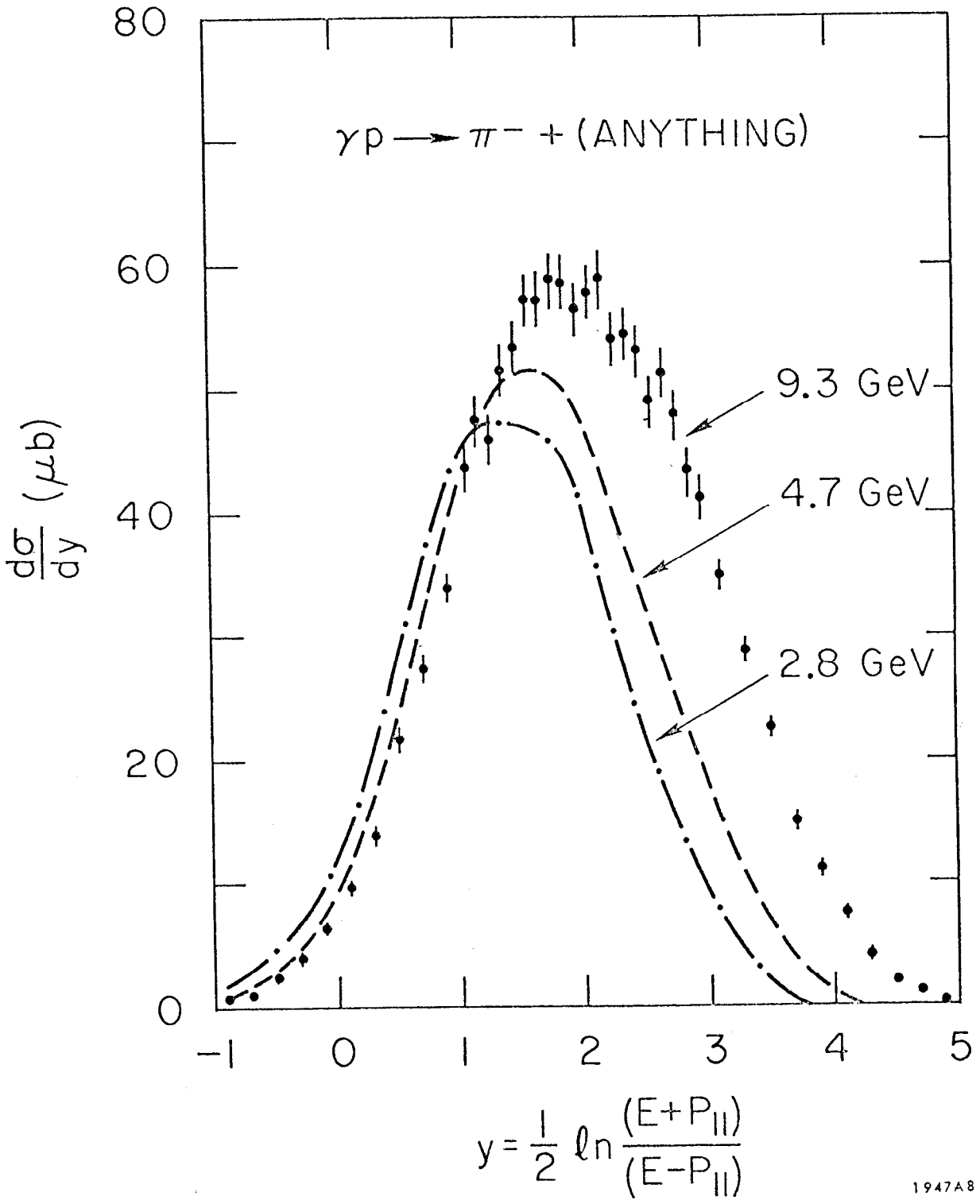
80
60
40
20
0
$\gamma p \longrightarrow \pi^- + (ANYTHING)$
9.3 GeV
4.7 GeV
2.8 GeV
$\frac{d\sigma}{dy}$ (μb)
-1
0
1
2
3
4
5
$y = \frac{1}{2} \ell n \frac{(E+P_{||})}{(E-P_{||})}$
1947A8

Fig. 30

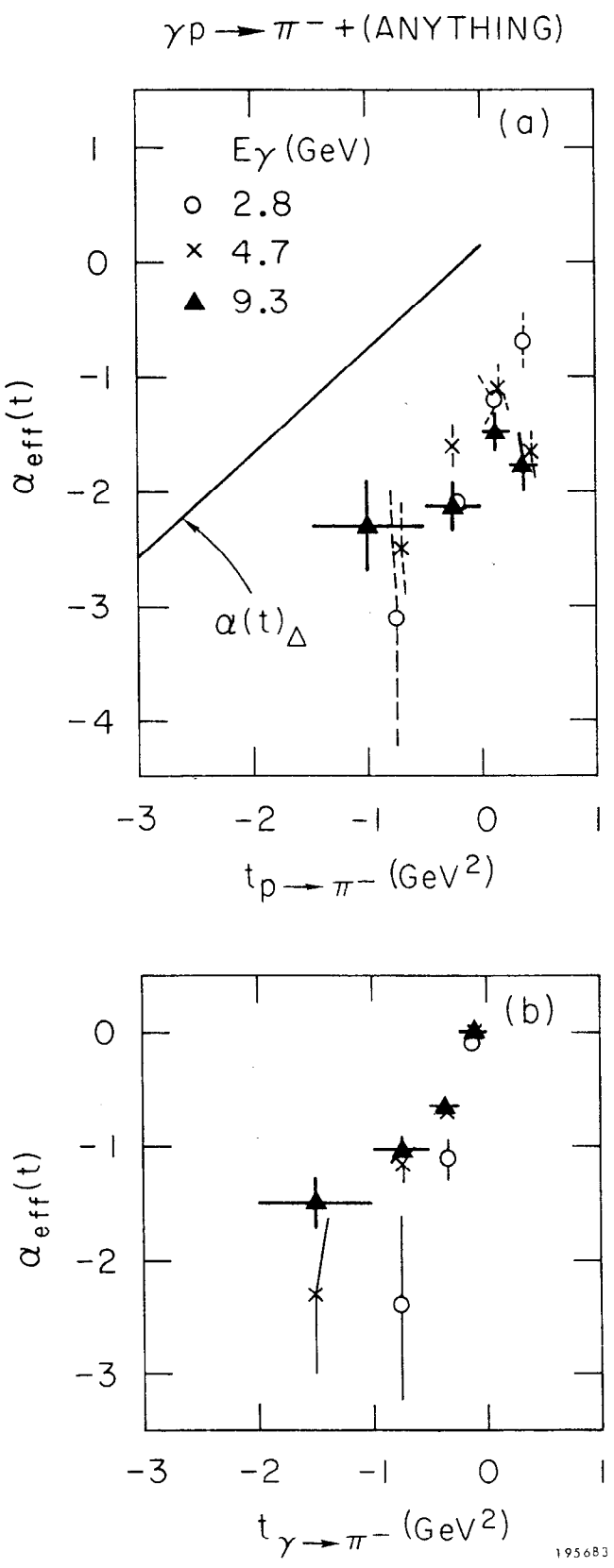
γp → π⁻ + (ANYTHING)
(a)
Eγ (GeV)
o 2.8
× 4.7
▲ 9.3
α(t)Δ
α eff (t)
t p → π⁻ (GeV²)
(b)
α eff (t)
t γ → π⁻ (GeV²)
195683

Fig. 31

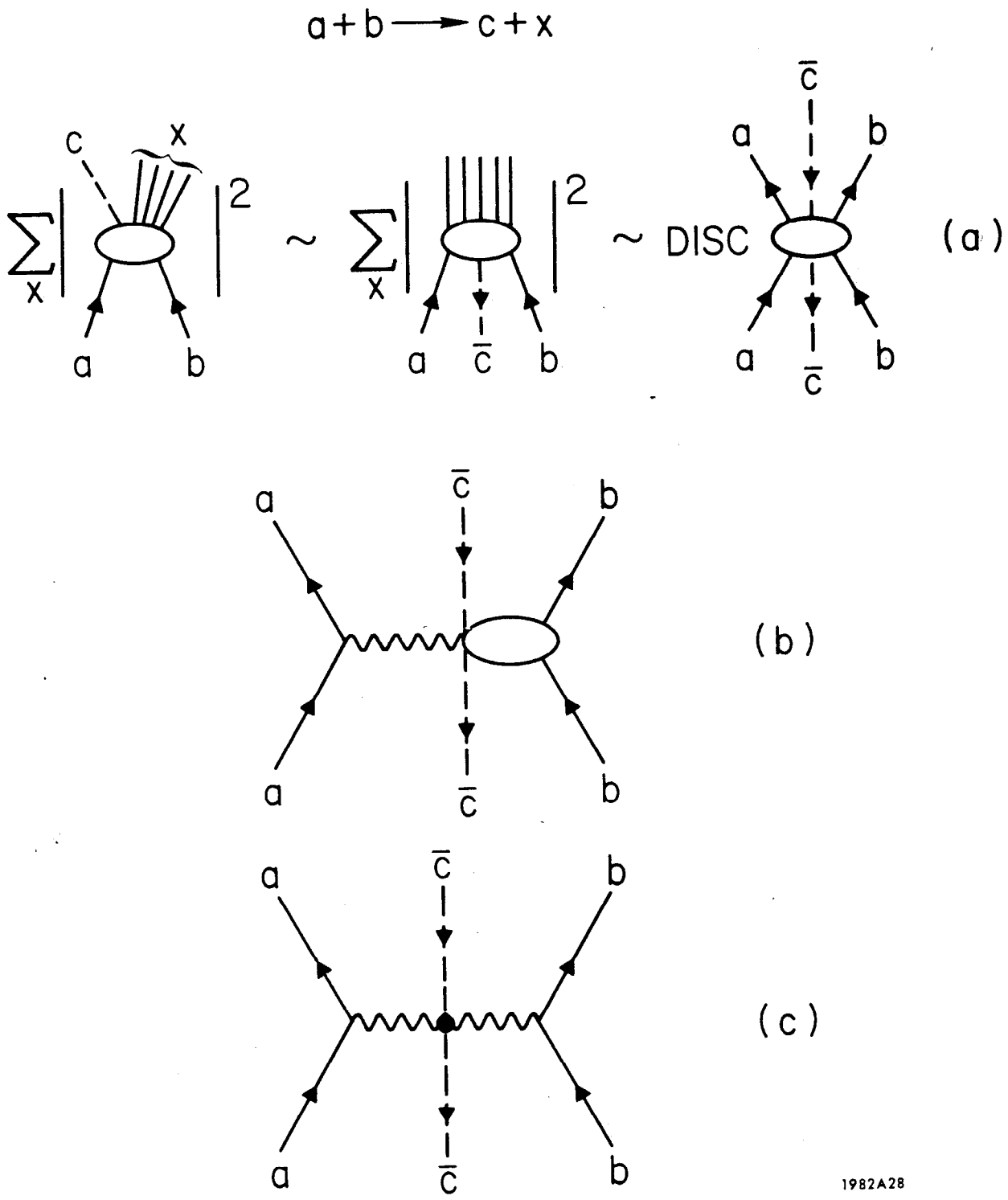

Fig. 32

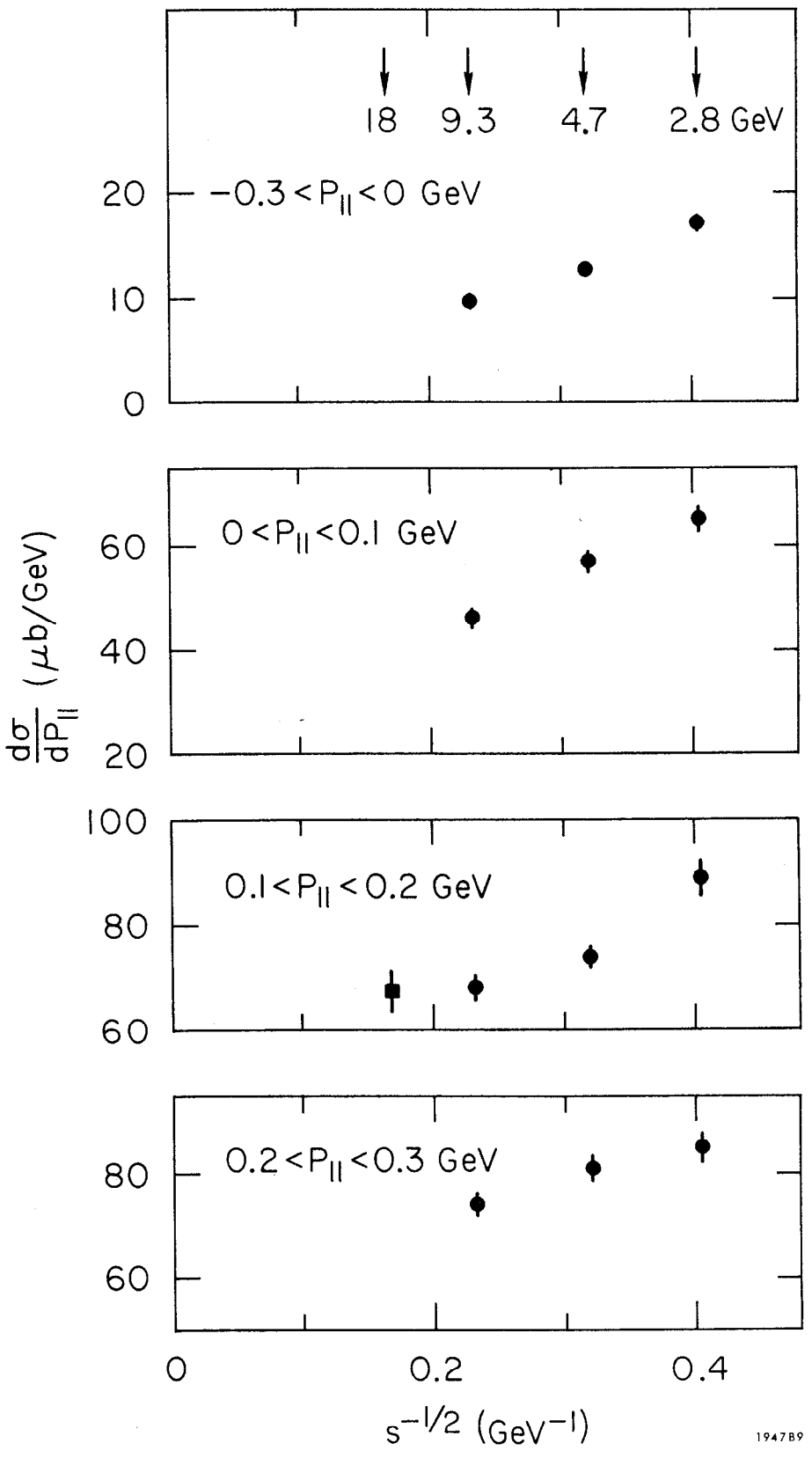
18
9.3
4.7
2.8 GeV
$-0.3 < P_{ll} < 0$ GeV
$0 < P_{ll} < 0.1$ GeV
$0.1 < P_{ll} < 0.2$ GeV
$0.2 < P_{ll} < 0.3$ GeV
$\frac{d\sigma}{dP_{ll}}$ (μb/GeV)
$s^{-1/2}$ (GeV^{-1})
194789

Fig. 33

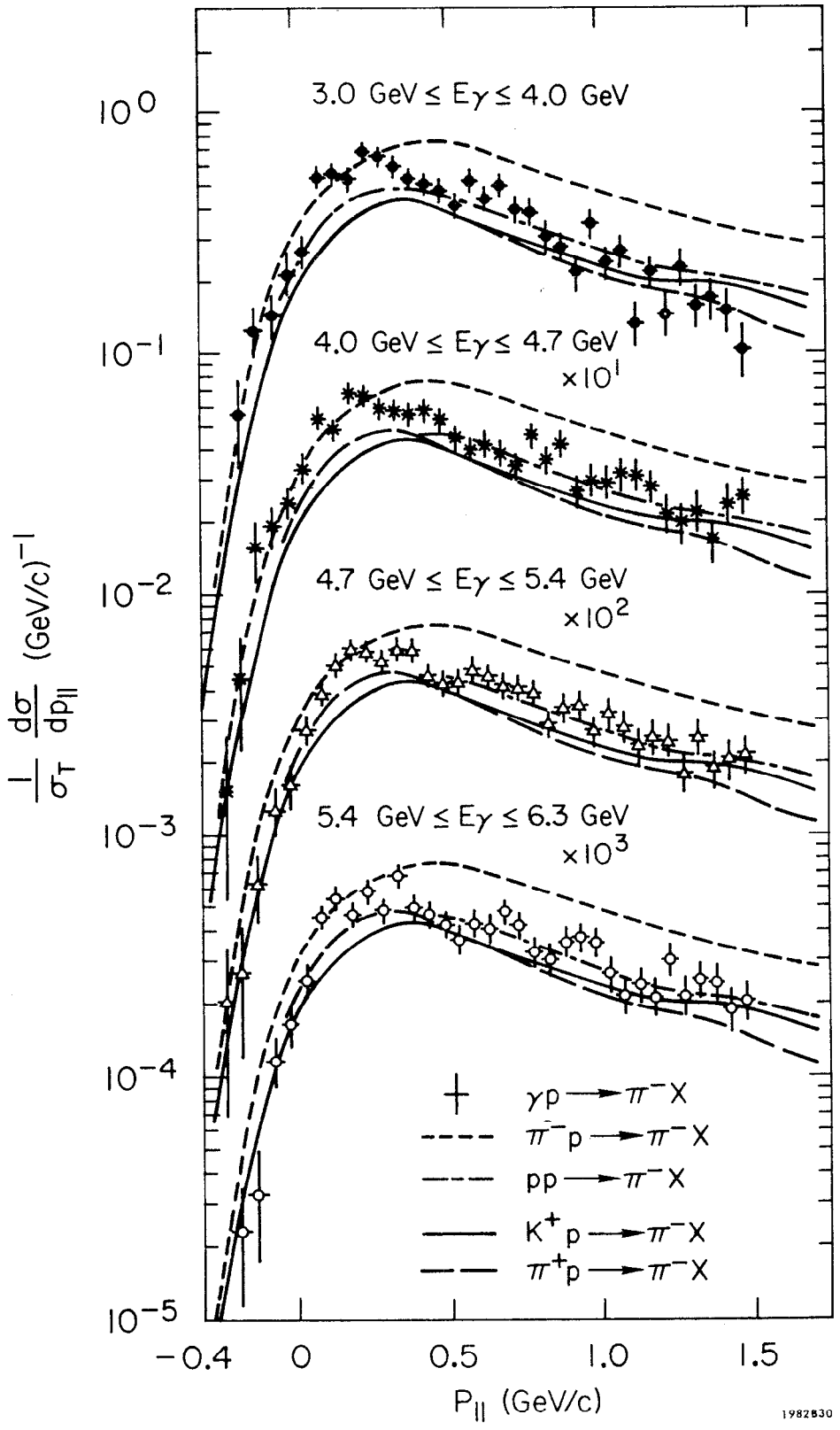
3.0 GeV ≤ Eγ ≤ 4.0 GeV
4.0 GeV ≤ Eγ ≤ 4.7 GeV
×10¹
4.7 GeV ≤ Eγ ≤ 5.4 GeV
×10²
5.4 GeV ≤ Eγ ≤ 6.3 GeV
×10³
γp → π⁻X
π⁻p → π⁻X
pp → π⁻X
K⁺p → π⁻X
π⁺p → π⁻X
10⁰
10⁻¹
10⁻²
10⁻³
10⁻⁴
10⁻⁵
−0.4
0
0.5
1.0
1.5
P|| (GeV/c)
1/σT dσ/dp|| (GeV/c)⁻¹
1982830

Fig. 34

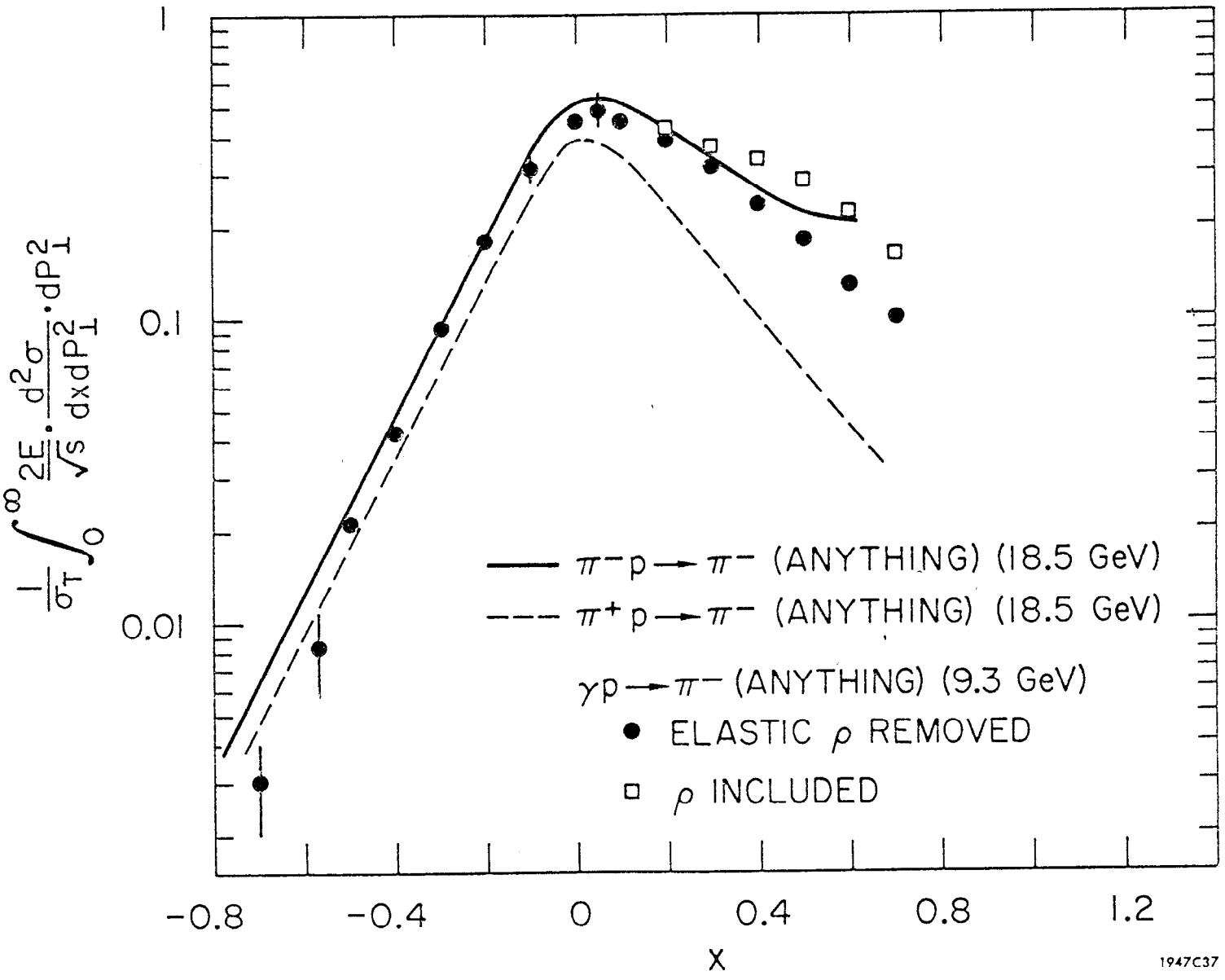
1
0.1
0.01
$\frac{1}{\sigma_T}\int_0^\infty \frac{2E}{\sqrt{s}}\cdot\frac{d^2\sigma}{dx\,dP_\perp^2}\cdot dP_\perp^2$
$\pi^- p \to \pi^-$ (ANYTHING) (18.5 GeV)
$\pi^+ p \to \pi^-$ (ANYTHING) (18.5 GeV)
$\gamma p \to \pi^-$ (ANYTHING) (9.3 GeV)
ELASTIC ρ REMOVED
ρ INCLUDED
-0.8
-0.4
0
0.4
0.8
1.2
X
1947C37

Fig. 35

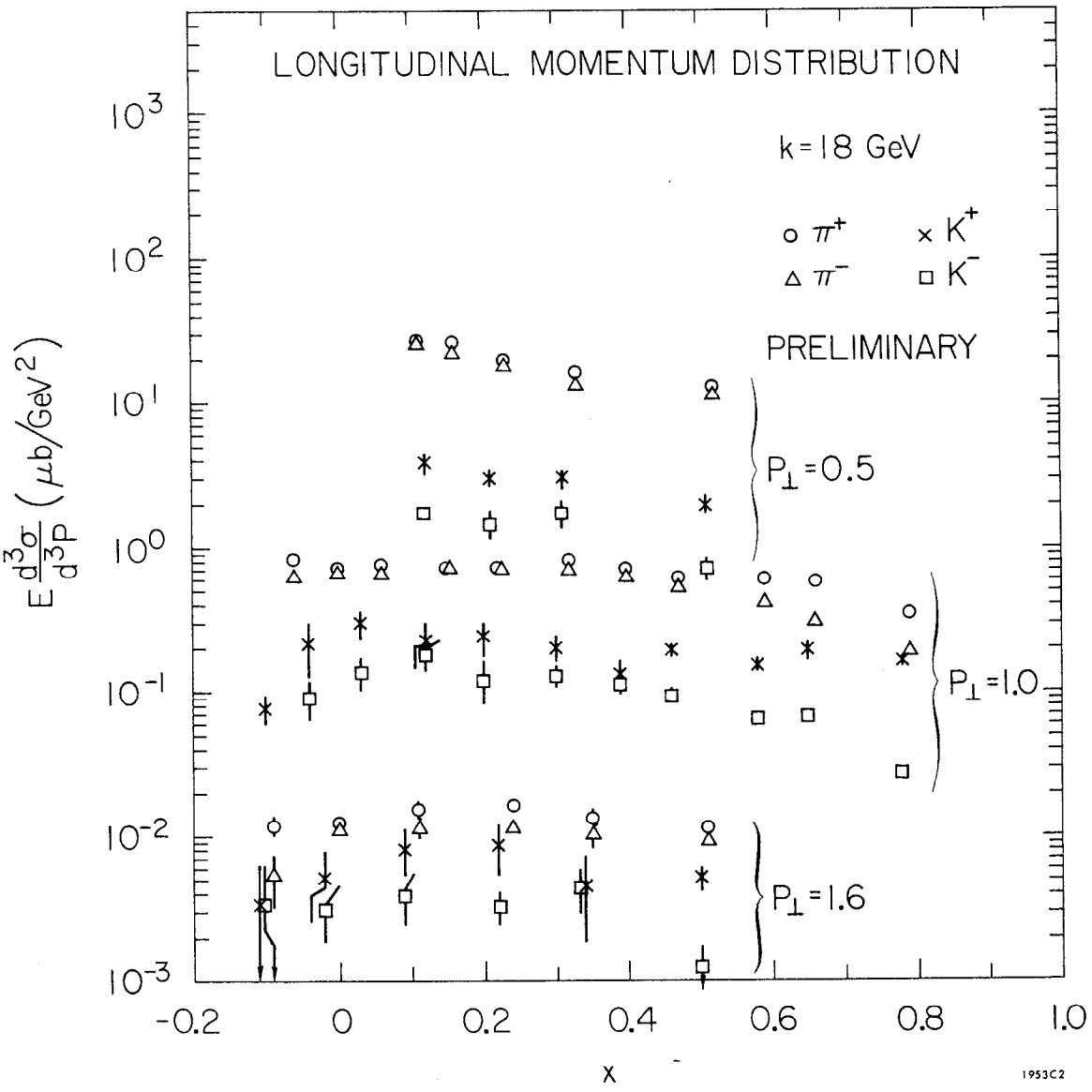
LONGITUDINAL MOMENTUM DISTRIBUTION
k = 18 GeV
o π+
× K+
Δ π−
□ K−
PRELIMINARY
P⊥ = 0.5
P⊥ = 1.0
P⊥ = 1.6
$E\frac{d^3\sigma}{d^3p}$ (μb/GeV²)
10^3
10^2
10^1
10^0
10^{-1}
10^{-2}
10^{-3}
-0.2
0
0.2
0.4
0.6
0.8
1.0
X
1953C2

Fig. 36

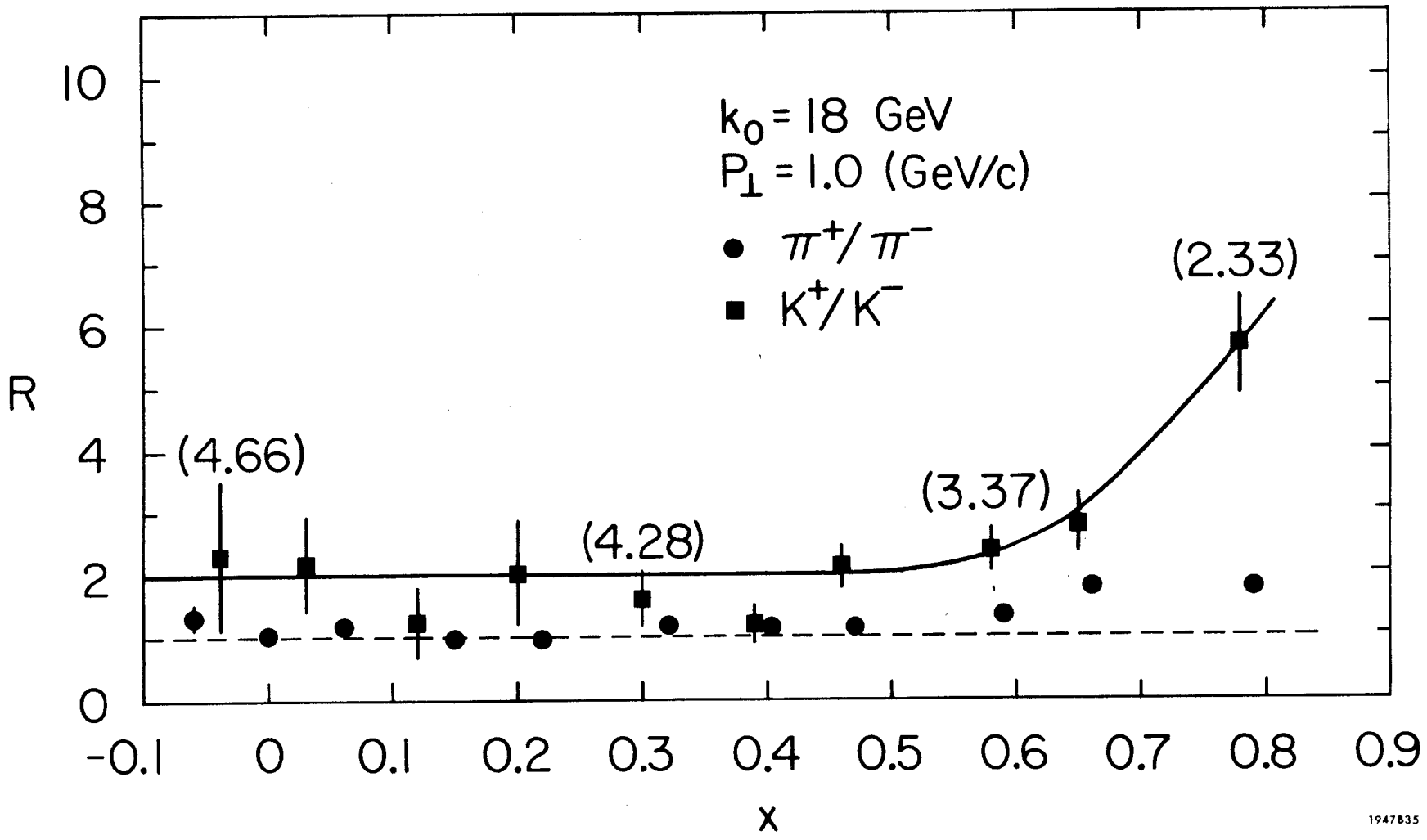
k_0 = 18 GeV
$P_\perp$ = 1.0 (GeV/c)
● π^+/π^-
■ K^+/K^-
(4.66)
(4.28)
(3.37)
(2.33)
R
x
10
8
6
4
2
0
-0.1
0
0.1
0.2
0.3
0.4
0.5
0.6
0.7
0.8
0.9
1947B35

Fig. 37

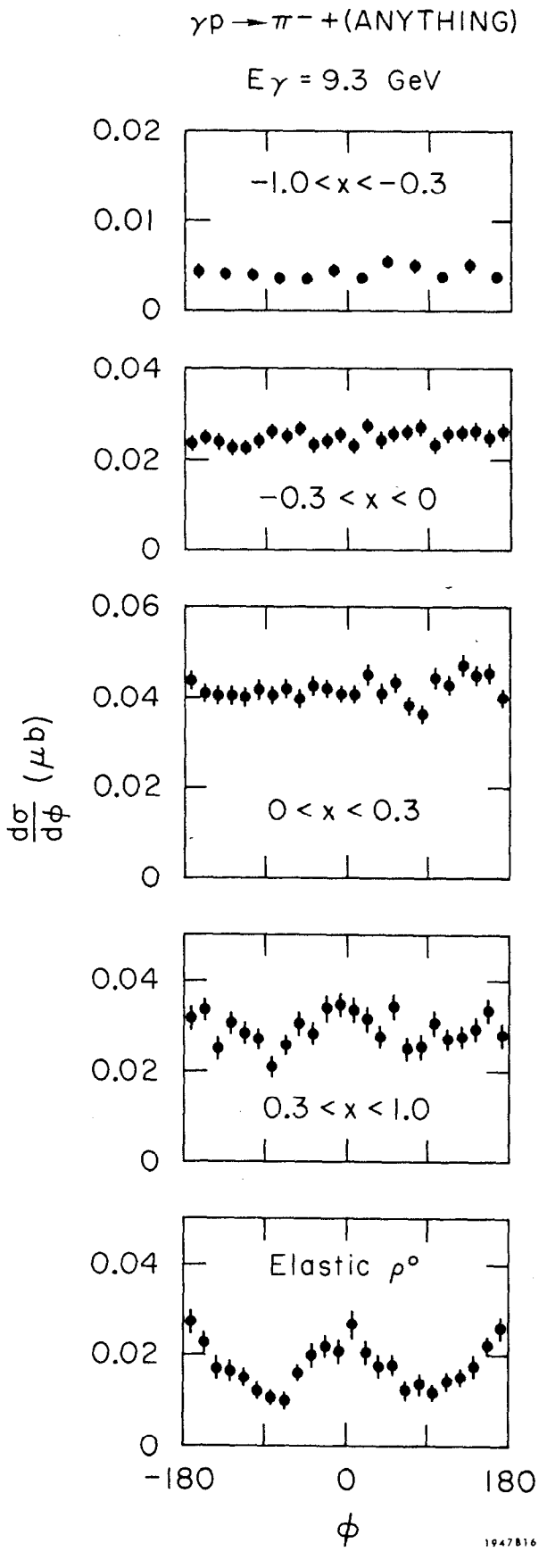
γp → π⁻ + (ANYTHING)
Eγ = 9.3 GeV
−1.0 < x < −0.3
−0.3 < x < 0
0 < x < 0.3
0.3 < x < 1.0
Elastic ρ°
dσ/dφ (μb)
φ
0.02
0.01
0
0.04
0.06
−180
180
1947B16

Fig. 38